

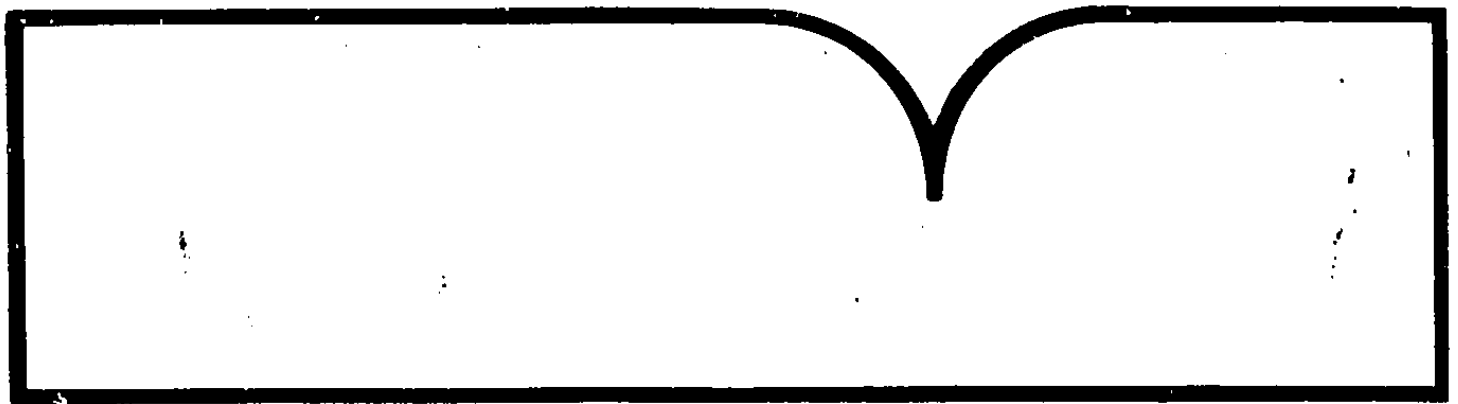
Desalination-Power Cycles with the
Biphase Rotary Separator Turbine, Phase 3

Biphase Energy Systems
Santa Monica, CA

Prepared for

Office of Water Research and Technology
Washington, DC

Feb 82



Biphase Energy Systems

A Research-Cottrell
Transamerica Delaval
Joint Venture

DESALINATION-POWER CYCLES WITH THE BIPHASE ROTARY SEPARATOR TURBINE, PHASE 3

FINAL REPORT

February 1982

Prepared for
U.S. Department of the Interior
Office of Water Research and Technology

Contract No. 14-34-0001-0490

by

Paul L. Limburg, Edward Walsh and Daniel Rovner

Approved by



William E. Amend
Technical Director

REPRODUCED BY
NATIONAL TECHNICAL
INFORMATION SERVICE
U.S. DEPARTMENT OF COMMERCE
SPRINGFIELD, VA. 22161

BIBLIOGRAPHIC INFORMATION

PB83-146753

Desalination-Power Cycles with the Biphase Rotary Separator Turbine, Phase 3.

Feb 82

Paul L. Limburg, Edward Walsh, and Daniel Rovener.

PERFORMER: Biphase Energy Systems, Santa Monica, CA.
Contract DI-14-34-0001-0490

SPONSOR: Office of Water Research and Technology,
Washington, DC.
W8301370 OWRTC-00156-D(0490)(1)
Final rept.

See also FB81-150237. Color illustrations reproduced in black and white.

Tests of a fluidized-bed seawater heat exchanger showed that 330F was the maximum temperature to which seawater could be heated without scale formation in the bed during once through flow of seawater. Twelve material and coating combinations were exposed to a two-phase salt-water jet to simulate the environment of rotary-separator-turbine rotor materials. The materials, except for bare aluminum and some brittle coatings, passed four-hour screening tests. A hydraulic version of the Biphase reaction turbine can recover reverse-osmosis reject-brine pressure energy with efficiency of over 70%. A two-phase version can recover pressure energy and provide additional power for pumping from a waste heat source. Integration of a high-pressure reverse-osmosis pump into the turbine is not as efficient as using a separate pump and turbine coupled together. A system configuration was developed for a desalination-power system which uses the waste heat from diesel engines in the power plant at San Nicolas Island, CA.

KEYWORDS: *Desalting, *Rotary filters, *Turbines, *Heat exchangers, *Fluidized bed processors, *Desalination plants, *Reverse osmosis.

Available from the National Technical Information Service, Springfield, Va. 22161

PRICE CODE: PC A07/MF A01

Selected Water Resources Abstracts

W 004539

3. Accession No.

W 83-01370

Input Transaction Form

4. Title Desalination — Power Cycles with the Biphase Rotary Separator Turbine, Phase 3, *(all caps)*

7. Author(s)

Paul L. Limburg, Edward Walsh, and Daniel Rovener,

9. Organization

Biphase Energy Systems

~~2800 Airport Avenue~~

Santa Monica, CA 90405 *California.*

10. Project No. C-00156-D
DES 7030-2 (0490)(1)

11. Contract/Grant No.

~~14-34-0007-0490 (7)~~

13. Type of Report and Period Covered

12. Sponsoring Organization ~~OWRT, DOI~~

15. Supplementary Notes

Final Report, February 1982. 121p, 58 fig, 7 tub, 11 ref.

16. Abstract

Tests of a fluidized-bed seawater heat exchanger showed that 330°F was the maximum temperature to which seawater could be heated without scale formation in the bed during once through flow of seawater.

Twelve material and coating combinations were exposed to a two-phase salt-water jet to simulate the environment of rotary-separator-turbine rotor materials. The materials, except for bare aluminum and some brittle coatings, passed four-hour screening tests.

A hydraulic version of the Biphase reaction turbine can recover reverse-osmosis reject-brine pressure energy with efficiency of over 70%. A two-phase version can recover pressure energy and provide additional power for pumping from a waste heat source. Integration of a high-pressure reverse-osmosis pump into the turbine is not as efficient as using a separate pump and turbine coupled together.

A system configuration was developed for a desalination-power system which uses the waste heat from diesel engines in the power plant at San Nicolas Island, CA.

(Author abstract)

17a. Descriptors

*fluidized-bed, *heat-exchanger, *turbines, waste-heat-recovery, scale, corrosion, erosion, rotary-separator turbine, energy-recovery, *Desalination, *California, San Nicolas Island.

17c. COWRR Field & Group

D3A, ~~86-08F~~

18. Availability
Available from the National
Technical Information Service

as PB ~~P88-3~~ 14675



Send to:
Water Resources Scientific Information Center
OFFICE OF WATER RESEARCH AND TECHNOLOGY
U.S. DEPARTMENT OF THE INTERIOR
Washington, D.C. 20240

Abstractor P.L. Limburg

Institution Biphase Energy Systems

FOREWORD

This study was sponsored by the U.S. Department of the Interior, Office of Water Research and Technology, Contract No. 14-34-0001-0490. Dr. William McCoy of OWRT's Research Division directed the effort.

At Biphase Energy Systems, Walter R. Studhalter provided valuable direction of the project, Louis Drobnick assisted the experimental work, Emil Ritzi contributed to turbine analysis and Treva Meredith helped prepare this report.

Mr. Brian E. Swaidan of the U.S. Navy Civil Engineering Laboratory, NCBC at Port Hueneme, CA, and ENS J.E. Power and Mr. G.E. Trask of the Public Works Department at the Naval Air Station at Pt. Mugu, CA, provided information and assistance.

CONTENTS

<u>Section</u>		Page
	ABSTRACT	1
1	INTRODUCTION	2
2	SUMMARY	
	Heating Seawater with a Fluidized Bed	4
	Corrosion-Erosion Test of Rotor Materials	4
	Turbine-Pump Unit for Reverse Osmosis	5
	Desalination-Power Cycle Application	5
3	HEATING SEAWATER WITH A FLUIDIZED BED	
	Why Fluidized-Beds?	6
	Biphase System Requirements	6
	Fluidized-Bed Tests	10
	Test System	10
	Test Heat Exchangers	14
	Bed Materials	19
	Test Results	20
	Bare Tube Tests	28
	Two Fluidized-Bed Heat Exchangers in Series	28
	Tests with One Heat Exchanger	30
	Two-Stage Fluidized Bed	35
	Filtering Scale Precipitates	35
	Conclusions	37
4	CORROSION-EROSION TEST OF ROTOR MATERIALS	
	Objectives	39
	Test Apparatus	40
	Results	40
	Conclusions	59

CONTENTS (cont'd)

<u>Section</u>		Page
5	TURBINE PUMP UNIT FOR REVERSE OSMOSIS	
	Development	60
	Hydraulic Reaction Turbine	62
	Two-Phase Turbine	67
	Combination of High-Pressure Pump and Turbine	67
	Conclusions	73
6	DESALINATION/POWER CYCLE APPLICATION	
	San Nicolas Island	74
	Biphase Desalination/Power System	81
	Prototype Systems Costs	84
	APPENDIX A - LIQUID FLUIDIZED BED ANALYSIS	88
	APPENDIX B - TEST SYSTEM INFORMATION	94
	APPENDIX C - REACTION TURBINE FLUID MECHANICS AND THERMODYNAMICS	111
	REFERENCES	121

LIST OF FIGURES

Figure		Page
3-1	Biphase Desalination/Power System	7
3-2	Seawater Heater General Arrangement	9
3-3	Liquid Fluidized-Bed Heat Exchanger Designed for Improved Flow Distribution	11
3-4	Test System Schematic	12
3-5	Test Heat Exchanger (Assembly Drawing)	15
3-6	Expansion Seal	16
3-7	Check Valve	17
3-8	Fluidized-Bed Heat Exchangers	18
3-9	Three Tubes in Series (Bare Tube Tests)	29
3-10	Plug Formation	31
3-11	Fluidized Bed with Two Sight Glasses	33
3-12	Two-Stage Fluidized Bed	36
3-13	Precipitate-Removal Filter	38
4-1	Corrosion/Erosion Impingement-Test Apparatus . .	41
4-2	Impingement Test Sample Holder	42
4-3	Miniature Nozzle for Impingement Test	43
4-4	Aluminum After Exposure	45
4-5	6061T0 After Test	46
4-6a	6061T6 Before Test	47
4-6b	6061T6 After Test	47
4-7a	7075T73 Before Test	48
4-7b	7075T73 After Test	48
4-8a	7075T73 with Electroless Nickel Coating, Before Test	49
4-8b	7075T73 with Electroless Nickel Coating, After Test	49
4-9	HY80 After Test	50
4-10a	HY80 with Inconel Flame Spray, Before Test . . .	51
4-10b	HY80 with Inconel Flame Spray, After Test . . .	51
4-11a	HY100 with CM500 Coating, Before Test	52
4-11b	HY100 with CM500 Coating, After Test	52

LIST OF FIGURES (cont'd)

<u>Figure</u>		<u>Page</u>
4-12a	AISI610 with TMT Coating, Before Test	53
4-12b	AISI610 with TMT Coating, After Test	53
4-13a	316 Stainless Steel, Before Test	54
4-13b	316 Stainless Steel, After Test	54
4-14a	Adiprene Coating on 316 Stainless Steel, Before Test	55
4-14b	Adiprene Coating on 316 Stainless Steel, After Test	55
4-15a	Inconel 625, Before Test	56
4-15b	Inconel 625, After Test	56
4-16a	Ti-6Al-4Vn, Before Test	57
4-16b	Ti-6Al-4Vn, After Test	57
5-1	Biphase/RO Machinery Simplification	61
5-2	Reaction-Turbine Concept	63
5-3	Baseline RO Cycles - Seawater Feed	65
5-4	Biphase/Reverse-Osmosis System with Reject- Brine Working Fluid, Maximum Seawater Temperature 330°F, 50-Inch-Diameter Turbine . . .	68
5-5	Biphase Turbine/Pump/Energy Recovery Unit for Reverse Osmosis Application	69
5-6	Pumping Methods	71
6-1	Sketch of San Nicolas Island Power Plant	75
6-2	San Nicolas Island Power Plant	76
6-3	San Nicolas Island Power Plant Log 5/22/79	78
6-4	San Nicolas Island Power Plant Log 1/23/79	79
6-5	Exhaust-Gas Temperature from San Nicolas Engines	80
6-6	Exhaust Ducts from 1000-kw Engines	82
6-7	Single-Stage Biphase Desalination Cycle 400°F Maximum Seawater Temperature, 5-psia Con- densing Pressure.	83

LIST OF FIGURES (cont'd)

Figure		Page
A-1	Reynolds Number vs Gailleo Number for Fluidized Beds	90
A-2	Fluidized-Bed Superficial Velocity as a Function of Particle Diameter and Density . .	91
A-3	Bed Void Fraction as a Function of Fluid Velocity	92
A-4	Bed-Length Expansion as a Function of Bed Void Fraction	93
B-1	Test System Detail Schematic	96
B-2	Valves List	97
B-3	Measurements List	98
B-4	Data System	101
B-5	Seawater Heating Test Checklist	102
B-6	System Shutdown	105
B-7	Seawater Heating Test System Things to Check During Testing	106
B-8	Calibration/Checkout Tests	108
B-9a	Three Uninsulated Test Heat Exchangers, Top Section Showing Sight Glasses	109
B-9b	Three Uninsulated Test Heat Exchangers, Lower Section Showing Expansion Joints	110
C-1	Mollier Diagram of Reaction Turbine Thermodynamics	112
C-2	Reaction Rotor and Velocity Triangles	113
C-3	Optimum Efficiency, Speed Ratio and Radius Ratio	120

LIST OF TABLES

Table		Page
3-1	Seawater Composition	13
3-2	Bed Materials	19
3-3	Seawater Heat-Exchanger Test Runs	21
4-1	Impingement Test Results	44
5-1	Turbine Specifications	66
6-1	San-Nicolas-Island System	85
6-2	Prototype System Cost Estimate	87

ABSTRACT

Tests of a fluidized-bed seawater heat exchanger showed that 330°F was the maximum temperature to which seawater could be heated without scale formation in the bed during once through flow of seawater.

Twelve material and coating combinations were exposed to a two-phase salt-water jet to simulate the environment of rotary-separator-turbine rotor materials. The materials, except for bare aluminum and some brittle coatings, passed four-hour screening tests.

A hydraulic version of the Biphase reaction turbine can recover reverse-osmosis reject-brine pressure energy with efficiency of over 70%. A two-phase version can recover pressure energy and provide additional power for pumping from a waste heat source. Integration of a high-pressure reverse-osmosis pump into the turbine is not as efficient as using a separate pump and turbine coupled together.

A system configuration was developed for a desalination-power system which uses the waste heat from diesel engines in the power plant at San Nicolas Island, CA.

1. INTRODUCTION

The Biphase Rotary Separator Turbine (RST) produces power by expanding a two-phase (liquid and gas) fluid from a higher to a lower pressure. In a desalination system, the RST can produce both power and potable water. In previous work Biphase Energy Systems developed an RST for power production from geothermal, waste-heat and solar-energy resources.

In more recent work, Biphase Energy Systems developed the concept of using an RST in a desalination cycle that used waste heat as the energy source. The U.S. Department of the Interior, Office of Water Research and Technology, supported a study which optimized RST desalination - power cycles and identified beneficial use of components with conventional desalination processes (1). The operation of an RST using seawater for the working fluid was demonstrated and a conceptual design of a desalination-power system was developed.

This study raised three key issues for development of the desalination-power cycles. These issues are:

1. The efficiency of the Biphase desalination-power cycle is, like other thermal desalination processes, dependent on the maximum temperature to which saltwater can be heated in the equipment. Fluidized-bed technology provides potential for higher-than-conventional temperatures which are limited by scale formation. The maximum temperature that saltwater can be heated in a fluidized-bed heater and the materials that the RST must be made of for corrosion-and-erosion-free operation are important limitations on system performance and economics.
2. The RST has potential application in reverse-osmosis systems. The turbine can operate as the power source, high-pressure pump and energy-recovery device. The feasibility of this concept depends on the turbine performance limits which are not known.

3. The requirements for a demonstration desalination-power system for a typical application using a waste-heat energy source need to be delineated.

This report describes the investigation into these issues. The following section summarizes the results of the project. Later sections describe fluidized-bed experiments, corrosion-erosion tests, the design of a reverse-osmosis turbine and a desalination-power system application in greater detail.

2. SUMMARY OF RESULTS

HEATING SEAWATER WITH A FLUIDIZED BED

We tested seawater fluidized beds of metal and ceramic beads. The beads were contained in 1/2-inch diameter vertical tubes.

1. Bare tubes (without bed material) scaled as expected at 260°F and even more at higher temperatures.
2. The fluidized bed improves dramatically the heat transfer rate between the tube wall and the seawater.
3. Ceramic bed materials are not as effective as the more dense metal particles in eliminating scale on the tubes.
4. 330°F was the maximum temperature that the seawater can be heated to without scale forming in the fluidized bed during once through flow of the seawater.
5. Close attention must be paid to the bed geometry to provide a uniform flow throughout the bed. Lower flows in certain areas can lead to areas of unstable scale buildup.
6. For heating to higher than 330°F, a system that recirculates the seawater flow through the bed is required. Reducing the heat fluxes to the seawater (with a gas as the heating fluid instead of steam, for example) could reduce scaling tendency. Also, additives might reduce scaling.

CORROSION-EROSION TEST OF ROTOR MATERIALS

Twelve material-and-coating combinations were exposed to a two-phase saltwater jet for four-hour screening tests. The test simulated the environment of RST rotor materials in desalination-power systems. All materials except for bare aluminums and some brittle coatings passed the test. The materials which passed should be tested for longer periods to determine incubation time effects, and resistance to cavitation-type erosion.

TURBINE-PUMP UNIT FOR REVERSE OSMOSIS

We analyzed the performance of a turbine and pump in combination with reverse osmosis desalination systems.

1. A hydraulic reaction turbine is projected to economically recover reverse-osmosis reject-brine power with an efficiency of over 70%. The turbine will reduce the pumping power required by the RO plant by 35%. A prototype of the unit should be built and tested.
2. A two phase version of the turbine can be combined with a reverse osmosis plant to generate fresh water from waste heat sources. The system is projected to produce 5.6 pounds of fresh water per 1000 Btu of heat input.
3. The combination of the high-pressure reverse-osmosis pump and the power-recovery turbine in the same housing would provide a simple machine. However, this combination is not as efficient as using a separate pump and turbine that are coupled together.

DESALINATION-POWER SYSTEM APPLICATION

We developed the configuration for a desalination-power system. The configuration was based upon using the waste heat from the power plant at San Nicolas Island, California.

A demonstration desalination system using a Biphase rotary separator turbine can generate 29 hp and 2900 gpd of fresh water. During peak-power demand, production increases to 57 hp and 5700 gpd of fresh water.

3. HEATING SEAWATER WITH A FLUIDIZED BED

In a fluidized bed, a fluid flows vertically upwards through a bed of solid particles. If the fluid velocity is high enough, the particles become fluidized. The gravity force on the particles is balanced by the upward drag force of the fluid. The particles move irregularly within the bed. If the fluid velocity is not too high, the particles do not flow with the fluid out of the top of the bed.

WHY FLUIDIZED-BEDS?

Formation of calcium sulphate scale limits conventional seawater heat exchanger operation to about 275°F. Scale decreases heat-transfer rates and blocks flow. Higher seawater temperatures provide greater power- and water-production performance in Biphase and other desalination systems. Increasing the temperature from 275 to 400°F in Biphase desalination-power cycles doubles power-production efficiency from 3 to 6 percent (1). Seawater fluidized beds have potential to supply seawater at higher more-efficient temperatures. The action of the fluidized bed limits scale formation on the heat transfer surfaces.

Hatch and Weth (2) tested seawater fluidized beds in 1½-inch tubes in a steam-heated loop. The flow rate circulating through the beds was 20 to 50 times the seawater makeup added to the loop. Scale did not form on the heat transfer surfaces for at least up to 400°F maximum seawater temperature. Some scale deposited in the separation region above the fluidized bed and in the recirculating lines. Filters were able to remove precipitated scale compounds from the heated seawater as a muddy slurry. Hatch and Weth also operated fluidized beds with once-through seawater flow with no scale at 350°F maximum seawater temperature. Other investigators (3-8) have tested saltwater fluidized beds with similar results.

BIPHASE SYSTEM REQUIREMENTS

A single-stage Biphase desalination-power system, Figure 3-1, with a 400°F maximum seawater temperature can produce 9000 gallons per

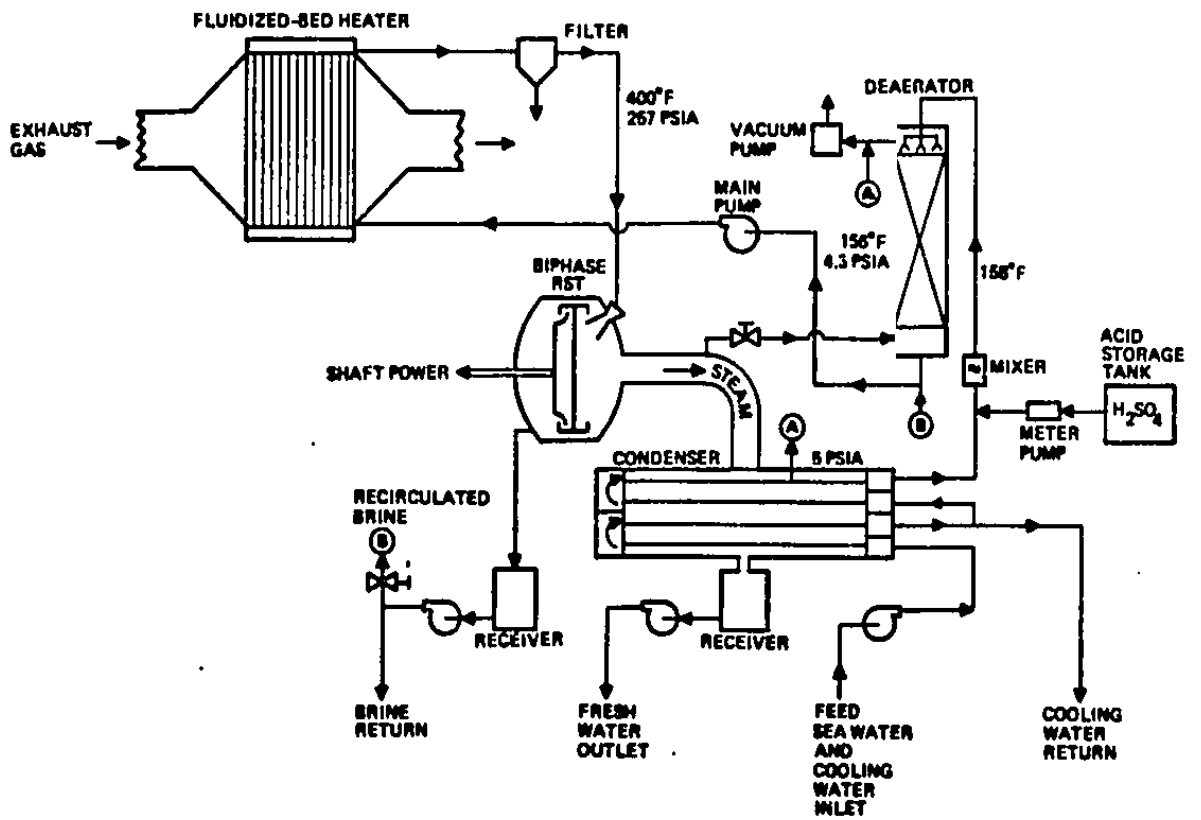


Figure 3-1. Biphase Desalination/Power System

0569A

day and 90 hp from the energy in 7.6 lb/s of 760°F exhaust gas (1). Larger systems can be scaled from this size. Waste exhaust gas heats the seawater in the fluidized-bed heater. The following are considerations for design of the fluidized-bed heater:

1. Seawater must flow vertically upward through the fluidized bed.
2. Fluidized beds have high heat-transfer rates between the fluid and the enclosing surfaces. In this application, the low gas-side film coefficient controls heat transfer, so a large gas-side surface area is necessary.
3. All surfaces which transfer heat to the seawater should be exposed to the fluidized bed to limit scaling.
4. Fluidized beds tend to be isothermal due to the mixing of particles. Staging or multiple passes are required to extract the most energy from the exhaust gas. For beds in thin long tubes, the isothermal tendency is probably reduced.
5. Liquid-side superficial velocity is limited to a narrow band which causes proper fluidization of the bed. The velocity is lower for smaller and less-dense particles.
6. Gas-side pressure drop should be about five in. H₂O to be compatible with exhaust-gas sources. Gas side should be designed to avoid fouling by exhaust-gas particles.
7. The minimum gas-side wall temperature must be above the acid dew point in the exhaust gas.

There are two possible fluidized-bed seawater-heater configurations in a Biphase desalination/power system. These are:

1. Fluidized-Bed Inside Finned Tubes (Figure 3-2). The seawater flows through a number of vertical passes. Each pass consists of several vertical tubes which join together in a manifold at

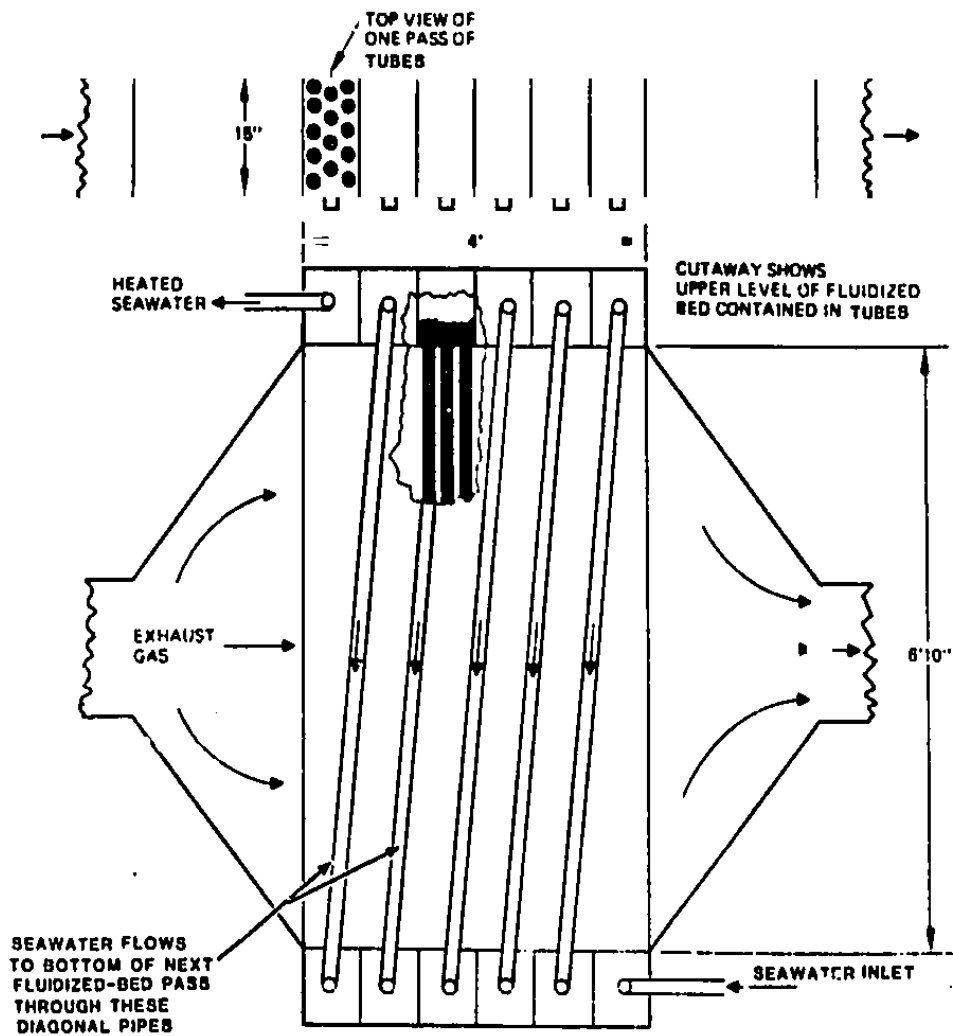


Figure 3-2. Seawater Heater General Arrangement

0571A

the top and bottom. The seawater fluidized bed is contained inside the tubes (solid black area in cutaway in Figure 3-2). After the seawater reaches the top of the bed, the seawater flows down through a pipe to the bottom of the next pass.

2. Fluidized-Bed on Shell Side (Figure 3-3). The gas flows through the tubes. The seawater flows through multiple passes on the shell side. This configuration has been developed by Allied Chemical Corp. (6-8) for transferring heat from hot geothermal brines. When exhaust gas is on the tube side, the gas side is less susceptible to particulate fouling than when exposed to externally-finned tubes. Maintaining uniform fluidization is more difficult with beds on the shell side. Also, shell-side beds require a large recirculating flow to keep the proper seawater velocity for fluidization. A vertical configuration is also possible. The fluidized bed limits scale and improves heat transfer more on vertical surfaces. However, tubes are exposed to hot sea water outside of the bed in the disengagement space above the bed.

The configuration with the fluidized bed inside the finned tubes is more practicable and was the basis for our fluidized-bed tests.

FLUIDIZED-BED TESTS

We tested seawater fluidized-beds contained in 1/2-inch inside-diameter tubes. We sought to determine the maximum temperature to which the seawater can be heated without scale forming in the fluidized-bed heat exchanger.

TEST SYSTEM

Figure 3-4 is schematic of the test system. Seawater flowed from a storage tank, through a 7 μ m filter and pump to a preheater. Low-pressure steam from a small boiler heated the seawater to 200^oF in the preheater. The seawater temperature was controlled by regulating the steam pressure.

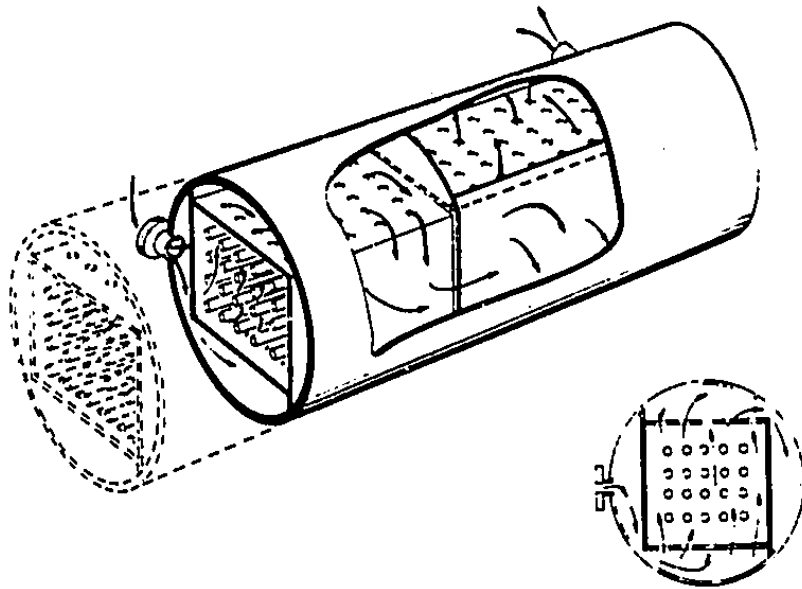


Figure 3-3. Liquid Fluidized-Bed Heat Exchanger Designed for Improved Flow Distribution

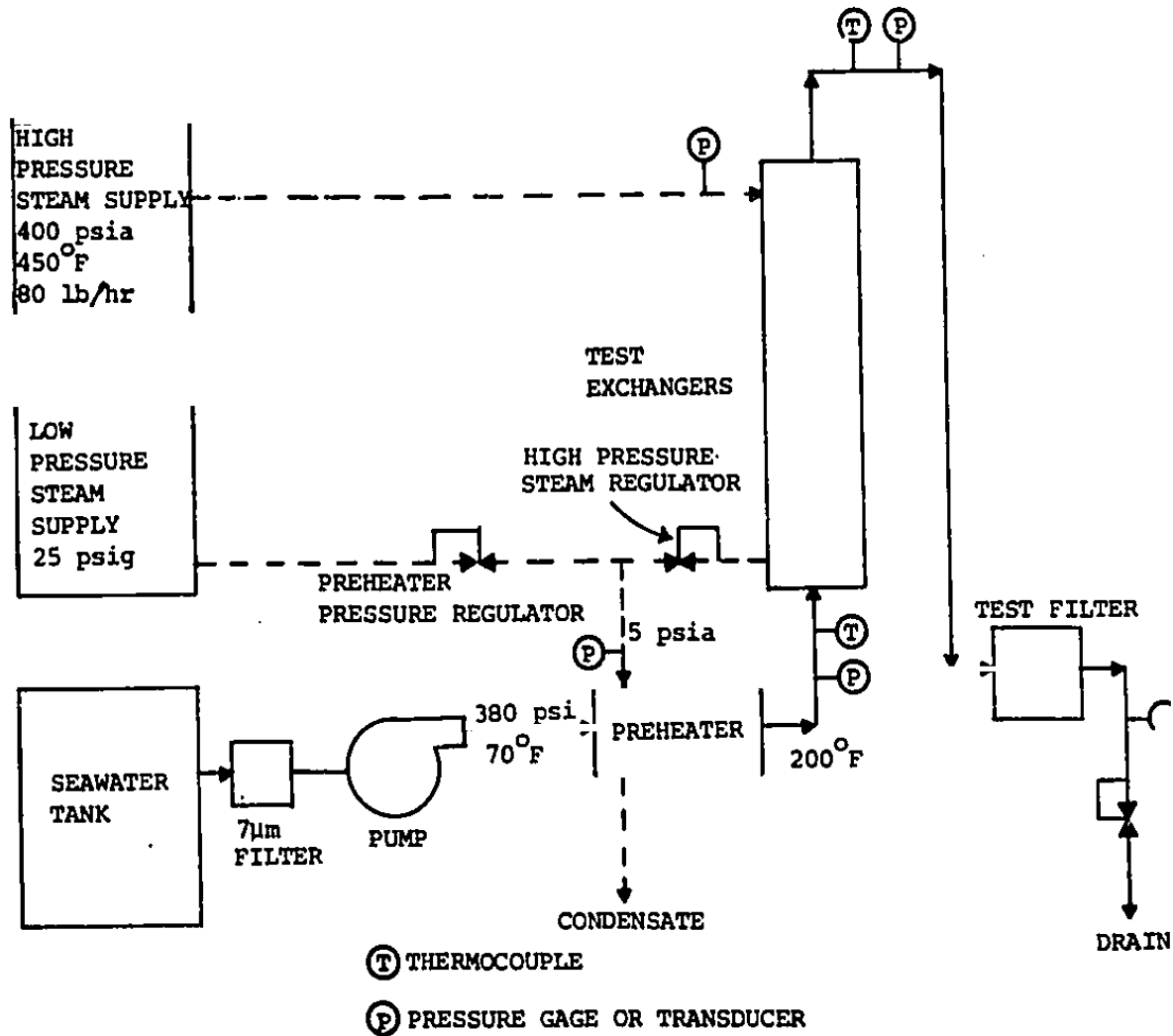


Figure 3-4. Test System Schematic

The seawater then flowed to one, two, or three test heat exchangers. A steam-supply system provided saturated steam up to 400 psia. Condensing steam heated the seawater in the test heat exchangers. The temperature of the seawater at the test-heat-exchanger outlet was controlled by regulating the steam pressure.

Next, the seawater flowed from the heat exchangers to a test filter. The filter removed scale precipitates from the seawater. After filtering, the seawater was discarded. Appendix B gives additional details about the test system.

The eventual application of seawater fluidized beds in Biphase systems points to seawater being heated by hot gas. The gas gives a much lower hot-side heat transfer coefficient than does condensing steam. The heat flux is also less. However, steam heating gave greater control over the hot-side temperature in the test heat exchanger.

A local utility supplied seawater from their power plant's seawater clear well. Table 3-1 lists the chemical composition of the seawater.

Table 3-1. Seawater Composition

	ppm
Chloride	21,000.0
Sodium	12,156.7
Sulfate	2,855.8
Magnesium	1,287.9
Calcium	400.4
Bicarbonate	170.9
Silica	16.0
Carbonate	0
Nitrate	0
Borate	0
Total Dissolved Solids	37,888

TEST HEAT EXCHANGERS

The fluidized beds that we tested were contained inside 5/8" OD (0.459" ID) 90-10 CuNi tubes. The tubes, about seven feet long, were surrounded by a 1½" 304SS pipe. Heating steam flowed through the annular space between the pipe and tube. The steam condensed on the tube and heated the fluidized bed. Figure 3-5 is an assembly drawing of the fluidized-bed heat exchanger. An expansion joint BE-933 at the bottom of the steam jacket allowed for thermal expansion of the tube. Before entering the fluidized bed, seawater flowed through a check valve which kept the bed material inside the tube when the seawater flow was stopped. Figure 3-6 and 3-7 show the details of the expansion joint and check valve. The size of the check valve ball was later decreased to eliminate clogging with bed material.

The tubes were secured in the steam-pipe jacket by a tube fitting screwed into the ends of the steam jacket and brazed to the tube. The tubes were easily removed for sectioning by cutting through these fittings. Then another tube could be installed in the steam jacket.

At the top of the bed, the seawater flowed through high-pressure 6"-high sight glasses. The sight glasses enabled us to observe the top of the bed. The sight glass, which had a flow area about three times the area of the 0.495" ID tubes, also provided a region for the bed material to disengage from the seawater flow because of lower water velocity. In some sight glasses we inserted a glass tube, with the same inside diameter as the copper-nickel tubes, in the flow path inside the sight glass. The sight glass body contained the 300 psig pressure, and the glass tube contained the flow. Thus, we were able to observe the action of the bed as it occurred in the tubes and more precisely control the bed height.

Figure 3-8 shows three uninsulated heat exchangers in the test stand. The preheater is the horizontal cyclinder behind the exchangers. The low-pressure steam boiler is beside the exchangers to the right.

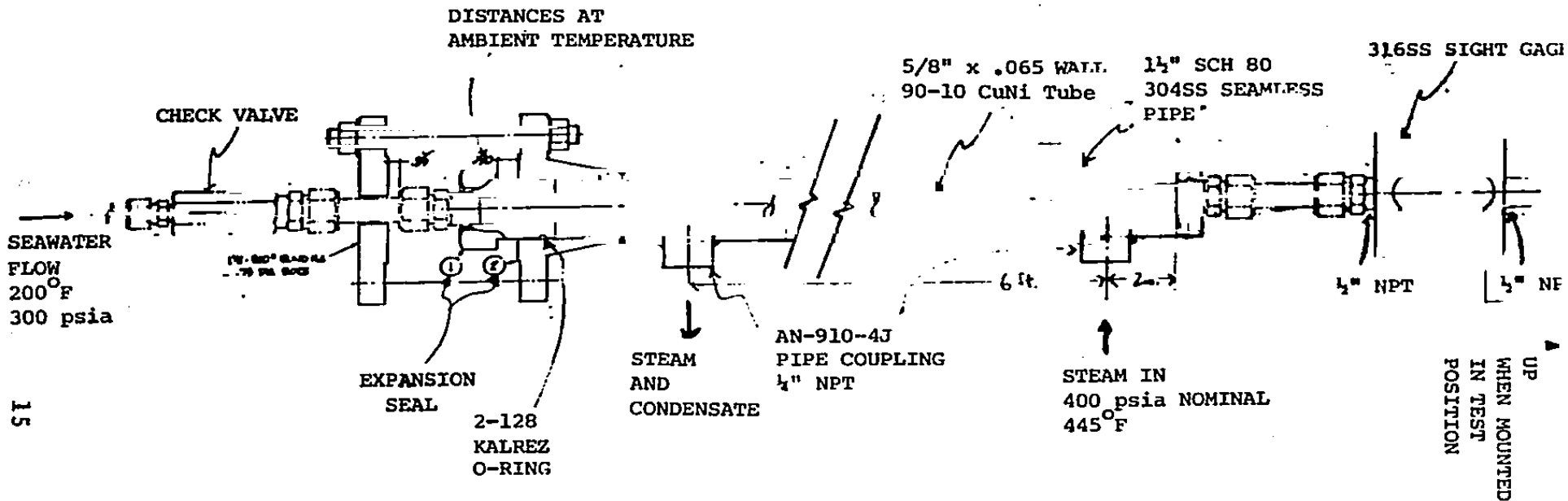


Figure 3-5. Test Heat Exchanger (Assembly Drawing)

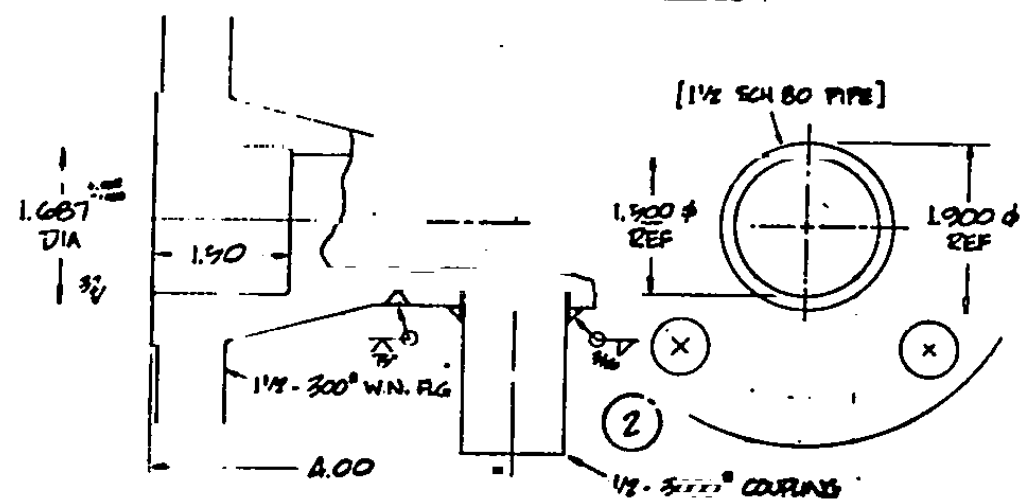
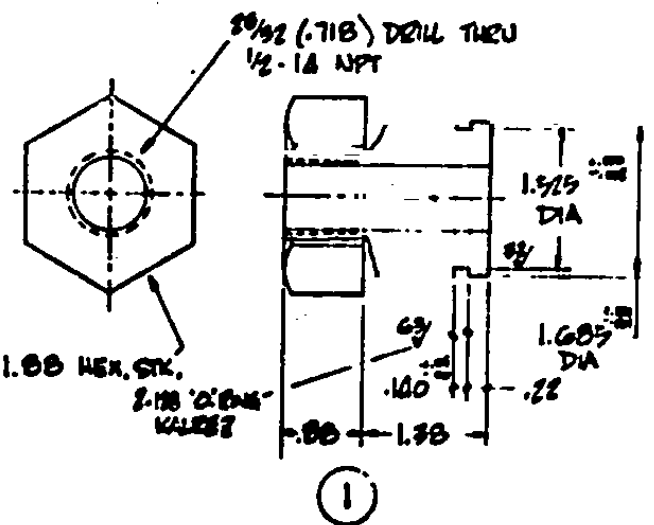
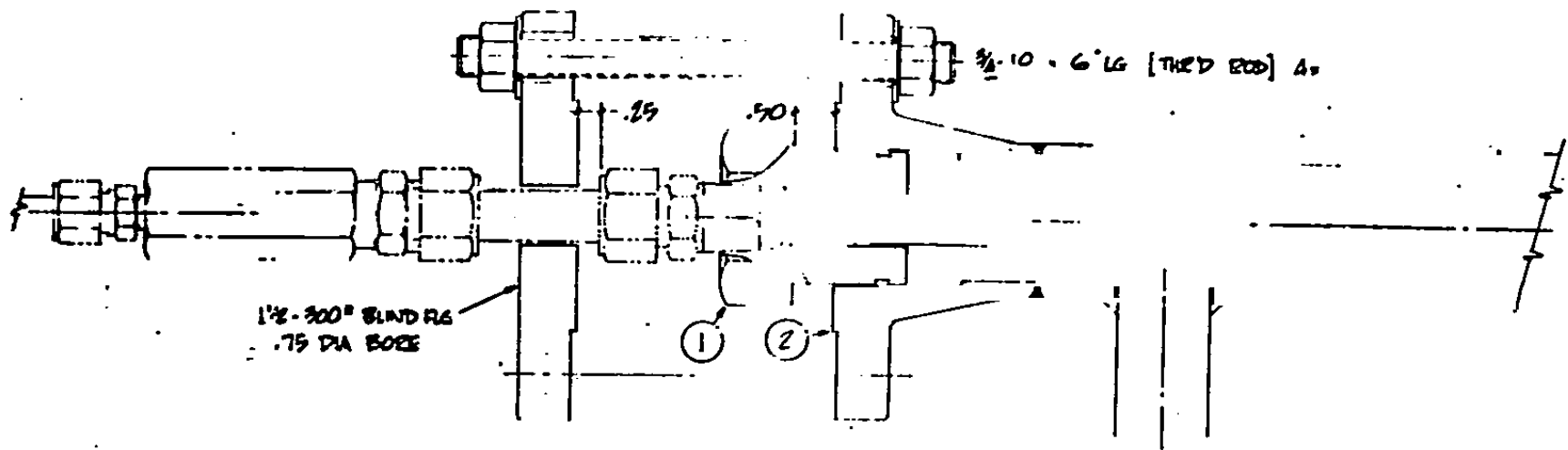


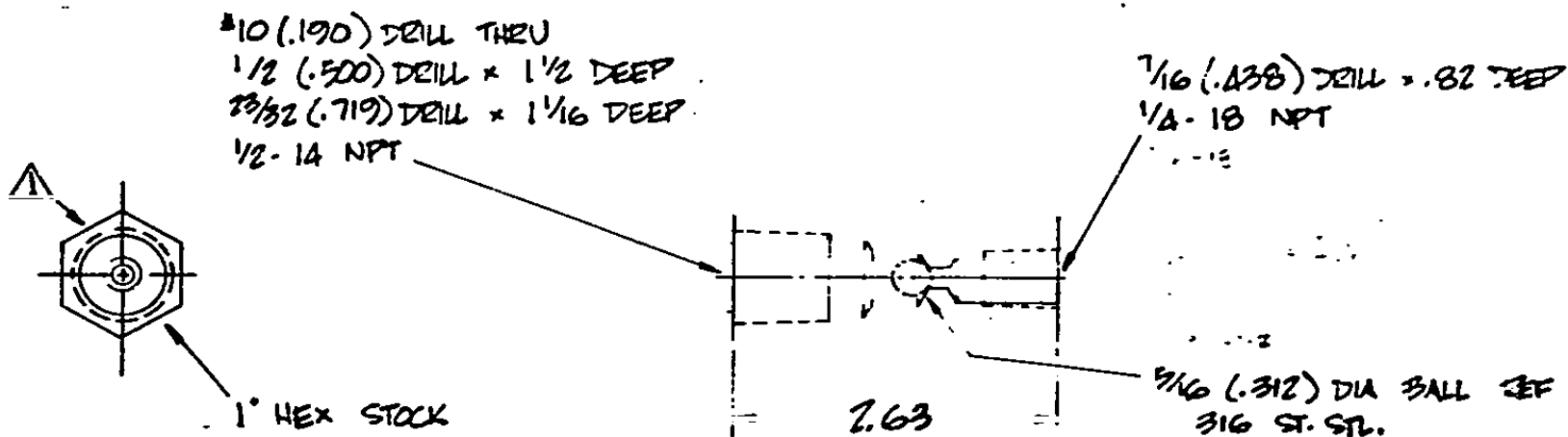
Figure 3-6. Expansion Seal

2	1	SEAL HOUSING	304 ST. STL.		
1	1	SEAL PLUNGER	303 SU ST STL	ASTM A-501	1 7/8 HEX - 2 1/2 LG
Description		MATERIAL		FINISH	
No Req'd		SPECIFICATION		CONTRACT NO 1031	
MATERIAL SPECIFIED		FINISH		BYE	
SEE DRAWING		25		C	
SEE DRAWING		25		BE-933	
SEE DRAWING		25		SCALE FULL	

Reproduced from best available copy.



SEE DRAWING



NOTES:
 STAMP "BE-930" FOR IDENTIFICATION

Figure 3-7. Check Valve

Item No	No Req'd	Description	Material	Specification	Size
Next Assy	BE	No Req'd	MATERIAL	303 S.U. ST. STL. COND B	Phase Energy Systems
Final Assy	BE		SPECIFICATION	ASTM A-581	SIZE
UNLESS OTHERWISE SPECIFIED All dimensions are in inches and apply after chemical treatment and/or plating All machined fillets G1.0 D20 P Break all sharp edges D05 D15 R TOLERANCES XX ± .03C Angles 5 XXX ± .01C			CONTRACT NO	1031	BE-930
DO NOT SCALE DRAWING			FINISH	ZS ZSBB	3
				PL 20 PER	3
					3

MEDIA BALL VALVE
 BE-930
 SIZE 3
 FINISH ZS ZSBB
 PL 20 PER



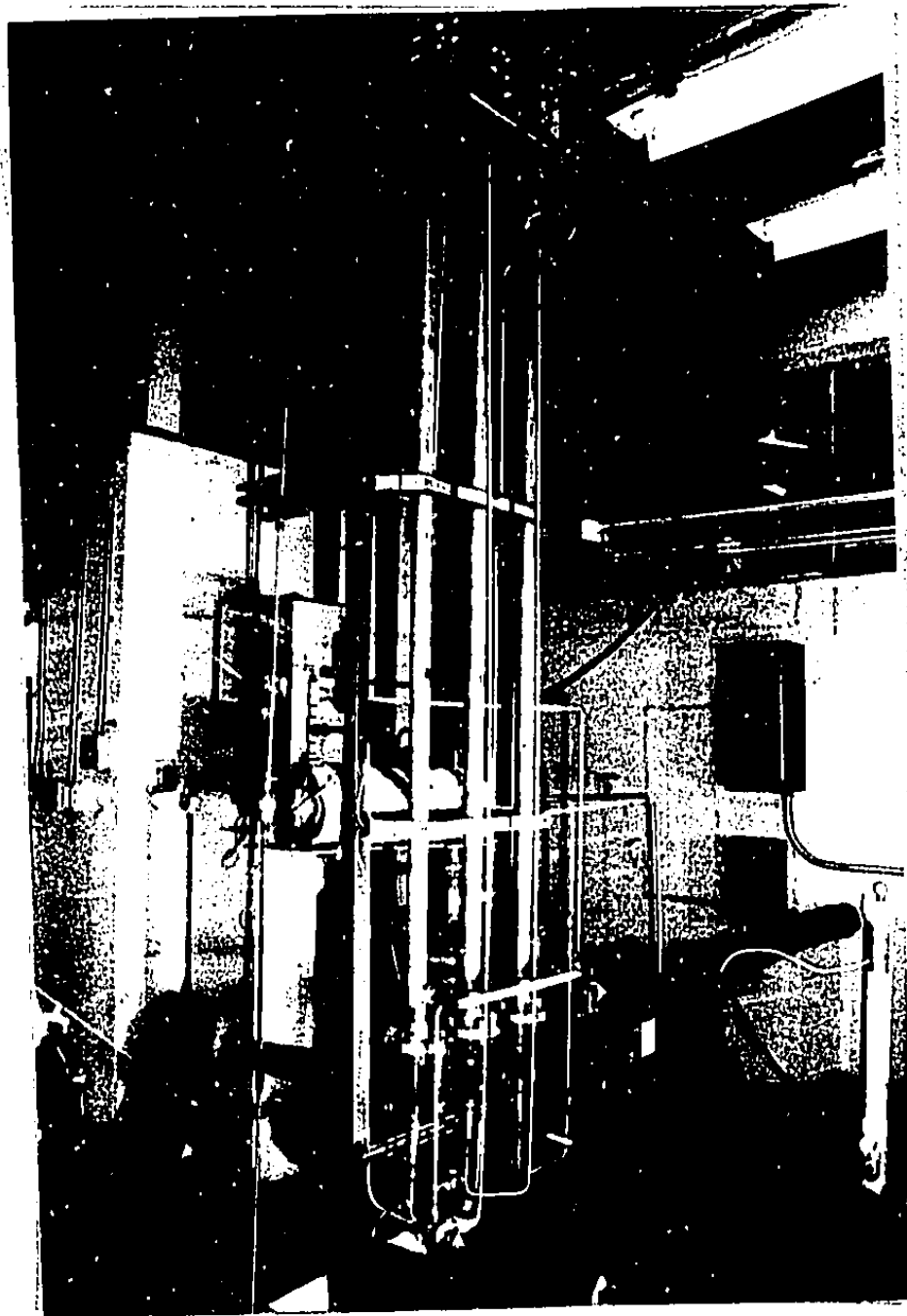


Figure 3-8. Fluidized-bed Heat Exchangers

BED MATERIALS

Table 3-2 lists the bed materials that we tested in the fluidized beds. The expansion of the fluidized bed is determined by seawater velocity in the tube, particle size and density. Appendix A summarizes the fluid-mechanics of liquid-fluidized beds. During the tests, the bed expanded to a height that was 2 to 6 times the height of the unexpanded bed.

Table 3-2. Bed Materials

<u>Material</u>	<u>Size</u>	<u>Specific Gravity</u>
Silica Glass Bead (Potters A-110)	.039-.047 in. dia.	2.8
Aluminum Oxide Bead (Coors Mini-Media)	.062 in. dia.	3.6
Zirconium Oxide Bead (Corning Glass)	.062 in. dia.	5.4
Cut-wire 304 Stain- less Steel Cylinders	.045 in. dia. x .060 in. long	7.8
Lead Shot #9	.075 in. dia.	11.4

TEST RESULTS

We ran four sets of tests, each with a different configuration of test heat-exchanger tubes. The first tests were baseline tests of bare-tube heat exchangers without any bed material. The seawater flowed through three of the tubes in series. In the second set of tests, we ran two tubes in series containing fluidized beds. The third set of tests were of a single-tube fluidized bed. The fourth set of tests used a two-stage arrangement. Two-tubes in series were heated by steam condensing at two-different temperatures.

The outlet temperature of the seawater, the bed material, and the bed expansion were varied during the tests. The seawater outlet temperature was controlled by adjustment of the heating-steam pressure.

During the tests we watched for scale formation in the sight glasses. After the tests we cut open the copper-nickel tubes to observe any scale that had formed. Ten identical copper-nickel tubes were run during the tests. Also, changes in the height of the fluidized bed indicated scale formation. The scale reduced the flow area of the tubes and increased the seawater velocity. The higher velocity expands the bed more and increases the bed height.

Table 3-3 is a list of the test runs.

Table 3-3. Seawater Heat Exchanger Test Runs

RUN	DURATION HRS	MAX SEAWATER TEMP °F	BED MATERIAL	EXPANSION	REMARKS	FILTER HRS
-----	-----------------	----------------------------	-----------------	-----------	---------	---------------

A. BARE TUBE TESTS: 3 IN SERIES

		<u>TUBE #1</u>	<u>TUBE #2</u>	<u>TUBE #3</u>	
1	8.5	260 /none	285/none	300 /none	All runs with seawater unless noted.
2	6.0	260	280	295	
3	7.7	270	295	305	
4	5.9	260	285	300	
5	2.3	260	285	300	
6	7.6	260	285	300	
7	8.1	260	285	300	
8	6.0	260	285	300	
9	4.6	260	280	300	
10	2.0	280	330	350	
	0.25	310	375	400	
11	0.5	300	360	385	Added Monel fittings.
12	5.0	320	380	410	Fresh water run.
13	4.0	285	330	340	"
14	2.0	-	-	200-400	"
15	6.5	295	330	350	
16	2.0	295	330	350	
17	-	80/Al ₂ O ₃	80/Al ₂ O ₃	80/Al ₂ O ₃	Al ₂ O ₃ beads in formerly bare tubes don't move freely because of scale, changed tubes.

21

Table 3-3 (continued)

RUN	DURATION HRS	MAX SEAWATER TEMP °F	BED MATERIAL	EXPANSION	REMARKS	FILTER HRS
B. TWO FLUIDIZED BEDS IN SERIES						
		<u>TUBE #4</u>	<u>TUBE #6</u>			
18	0.7	Al ₂ O ₃ /3X	210/Al ₂ O ₃ /3X		Fresh water run, check valves clogged so reduced size of check balls.	
19	2.0	"	350			
20	6.0	"	350		Clog in sight glass cleaned.	
21	4.5	"	350		Scale in sight glass.	
22	6.0	"	350		Flow required to fluidize is reduced.	
22	23	3.5	"	400		
C. SINGLE FLUIDIZED BED						
			<u>TUBE #6</u>			
24	1.5		400/Al ₂ O ₃ /3X		Outlet pipe clogged with scale, cleaned.	
25	1.5		"		Beads and scale clog sight glass and tube.	
26	1.5		"		Beads and scale clog sight glass and tube.	

Table 3-3 (continued)

RUN	DURATION HRS	MAX SEAWATER TEMP °F	BED MATERIAL	EXPANSION	REMARKS	FILTER HRS
27	2.0			<u>TUBE #5</u> 400/Al ₂ O ₃ /3X	#5 tube has unheated top section. Clog of beads and scale in tube.	
28	1.75			400/ZrO/3X	Clog of beads and scale in tube.	
29	2.75		<u>Tube #6</u> 400/ZrO/3X		Clogged. Two sight glasses at top of tube for this and subsequent tests.	
30	3.0		<u>TUBE #7</u> 350/ZrO/3X		Hard scale in lower sight glass (LSG), soft above.	
31	1.5	"	"	clogged		
32	1.25		340/ZrO/5X		Stable	
33	7.0	"	"		Stable but flow rate must be decreased to maintain bed height.	
34	7.0	"	"		Clog beginning, flow rate continues to decrease	

Table 3-3. (continued)

RUN	DURATION HRS	MAX SEAWATER TEMP OF	BED MATERIAL	EXPANSION	REMARKS	FILTER HRS
			<u>Tube #8</u>			
35	0.75		370/A110 glass/3X		Clog in upper sight glass (USG)	
36	1.5		350/lead/2X			
37	1.5		"		Clog in USG - stop, cleanout	
38	2.8		"		Clog developed in USG	
			<u>Tube #9</u>			
39	3.0		300/lead/2X			
40	7.5		300/lead/2X			
41	5.0		310/lead/2X			<u>Carbon Element</u> 5.0
42	6.0		320/lead/2X		Trace scale in tube.	5.0
43	7.0		330/Cut Wire/3X		Sight scale in LSG.	6.5
44	5.5		340/Cut Wire/3X		Heavy clog in lower 1/6 of tube, cleaned.	5.5
45	6.0		330/Cut Wire 4/X		Thin scale LSG.	2, hi Δ P

Table 3-3. (continued)

RUN	DURATION HRS	MAX SEAWATER TEMP OF	BED MATERIAL	EXPANSION	REMARKS	FILTER HRS
46	5.0	330/Cut Wire/4X				4.0
47	7.3	330/Cut Wire/4X				Cleaned filter. 4 layers of de- posits.

D. TWO-STAGE FLUIDIZED BED

25

		<u>Tube #9</u>	<u>Tube #10</u>		
48	2.0	330/Cut Wire/4X	340/Cut Wire/4X		2
49	8.0	"	"	Cleaned sight glasses and intermediate tube on hotter tube (#10)	8
50	6.7	"	345/Cut Wire/4X		6.7
51	6.0	"	"	6061T6 Test Cleaned sight glasses and intermediate tube,	6
52	6.0	"	"	316SS Test Cleaned sight glasses and intermediate tube,	5.5 back flush

Table 3-3 (continued)

RUN	DURATION HRS	MAX SEAWATER TEMP °F	BED MATERIAL	EXPANSION	REMARKS	FILTER HRS
53	4.0	330/Cut Wire/4X	345/Cut Wire/4X		6061T0 Test Cleaned clog in #10 upper sight glass and intermediate tube.	4
54	4.5	330/Cut Wire/4X	345/Cut Wire/4X		6061T0 Test Cleaned clog in #10 upper sight glass and intermediate tube.	New Carbon Element 4.5
55	5.5	330/Cut Wire/4X	345/Cut Wire/4X		HY-80 Test Cleaned scale from #10 upper sight glass and intermediate tube.	5.25
56	5.5	"	"		7075T73 Test Cleaned scale from #10 upper sight glass and intermediate tube.	5.2
57	5.5	"	"		Inconel 625 Test Cleaned scale from #10 upper sight glass and intermediate tube.	Monel Element 5
58	3.0	"	"		HY-80 & Inconel Test, Power failure, 1/2 hr boiling in tubes, cleared sight glasses and intermediate tube.	3
59	6.5	"	350/Cut Wire/4X		Cleaned as above, HY80 + Inconel Test , 7075T73 + Nickel Test.	6 Cleaned

Table 3-3 (continued)

RUN	DURATION HRS	MAX SEAWATER TEMP OF	BED MATERIAL	EXPANSION	REMARKS	FILTER HRS
60	5.0	330/Cut Wire/4X	350/Cut Wire/4X		Adiprene Test, cleaned clog in intermediate tube	4.5
61	6.0	"	"		Completed Adiprene tests, began AISI610 + TMT Test	4.0
62	6.0	"	"		Ti Test, cleaned scale from #10 USB and intermediate tube	Old Carbon Element
63	5.5	"	"		HY-100 + CM500 Test	5.5

Bare Tube Tests

In the first test series we ran the heat exchangers without any bed material. These tests allowed checkout of the system and provided a baseline for comparison to the fluidized bed tests. Seawater flowed through three tubes in a series (#1, #2, #3), Figure 3-9. The preheater heated the seawater to 220°F before the first tube. Steam inside the tube jackets condensed on the tubes providing heat to the seawater. We ran the tubes with a maximum seawater temperature of 300°F for 57 hours in a series of daily runs averaging six hours. Then we ran at higher temperatures up to 400°F for eleven hours. Special precautions were taken when stopping a run to avoid boiling the seawater in the tubes. First the steam flow was stopped and then the seawater flow was maintained until the seawater outlet temperature cooled to below 200°F.

After the runs we cut the tubes lengthwise to examine the scale. The first tube showed a dark scale, a combination of magnesium hydroxide and calcium sulphate, which increased in thickness from 0.0 at the bottom to 0.02 inches at the top. In the second tube, the scale color changed gradually to a white scale ~0.06 inch thick at the top. In the third tube the scale formed small crystal fingers about 0.07 inches thick which increased in length from the bottom to the top where they almost completely blocked the tube. Chemical analysis showed this scale was predominately calcium sulphate.

Two Fluidized-Bed Heat Exchangers in Series

Next we ran two-tubes in series (#4 and #6) with 1/16 inch diameter Al_2O_3 beads. The configuration was the same as Figure 3-9, but with two instead of three tubes. The fluidized bed breaks up the boundary layer next to the tube walls. This increases the transfer of heat from the tube wall to the seawater. Thus, two tubes provided enough heat transfer area to heat the seawater to 400°F. The tubes were filled with beads to give a 3x expansion of the bed at 0.3 gpm flow.

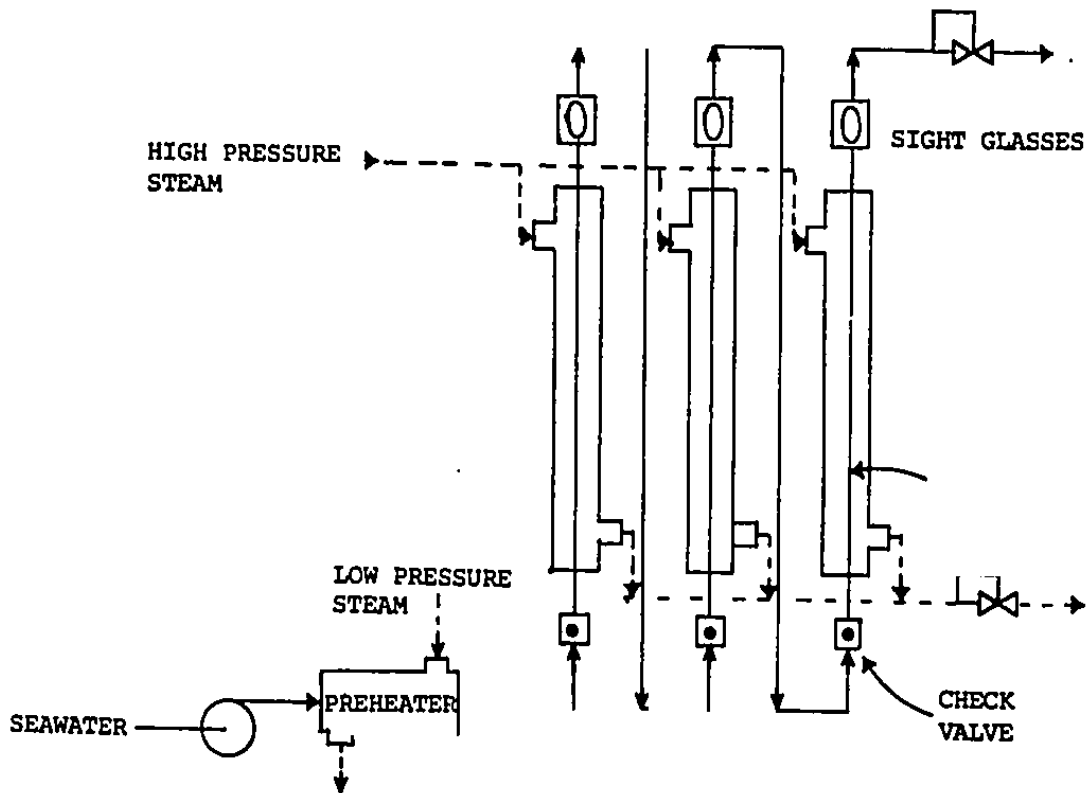


Figure 3-9. Three Tubes in Series (Bare Tube Tests)

The tubes ran with 350°F maximum seawater temperature for 18.5 hrs and for 3.5 hrs at 400°F. Clogs of beads and scale precipitate formed at the bottom inlet to the sight glasses which had to be cleaned about every four hours. Beads entered the enlarged flow area region in the sight glass where the bed expansion was locally reduced. The beads were stuck together by scale precipitates. Then the scale and bead plugs backed up into the tubes. Scale deposited on the sight glasses and in the tubes downstream of the fluidized beds. We next ran the hotter #6 tube by itself at 400°F for 4.5 hrs.

When sectioned, both tubes had a hard white scale averaging 0.07 inches thick. The #6 tube had regular plugs of scale about every two feet. This can be explained as follows. When the scaling started at a spot in the tube, the local water velocity increases and keeps beads away from the surface as shown in Figure 3-10. This creates an unstable condition and forms a local obstruction. These plugs impeded the movement of the beads so that solid cylinders of beads and scale formed inside the tubes.

Clearly, the scale and bead plug-up was not satisfactory for long term operation.

Tests with One Heat Exchanger

The next test series employed only one tube. With one tube, the heat transfer area was still sufficient to heat the seawater. And with one tube, the number of locations susceptible to plugging was reduced.

Also, to reduce the sight glass plugging, we increased the length of the unheated section of tube between the top of the steam jacket and the sight glass to 2 feet long (tube #5). In this manner, the top of the bed was kept below the sight glass. After two hours at 400°F, with Al_2O_3 particles at 3X expansion, the pressure drop through the tube increased from 8 to 195 psi due to a plug of beads

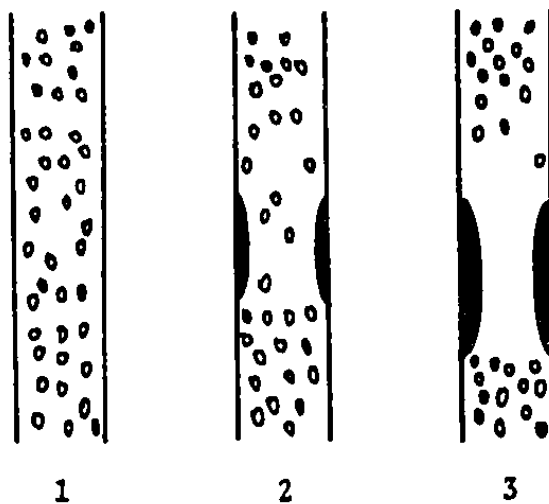


Figure 3-10. Plug Formation

and scale forming in the tube. Precipitate particles could be seen flowing through the sight glass during the test. After clearing the plug, we ran for 2 hours with ZrO (zirconium oxide) beads at 400°F. The pressure drop only increased to 40 psi, but the same plugging was occurring.

For the rest of the tests we ran at lower temperatures and mounted two sight glasses downstream of the tubes as shown in Figure 3-11. The first sight glass (lower one) had a glass tube inserted in the flow path. The glass tube had the same inside diameter as the test-heat-exchanger tubes. So, the flow area did not increase in the bottom sight glass and we could watch the bed action. We maintained the bed level in the lower sight glass to keep the particles away from the upper sight glass. The upper sight glass still functioned as a disengagement region for bed particles that traveled that high.

We ran tube #7 with ZrO beads at 3X expansion at 350°F maximum seawater temperature for 4.5 hours. The top of the bed was maintained in the lower sight glass by adjusting the flow. During the test the flow required to maintain the level decreased about 20% indicating that scale was building on the tube walls and reducing the flow area. A thin hard scale developed in the glass tube in the lower sight glass. This area was exposed to the top of the bed. Above this, the unheated section of tube had a 0.1 inch thick layer of softer scale. The tube was run for an additional 15 hours with ZrO beads at 5X expansion to see if the more active bead action would remove the scale or at least prevent additional buildup. After 15 hours the pressure drop across the tube increased to 20 psi indicating that the tube was clogging with scale. Cutting open the tube revealed a hard white scale over its entire length.

In a new tube (#8), smaller less-dense glass beads with a 4X expansion developed clogs in the sight glasses in one hour. Maximum seawater temperature was 370°F.

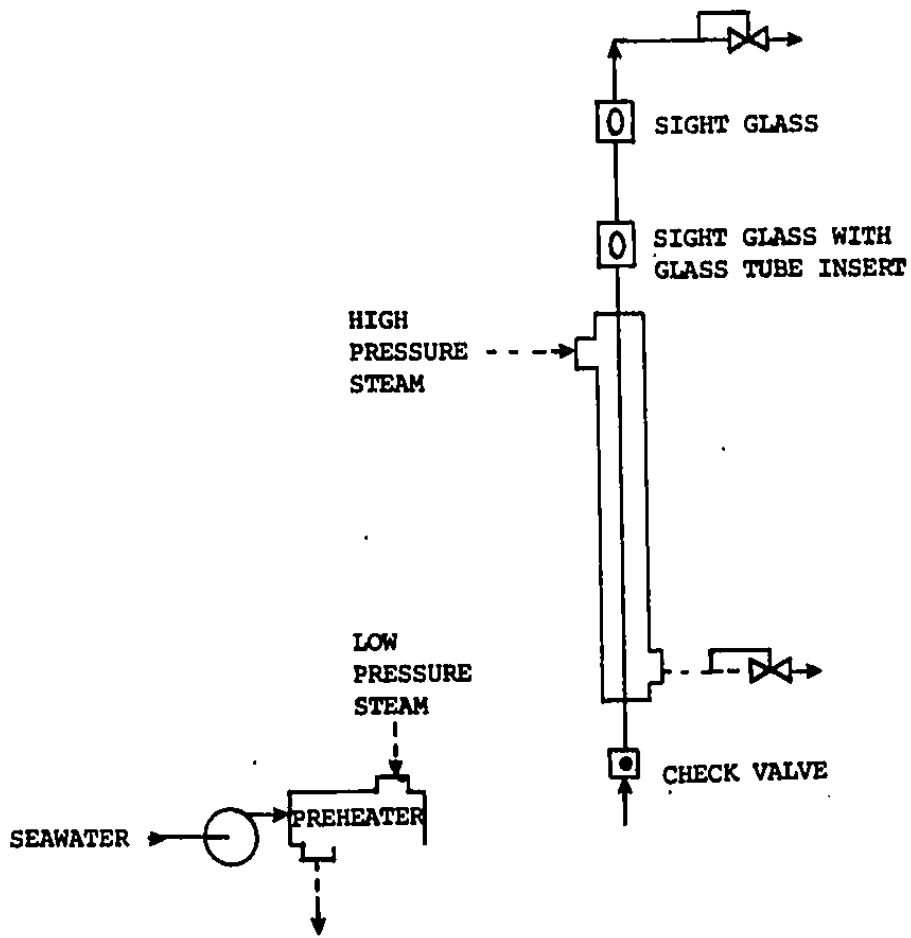


Figure 3-11. Fluidized Bed with Two Sight Glasses

We concluded that the ceramic materials were not dense enough to provide cleaning action in the bed at the temperature and heat rates we were testing.

Next we tested the lead shot and cut-wire stainless steel cylinders. The denser material scours the tube walls more effectively. However, the denser material requires a larger seawater velocity to fluidize the bed. The scale-forming dissolved solids flow increases as the seawater flow increases. The dissolved solids are a constant fraction of the seawater flow. Also, a higher heat flux at the tube wall is necessary to heat a higher flowrate to the same temperature. This increases the temperatures in the boundary layer along the tube wall.

Lead shot at 2X expansion and 350°F maximum seawater temperature (#8 tube) produced clogs after 2 hours of operation. A thin hard scale was observed over the entire length of tube #8.

Lead shot at 2X expansion in a new tube (#9) did not clog after 21.5 hours of operation at 300-320°F maximum seawater temperature. Only a trace of scale deposits appeared at the top of the heat exchanger tubes.

In the next tests in the same tube, cut-wire stainless steel cylinders ran at 3X expansion, 340°F maximum seawater temperature. After 12.5 hours, the bed material became stuck in the lower half of the heat exchanger. We cleaned out the cylinders, then ran the tube for 18 hours at 330°F with less bed material giving a 4X expansion. After 6 hours at the lower flowrate (still 330°F) only a very thin layer of scale formed on the glass tube in the lower sight glass. After 13 more hours, no clogging had occurred.

Thus, we concluded that 330°F was the limit for successful short term operation of the fluidized-bed seawater heat exchanger using the one-tube configuration. The high heat-flux rates at the higher temperatures and flows probably encouraged scale formation. Higher heat fluxes make the tube walls exposed to the seawater hotter. To determine if the seawater could be heated higher than 330°F, if the heat flux through the tube was kept low, we built a two-stage heat exchanger.

Two-Stage Fluidized Bed

In the two-stage configuration, Figure 3-12, the heating steam was a different pressure in each heat exchanger shell. In the first stage the 110 psig (344°F) steam heats the seawater to 330°F. In the second stage steam at up to 138 psig (360°F) heated the seawater up to 350°F. The preheater first heats the seawater to 220°F as in earlier tests. The heat flux at the highest seawater temperatures is lower for this configuration than for the case when only one exchanger heated the seawater to the top temperature.

Both stages ran with stainless steel cylinders at 4X expansion. We kept the lower-temperature first-stage (tube #9) at 330°F maximum seawater temperature. The second stage ran at 340 to 350°F maximum temperature. During 86 hours of running the first stage operated without additional scaling or clogging. Scale continually built up in the hot side intermediate tube and upper sight glass. But, clogging was eliminated if the scale was cleaned out about once every six hours. When cut open, the first stage tube (#9) showed a thin dark scale at bottom gradually changing to a thin white scale at its top. The second stage tube (#10) had a thicker .05 inch white scale over its whole length.

FILTERING SCALE PRECIPITATES

After flowing through the fluidized bed heat exchanger, the seawater contains scale particles. The particles are removed mechanically from the bed material and tube walls. Also, the scale particles precipitate from the supersaturated seawater and may continue to precipitate downstream of the fluidized bed.

Tests by Hatch and Weth (2) showed that when the seawater is heated above 370°F (in a recirculating loop) the scale particles formed a muddy slurry on filter elements. The slurry sloughed off of the elements so the filtering could potentially operate continuously.

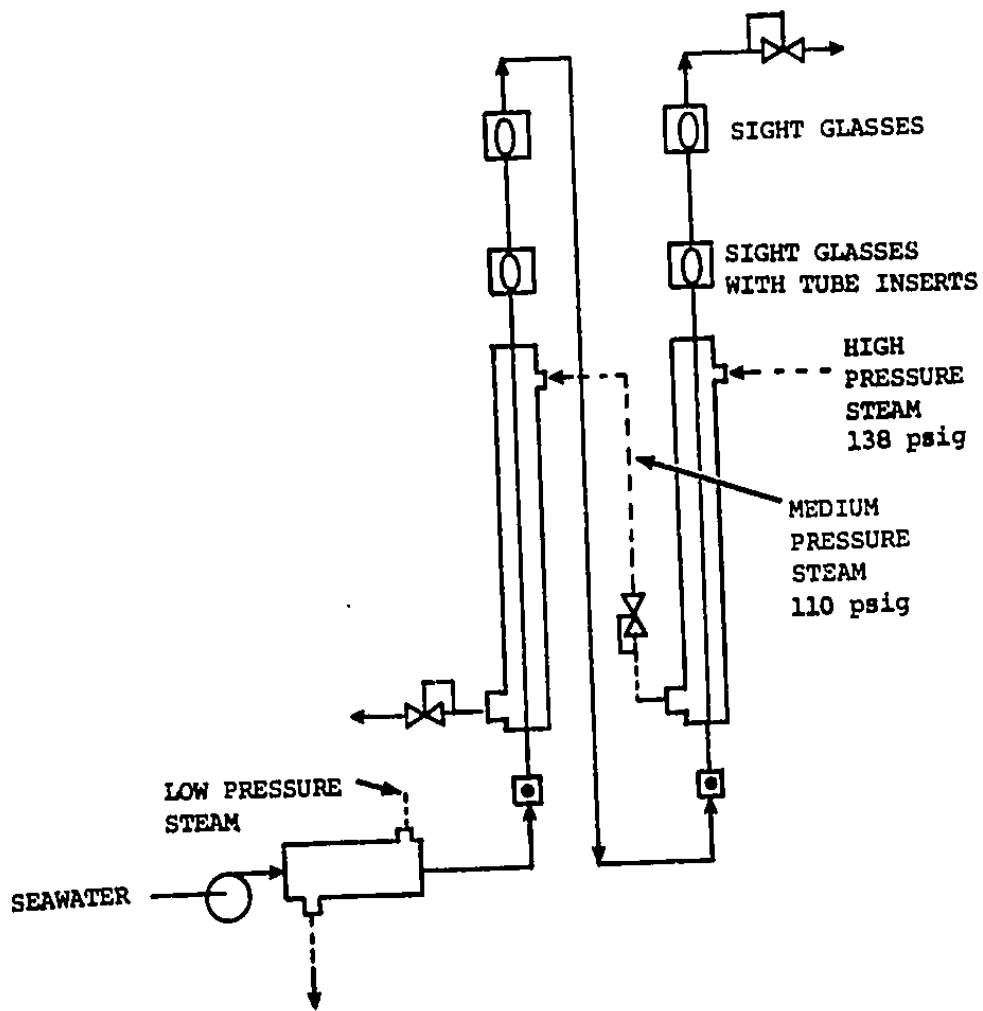


Figure 3-12 Two-Stage Fluidized Bed

We constructed a seawater filter shown in Figure 3-13 to filter seawater downstream of the fluidized beds. During runs of the fluidized bed at 330° - 350°F, hard white plaster-like scale formed on the filter during 3X bed-expansion. At 4X bed-expansion (higher flow and higher precipitate loading), the scale on the filter was softer but still adherent. The scale did not flow off the filter element in any of the filter tests. These tests occurred at a lower temperature and higher precipitate and particle load (per unit of flow) than in Hatch and Weth's tests.

CONCLUSIONS

1. Bare tubes (without bed material) scaled as expected at 260°F and even more at higher temperatures.
2. The fluidized bed dramatically improves the heat transfer rate between the tube wall and the seawater.
3. Ceramic bed materials are not as effective as the more dense metal particles in controlling scale on the tubes.
4. 330°F was the maximum temperature that the seawater can be heated to without scale forming in the fluidized bed during once through flow of the seawater.
5. Close attention must be paid to the bed geometry to provide a uniform flow throughout the bed. Lower flows in certain areas can lead to areas of unstable scale buildup.
6. For heating to temperatures higher than 330°F, a system that recirculates the seawater flow through the bed is required. Reducing the heat fluxes to the seawater (with a hot gas as the heating fluid instead of steam, for example) could reduce scaling tendency. Also, additives might reduce scaling.

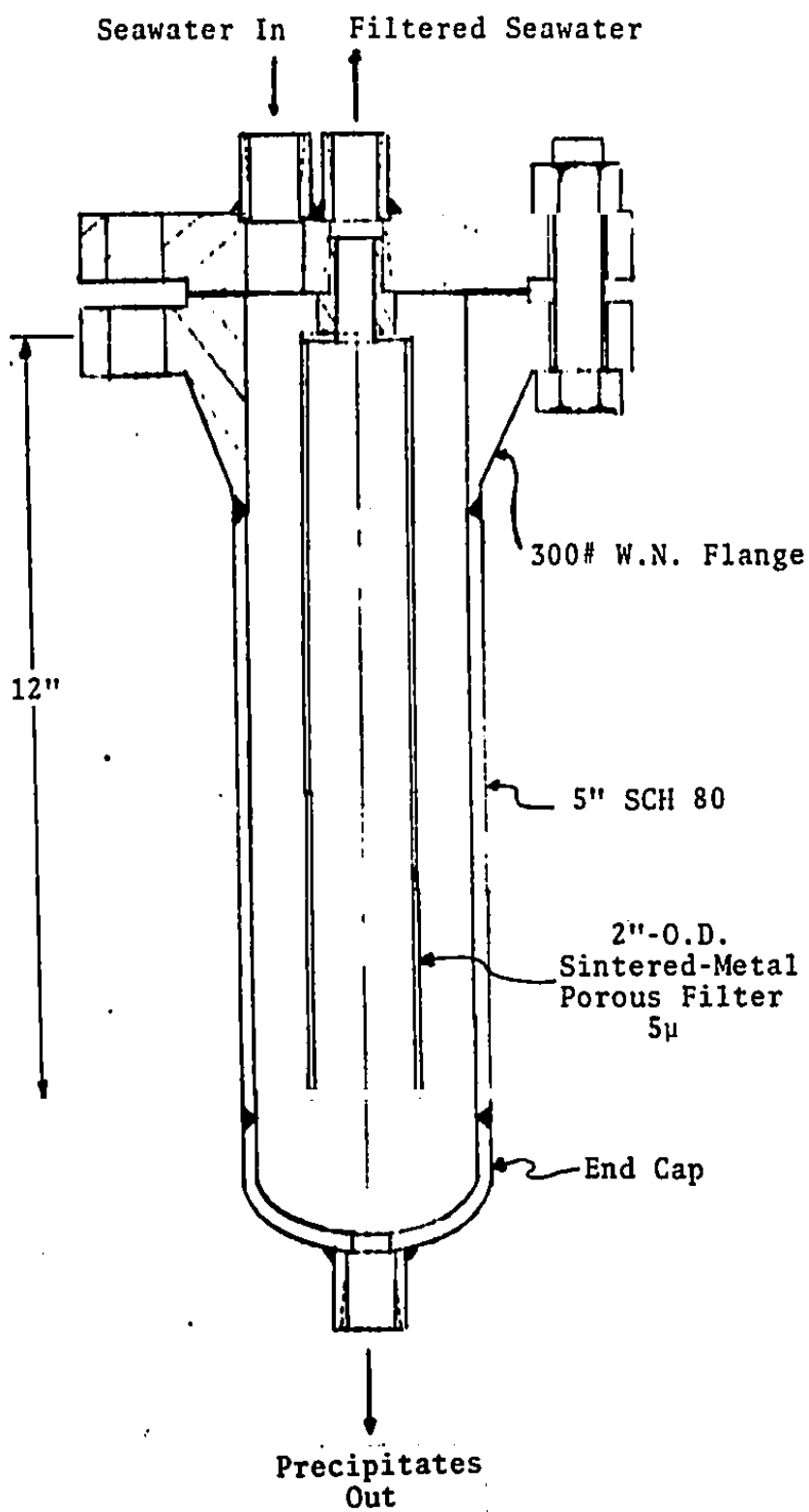


Figure 3-13. Precipitate-Removal Filter

4. CORROSION-EROSION TEST OF ROTOR MATERIALS

In the Biphase desalination-power system, a two-phase turbine expands hot seawater. In the turbine, a two-phase jet of seawater and steam flows from a nozzle on to the turbine rotor. A corrosion and erosion resistant rotor material is necessary for acceptable turbine life. The rotor material also experiences stresses due to rotational forces which limit the rotor speed.

We built an experiment to simulate the rotor-material environment where the two-phase jet impinges on the rotor. Twelve material-and-coating combinations were exposed to a two-phase jet in 4-hour screening tests.

OBJECTIVE

Identify rotor materials which can withstand the corrosion and erosion due to impingement of a high-velocity steam-and-salt-water jet.

TEST APPARATUS

Figure 4-1 shows the test apparatus. Hot seawater expanded through a small nozzle and impinged onto a material sample. The two-phase jet bulk velocity was 500 ± 50 ft/s, determined by measuring the nozzle thrust and flowrate. The jet impinged at a 30° angle to the face of the sample. A fixture held the sample and induced a tensile stress on the sample surface. A strain gage on the reverse (compression) side of the sample measured the stress. Figure 4-2 shows the sample and holder demensions. Figure 4-3 shows the details of the small two-phase steam-and-seawater nozzle. The housing around the sample maintained a steam environment at slightly above ambient pressure. A small stream of nitrogen flowed into the housing to eliminate air at the start and maintain a slight positive pressure.

RESULTS

Table 4-1 summarizes the composition of the samples, and the tests results. Each sample was exposed to the steam/seawater jet for four hours. Because of the limited time only qualitative results are possible. Additionally, the test probably does not show the effects of incubation time typical for cavitation-type erosion. The materials may begin to deteriorate rapidly after showing little deterioration for this incubation period.

Figure 4-4 is a photo of a 6061T6 aluminum sample after exposure to the two-phase jet. There is an elliptical impingement zone. The triangular area below the impingement zone is the area over which the flow traveled after hitting the sample. Figures 4-5 to 4-16 are enlarged photos (14X) of the impingement zones before and after the tests.

The bare aluminum samples 6061T0, 6061T6, and 7075T73 all experienced pitting in the impingement zone, an irregular scale buildup downstream, and general pitting on the rest of the sample.

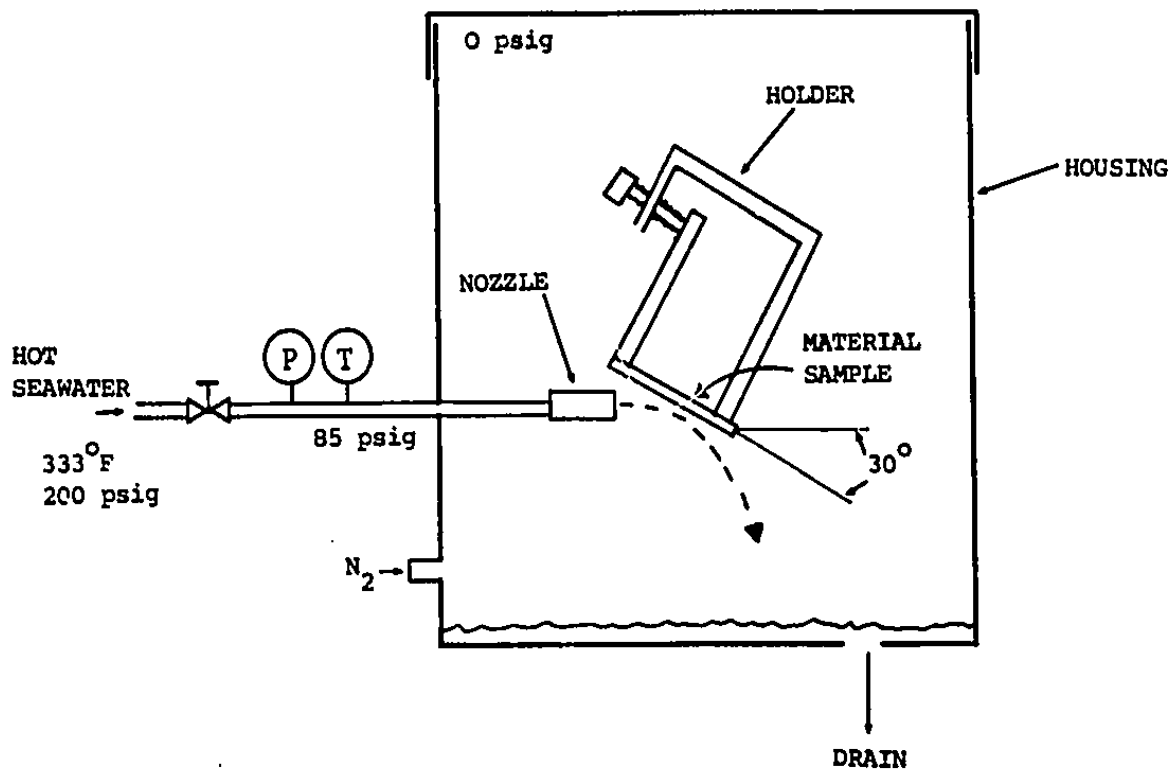
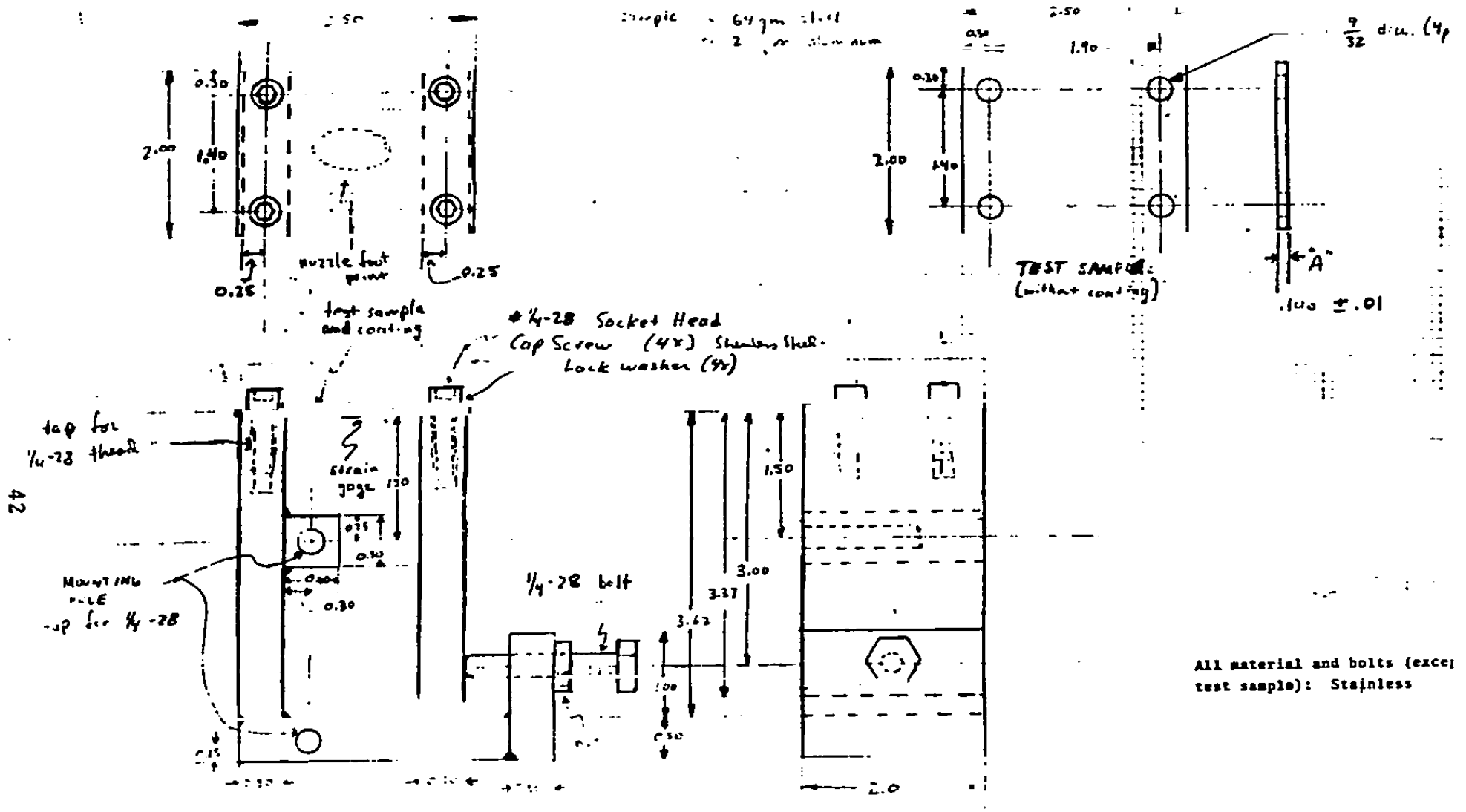


Figure 4-1. Corrosion/Erosion Impingement Test Apparatus



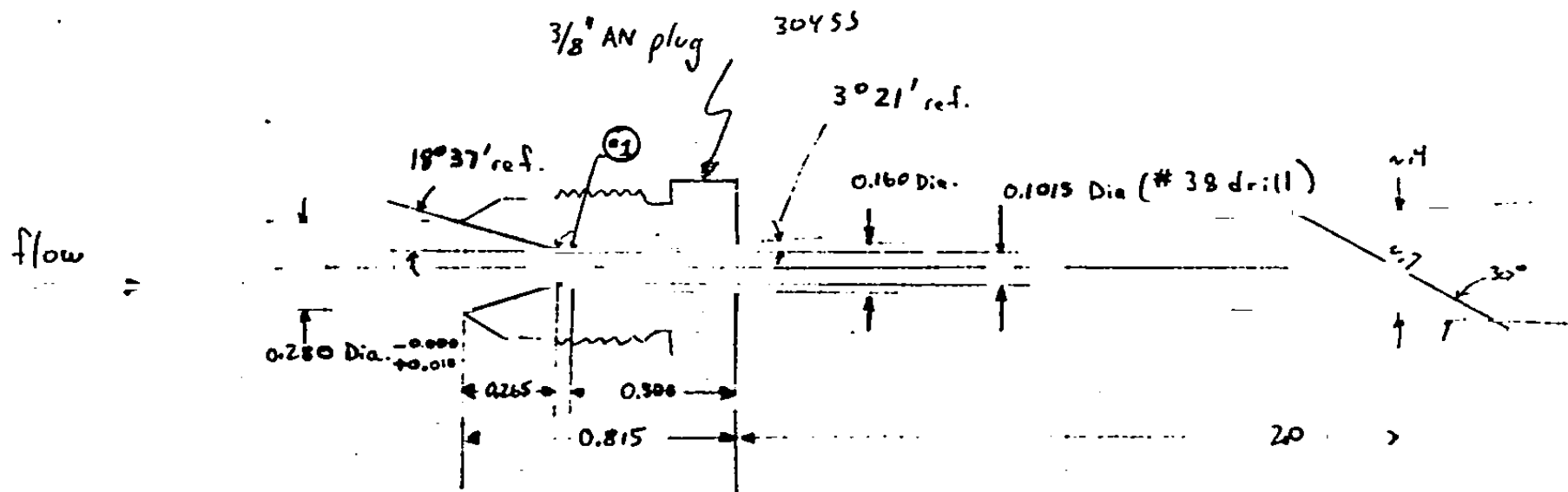
Reproduced from
best available copy. 

Figure 4-2. Impingement Test Sample Holder.

PLL 5-21-81

Rev. 1 5-22-81

Rev. 2 6-30-81



43

inlet : tube : $3/8" \times .049"$ wall

⊙1 : round off edges at throat

AR = 2.48

$L/D = 4.93$ (discharge)

inlet ~85 psig, 1% quality

outlet ~500 ft/s, 0.05 lbm/s

Scale : 2x

PLL 5-21-81

Figure 4-3. Miniature Nozzle for Impingement Test

Table 4-1. Impingement Test Results

BASE MATERIAL	COATING	BASE METAL PROPERTIES (212 F)			OBSERVATION	
		YIELD 10 ³ psi	MODULUS 10 ⁶ psi	DENSITY lb/in ³	PITTING	SCALE/DEPOSITS
		1. 6061T0	-	7.2	10.1	0.10
2. 6061T6	-	36	10.1	0.10	YES	YES
3. 7075T73	-	51	10.5	0.10	YES	YES
4. 7075T73	ELECTROLESS NICKEL	51	10.5	0.10	NO	NO
5. HY-80	-	80	29	0.29	NO	YES
6. HY-80	INCONEL FLAME SPRAY	80	29	0.29	NO	NO
7. HY-100	CM500	100	29	0.29	NO *	NO
8. AISI610	TMT VAPOR DEPOSIT	215	27	0.29	YES	NO
9. 316 STAINLESS STEEL	-	39	28	0.29	NO	NO
10. 316 STAINLESS STEEL	ADIPRENE	39	28	0.29	NO	NO
11. INCONEL 625	-	72	31	0.30	NO	NO
12. Ti-6Al-4Vn	-	122	14.9	0.16	NO	NO

* Surface Cracks in Impingement Zone.



Reproduced from
best available copy. 

Figure 4-4. Aluminum After Exposure

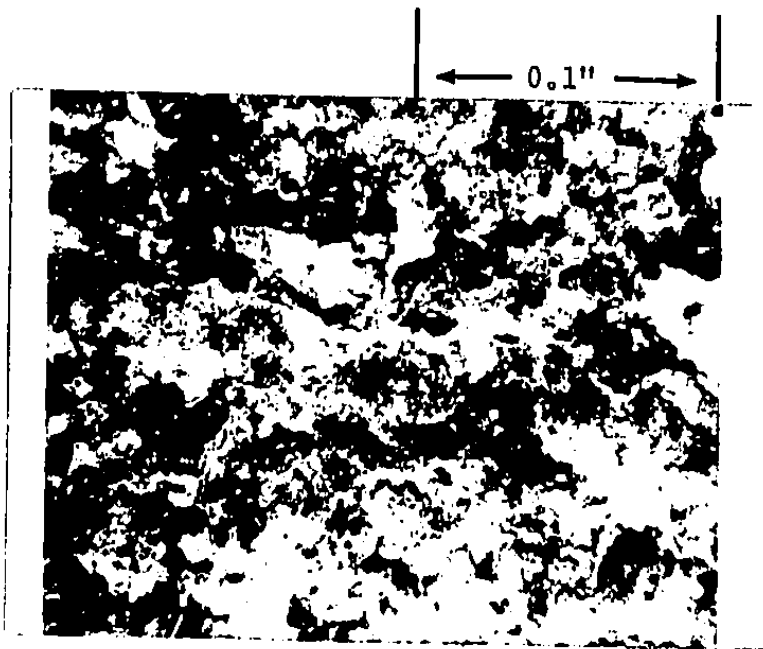


Figure 4-5. 6061T0 After Test

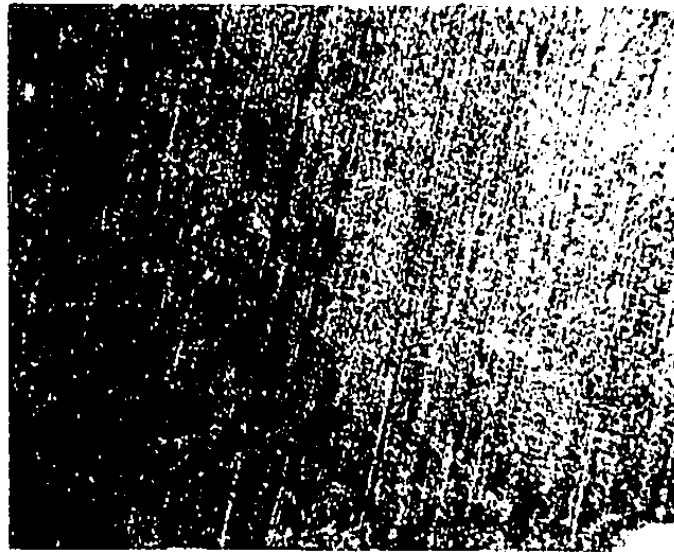


Figure 4-6a. 6061T6 Before Test

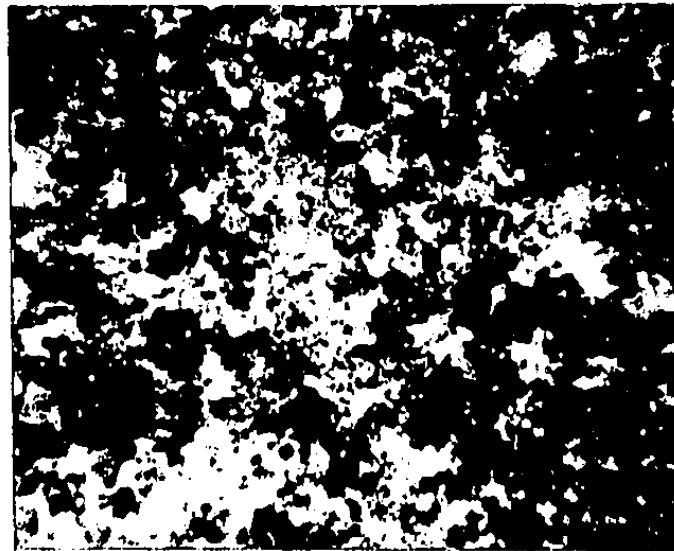


Figure 4-6b. 6061T6 After Test

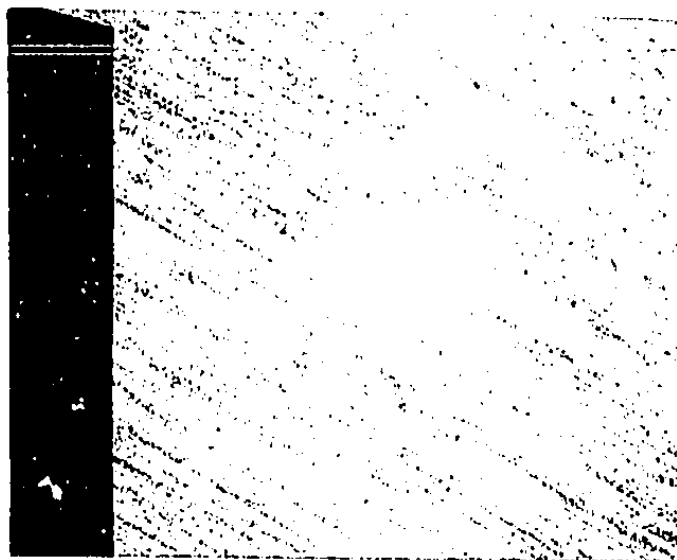


Figure 4-7a. 7075T73 Before Test

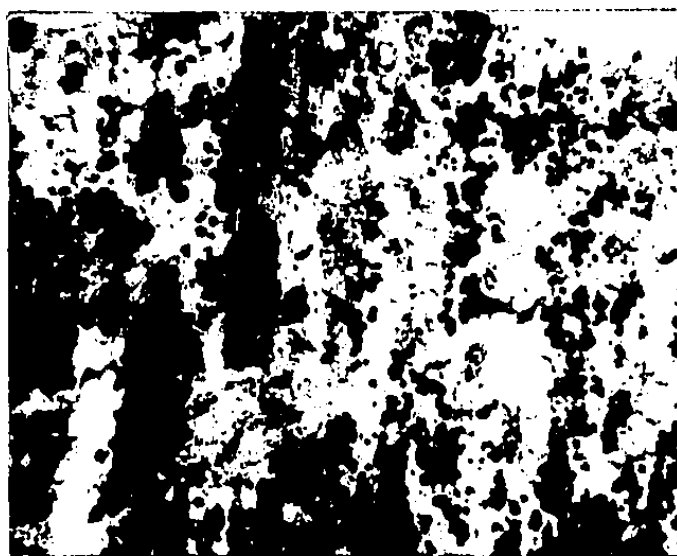


Figure 4-7b. 7075T73 After Test

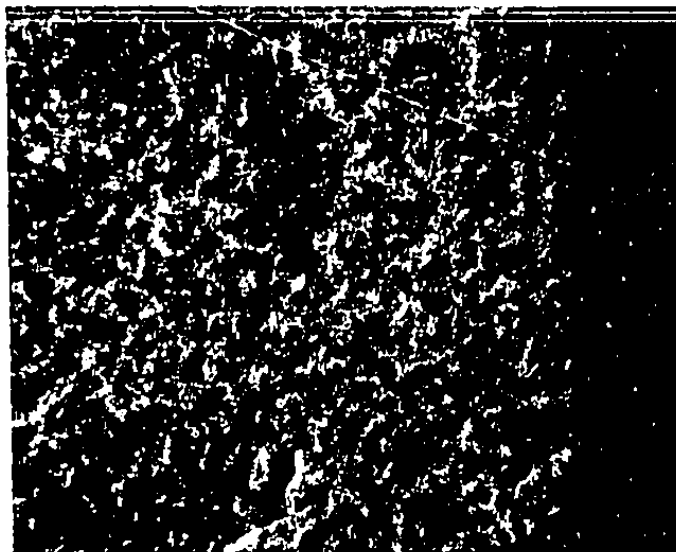


Figure 4-8a. 7075T73 With Electroless Nickel Coating, Before Test



Reproduced from
best available copy. 

Figure 4-8b. 7075T73 With Electroless Nickel Coating, After Test

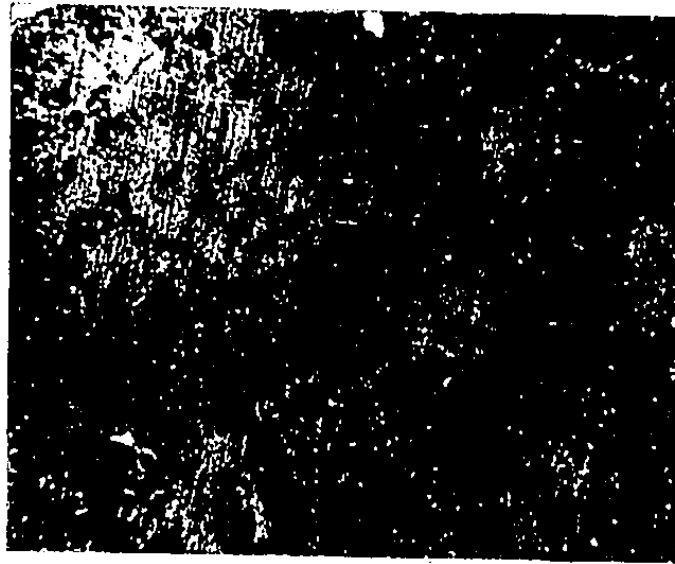


Figure 4-9. HY80 After Test

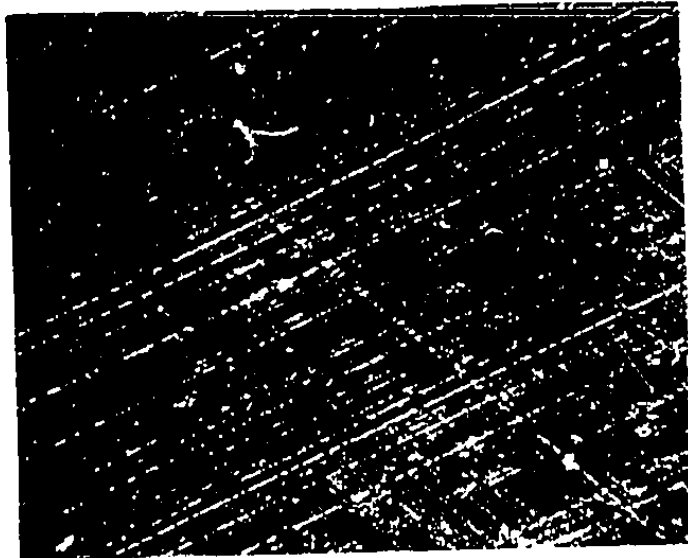


Figure 4-10a. HY80 With Inconel Flame Spray, Before Test



Figure 4-10b. HY80 With Inconel Flame Spray, After Test

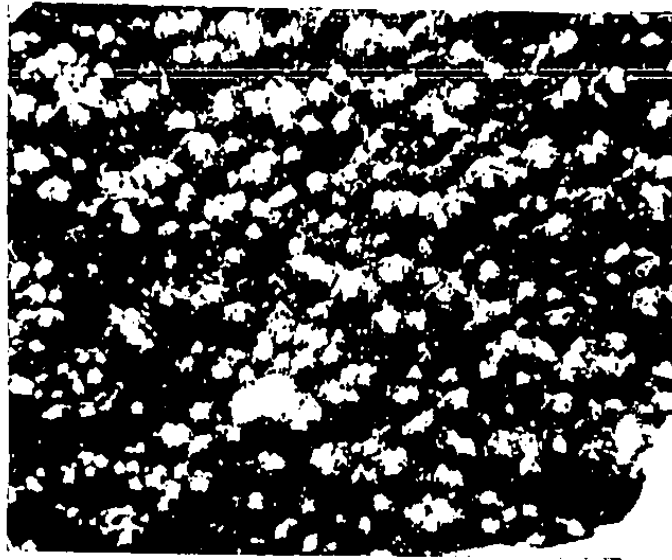


Figure 4-11a. HY100 With CM500 Coating,
Before Test

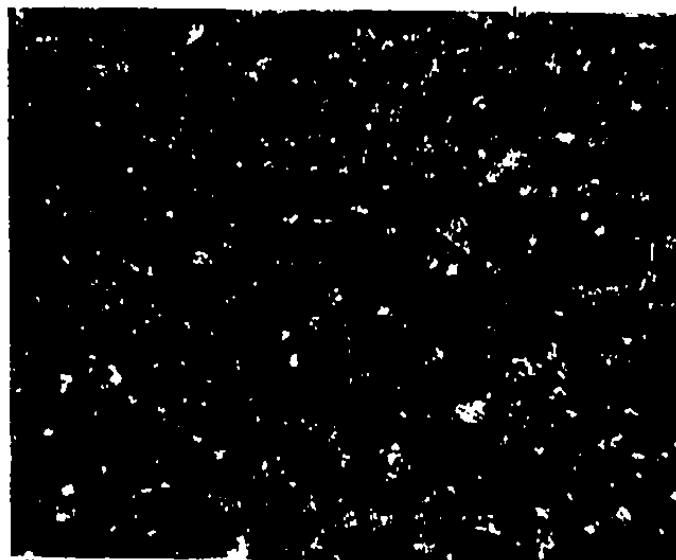


Figure 4-11b. HY100 With CM500 Coating,
After Test

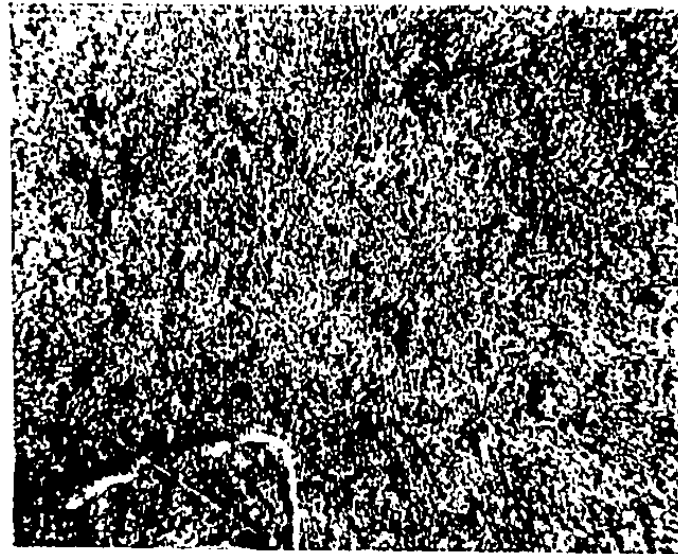


Figure 4-12a. AISI610 With TMT Coating,
Before Test



Figure 4-12b. AISI610 With TMT Coating,
After Test

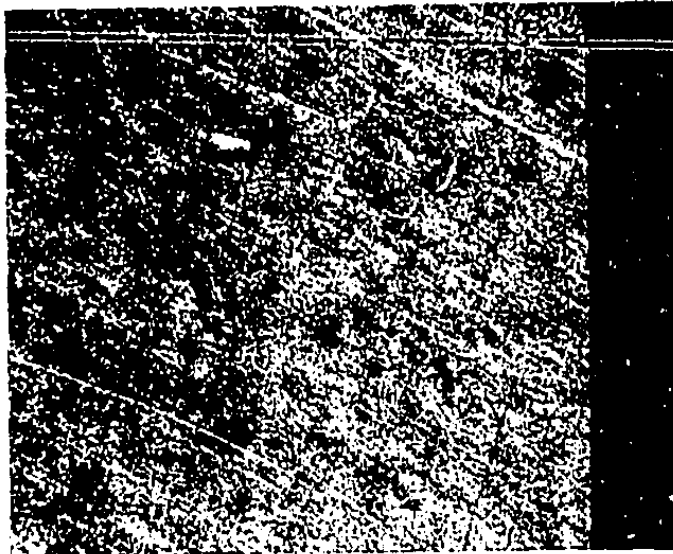
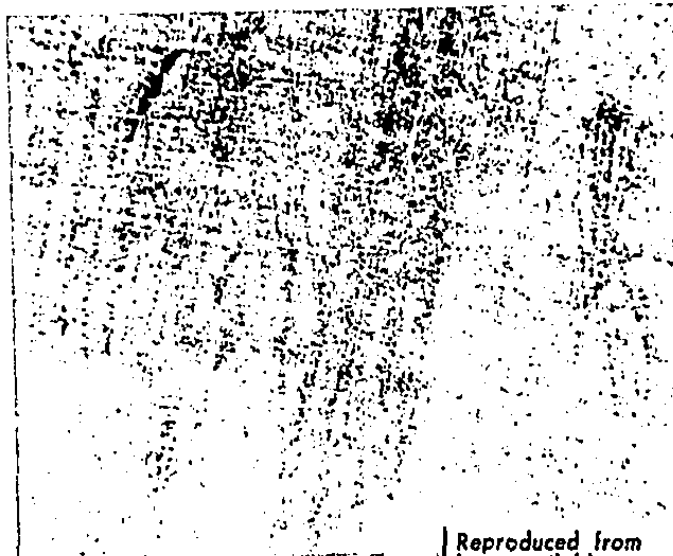


Figure 4-13a. 316 Stainless Steel,
Before Test



Reproduced from
best available copy. 

Figure 4-13b. 316 Stainless Steel,
After Test

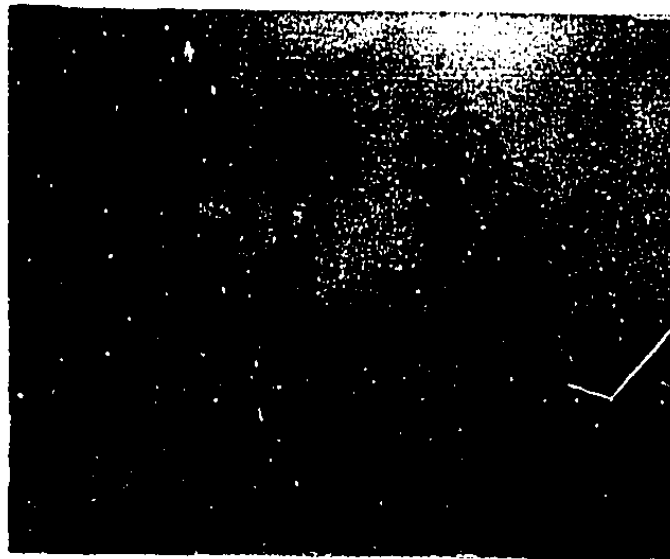


Figure 4-14a. Adiprene Coating on
316 Stainless Steel, Before Test



Figure 4-14b. Adiprene Coating on
316 Stainless Steel, After Test

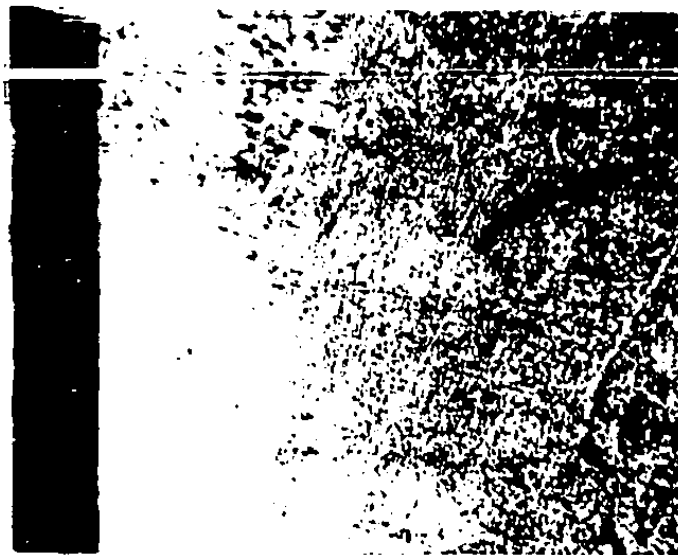


Figure 4-15a. Inconel 625, Before Test

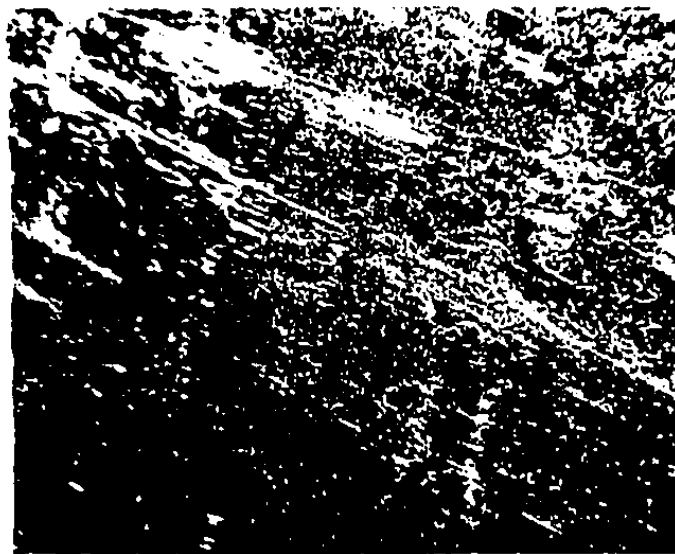


Figure 4-15b. Inconel 625, After Test

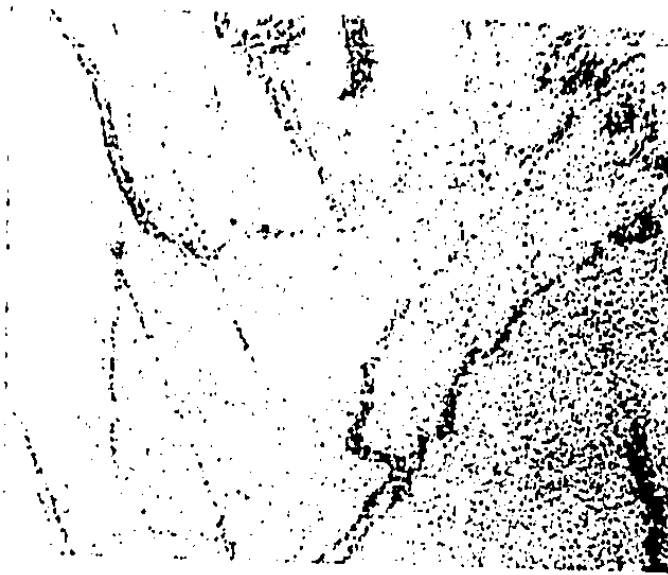


Figure 4-16a. Ti-6Al-4Vn, Before Test

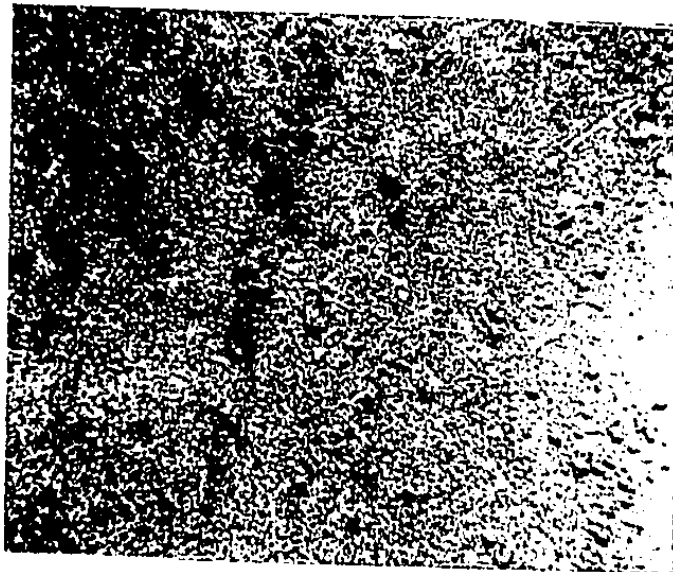


Figure 4-16b. Ti-6Al-4Vn, After Test

The 7075T73 aluminum with a 0.002 inch coating of electroless nickel showed no effects in the impingement zone. Around the impingement zone the surface turned a brown-orange color but the surface texture remained the same. Both 7075T73 samples were stressed to 42% of yield stress instead of 70%. This is the stress in a rotor made of 7075T73 that is rotating with a 900ft/s tip speed. For other materials (except AISI 610) the 70%-of-yield stress corresponds to a tip speed less than 900 ft/s.

HY-80 is proprietary high-strength, low-alloy steel produced by Lukens Steel Co., Coatesville, PA. The HY-80 sample showed orange deposits over the whole surface of the sample. The deposits were worn away in the impingement zone, exposing a smooth surface with no pits.

An HY-80 sample with an Inconel 625 flame-spray coating showed no effects of the jet impingement on the coating. The back side of uncoated HY-80 had the same orange deposits as the uncoated HY-80.

HY-100 is HY-80 with a different temper providing higher strength but not as good corrosion performance. An HY-100 sample was coated with CM-500, a very hard vapor-deposited tungsten-carbon material which is a proprietary product of San Fernando Laboratories. The CM-500 coating looks like shiny bumps about 0.01 inch across. After exposure to the jet, in the impingement zone, the bumps appeared laced with small cracks about 0.001 inch apart. A longer test is necessary to determine if the observed cracks will develop into pits.

A sample of AISI 610 (D4 tool steel) was coated with TMT vapor deposit, a proprietary coating applied by Turbine Metal Technology, Burbank, CA. The coating appeared to be worn away in the impingement zone with pits in the coating around the zone. The AISI 610 sample was stressed to 29% of yield stress instead of 70%.

Samples of 316 stainless steel, Inconel 625, Titanium (Ti-6Al-4Vn), and 316SS with a 0.2 inch thick Adiprene covering showed no effects from the jet impingement. Adiprene is a proprietary abrasion resistant urethane rubber made by DuPont.

The two-phase nozzle built up a thin layer of calcium sulphate during the course of testing.

CONCLUSIONS

All materials and coatings tested held up for 4-hour screening tests except the bare aluminums and the TMT coating on AISI 610. The CM-500 coating is suspicious due to the appearance of surface cracks. The materials which passed so far should be tested for longer periods to determine incubation time effects, and resistance to cavitation type erosion.

5. TURBINE PUMP UNIT FOR REVERSE OSMOSIS

The Biphase turbine can use the brine rejected by a reverse-osmosis plant as a working fluid. The turbine recovers pressure energy from the waste brine. If the brine is heated, the turbine can produce additional power from the input heat. Previous cycle studies (1) showed that the turbine can beneficially provide power for the reverse-osmosis high-pressure pumping.

DEVELOPMENT

Figure 5-1 shows the expected evolution of the application of the Biphase turbine to reverse-osmosis desalination. Currently available is a system combining a RO high-pressure pump, a Pelton wheel hydraulic turbine, an induction motor/generator and a Biphase waste-heat-recovery turbine. In this case the Biphase-turbine working fluid is fresh water circulating in a closed loop. The turbine converts waste-heat to shaft power. The motor-generator provides flexibility and control by either generating excess electricity or providing additional power to run the RO pump.

The first step in development is to improve the power recovery of the hydraulic turbine by using a Biphase reaction turbine. This turbine has the potential for both improved efficiency and simple integration with the two-phase-flow turbine. The next step combines both the hydraulic-power recovery and waste-heat recovery into one machine. Finally, the high pressure RO pump is added to the turbine. The result is one machine providing hydraulic-power recovery, RO pumping and power production from waste-heat sources. The intermediate machines are potentially valuable themselves, depending on the particular RO environment. The hydraulic turbine alone with pump and motor would be used where no waste-heat source is available.

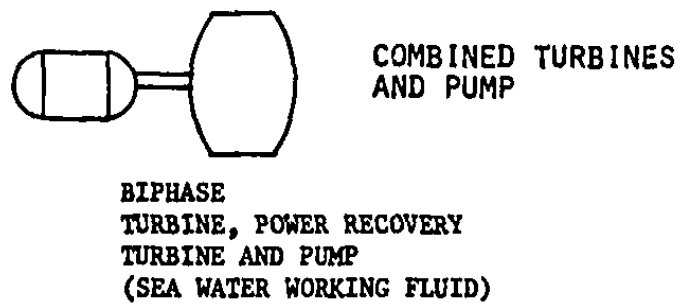
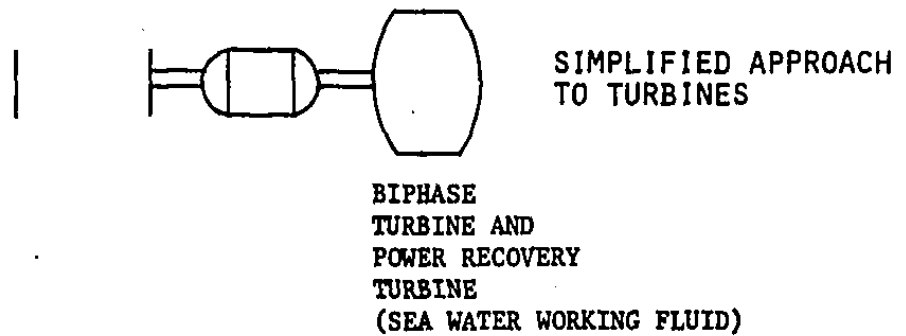
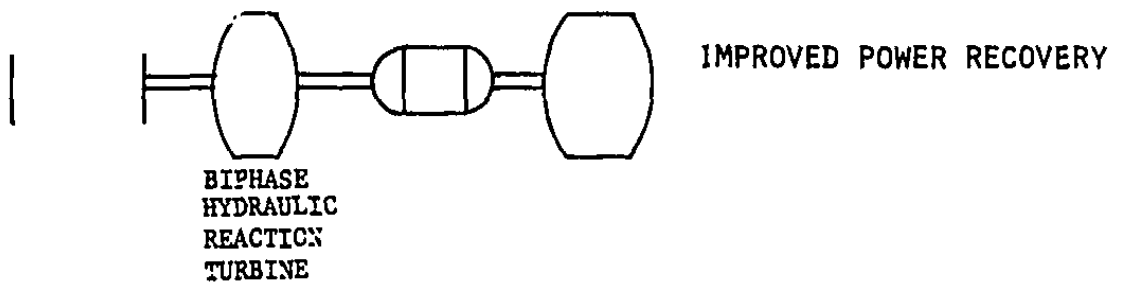
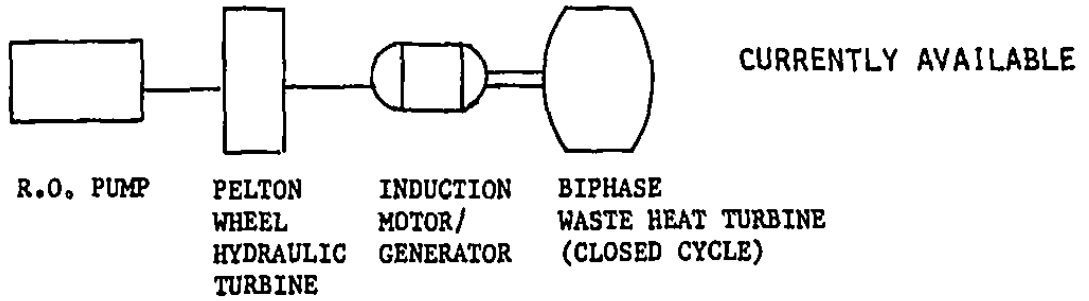


Figure 5-1. Biphase/RO Machinery Simplification

HYDRAULIC REACTION TURBINE

The reaction turbine concept has potential for high efficiency recovery of the RO reject-brine pressure energy. Also the mechanical configuration of the reaction turbine makes it easy to integrate in a single machine with two-phase-power production.

Figure 5-2 shows the reaction turbine concept. High-pressure fluid expands through an entry nozzle. This nozzle converts the pressure energy to kinetic energy. The jet of fluid with large kinetic energy enters a rotor whose speed at the point of entry is nearly the speed of the jet. The fluid then flows through passages in the rotor to a larger radius, where reaction nozzles expel the flow out of the rotor. The large centrifugal pressure gradient supplies the driving force. The velocity of the flow out of the reaction nozzles is in an opposite direction and almost as large (in magnitude) as the rotor speed at the reaction nozzles. So, the absolute velocity and hence, the kinetic energy of the flow leaving the rotor is low. The energy difference between the mass flow entering and leaving the rotor is the energy converted by the rotor to shaft power.

Appendix C describes the fluid mechanics of the reaction turbine operation. The overall turbine performance is derived from analysis of the losses in the turbine. The losses are specified as follows:

1. Inlet nozzle efficiency (nozzle-exit kinetic energy divided by isentropic energy drop through nozzle). Based on pipe friction data, 95% nozzle efficiency is reasonable.
2. Reaction nozzle velocity ratio (reaction-jet relative velocity divided by isentropic velocity). Again, based on pipe friction data, a velocity ratio of .975 is reasonable. This corresponds to a nozzle efficiency of 95%.
3. Angle of inlet jet relative to rotor inlet. This specifies losses in the transition of flow from the inlet nozzles to the rotor. The angle depends on how well the inlet nozzles

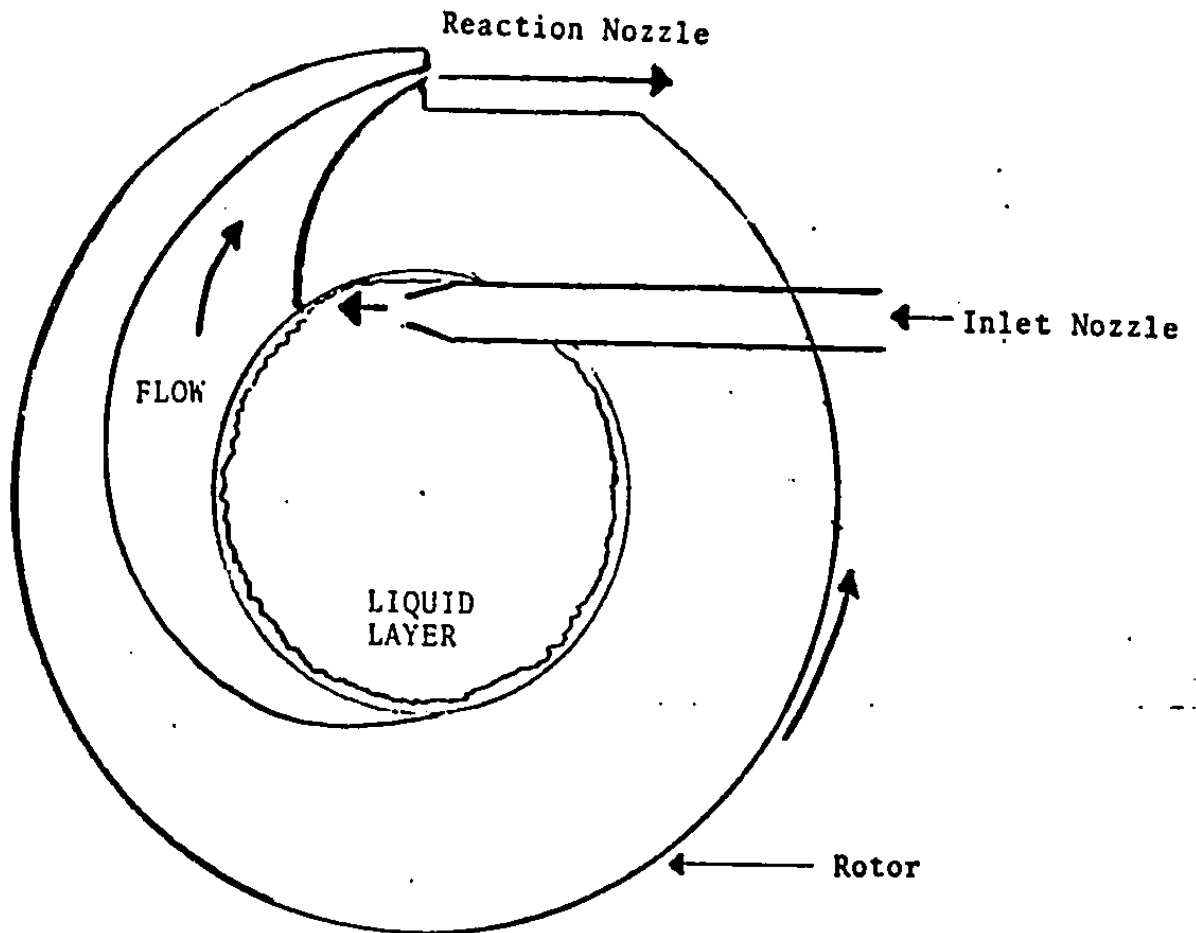


Figure 5-2. Reaction-Turbine Concept

are packaged around the rotor inlet. Increasing the rotor size, increasing the number of nozzles, or decreasing the flow and nozzle size gives a better (smaller) inlet angle. A 15° angle is reasonable which results in an efficiency of 93.3%.

4. Windage and bearing losses. These are a function of the rotor size and speed. A reasonable assumption is that these losses are 2% of the isentropic power available in the brine flow. The losses will probably be less than 2% for larger flows.

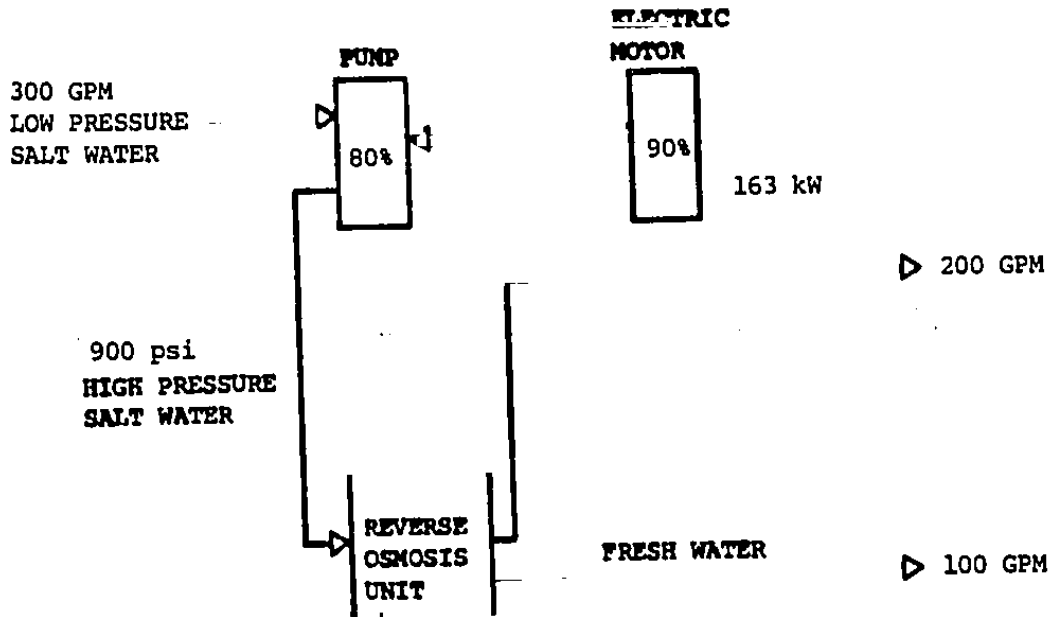
With these assumed losses, the turbine will have an efficiency of 70% (shaft power divided by isentropic power in brine flow) at the turbine design point.

Figure 5-3 shows that adding the hydraulic reaction turbine to a 100 gpm RO plant (seawater feed, 33% recovery) reduces the pumping power consumption by 35%. Assumed component efficiencies are marked on each component. The reaction turbine operates at about 10,000 rpm and so the turbine power includes an additional 1% loss for a speed reducing connection. Table 5-1 summarizes the turbine specifications for this system.

The nozzle sizes and rotor speed set the design point of the turbine. Efficiency can be kept at the design point level by adjusting the turbine speed for changes in the inlet pressure. If the speed and inlet pressure are not adjusted together, the efficiency drops. For example, with speed constant, efficiency drops 78% when inlet pressure drops 35% from the design point level. Increases in inlet pressure at constant speed do not penalize turbine efficiency as much. A 30% increase in pressure decreases efficiency by 7%. Reverse-osmosis systems run at a nearly fixed condition. The reject brine pressure may increase slightly in time as the RO membranes age and become dirty. Active control of the turbine speed (after tuning to the system) is not necessary.

A 200 gpm turbine would have an 11-inch diameter rotor. The size is a compromise between lower-inlet-nozzle angle losses in larger turbines and lower windage and lower costs for smaller turbines. The optimum size is about the same for 5 to 200 hp turbines.

a) 100 GPM RO SYSTEM



b) 100 GPM RO SYSTEM WITH HYDRAULIC REACTION TURBINE

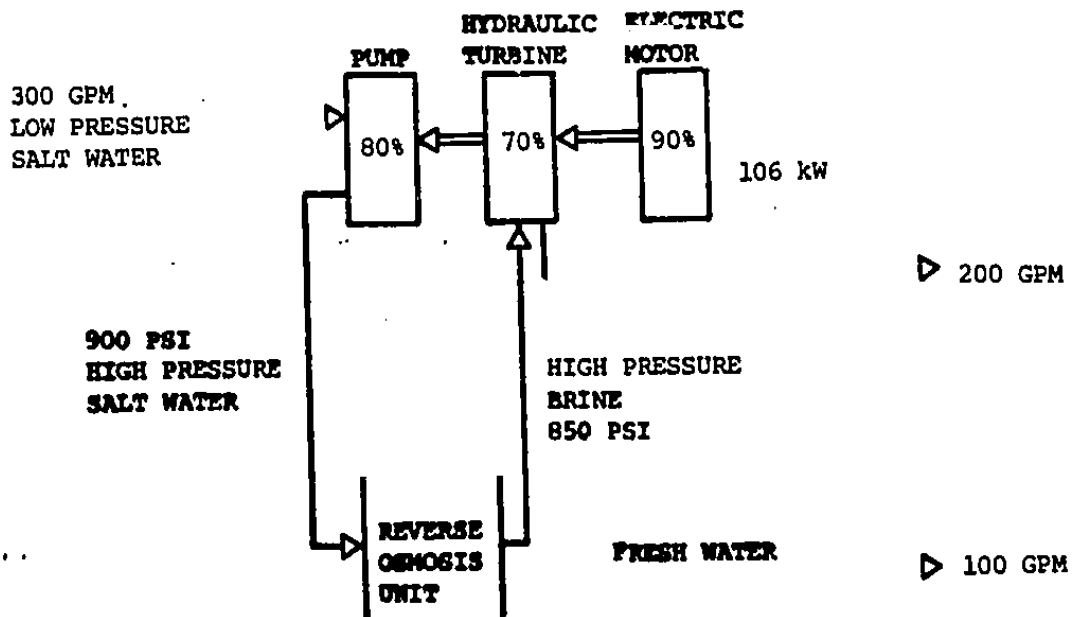


Figure 5-3. Baseline RO Cycles - Seawater Feed

Table 5-1. Turbine Specifications

Inlet Pressure	850 psig
Flow (concentrated seawater)	200 gpm
Rotor Diameter at Reaction Jets	11 inch
Rotor Inner Diameter	6.65 inch
Rotor Speed	9300 rpm
Shaft Power Output	69 hp

Figure 5-3 shows how a 69 hp, 200 gpm turbine would save 57 kW in a RO system. If these units sold for \$12,000 each, simple payback period for the user is 0.55 yr. This assumes electricity cost of \$0.05/kW-hr and a 90% on-line factor.

TWO PHASE TURBINE

The two-phase version of the Biphase turbine can generate additional shaft-power for RO pumping. A heat source heats the reject brine which then expands through a two-phase turbine. The turbine recovers the hydraulic power in the brine and produces additional power from the heat source. Figure 5-4 is a schematic of a combined reverse-osmosis and two-phase turbine system. This system is used when a source of waste-heat is available. The 330°F maximum temperature of the waste brine is based on our seawater fluidized bed heat exchanger experiments. The overall performance ratio for this desalination system is 5.6 pounds of fresh-water output per 1000 Btu of heat input.

COMBINATION OF HIGH PRESSURE PUMP AND TURBINE

The high-pressure pump and Biphase turbine shown in Figure 5-4 have the potential of being combined in a single machine. This machine provides the pumping power, the pump, and pressure recovery device. Figure 5-5 shows one concept for this machine's design. Heated high-pressure brine enters the housing through nozzles on the right side of section A-A. The high velocity flow from the nozzles enters a Biphase reaction-turbine rotor, leaving the rotor through reaction nozzles. The brine flow provides power to the rotor which is absorbed by a Pitot-type seawater pump attached to the back side of the rotor.

The liquid is introduced on to the pumping side of the machine rotor (four different schemes for introducing liquid have been considered and are described below). A pitot diffuser then converts

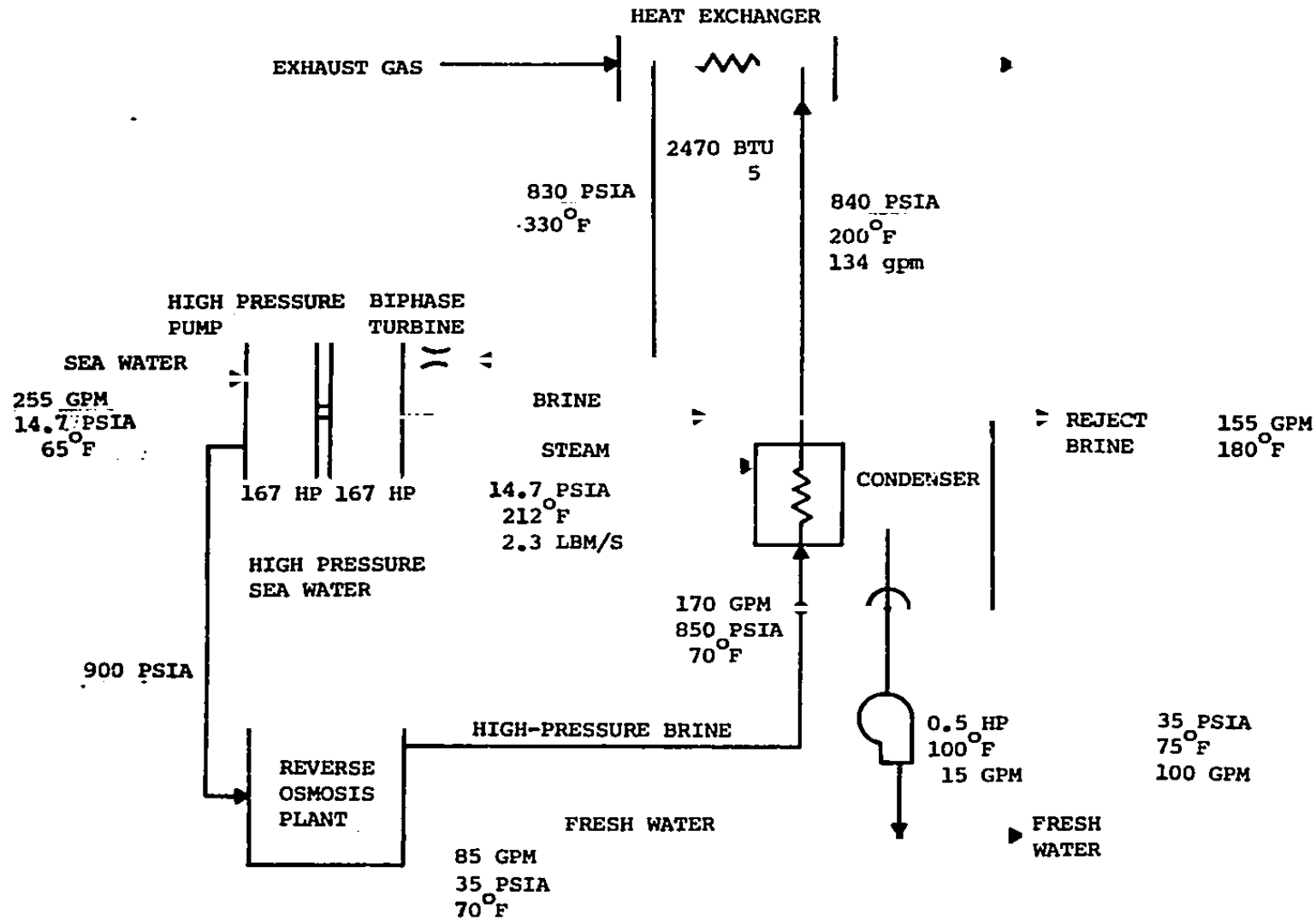


Figure 5-A. Biphase/Reverse Osmosis System with Reject Brine Working Fluid, Maximum Seawater Temperature 330°F, 50-Inch-Diameter Turbine

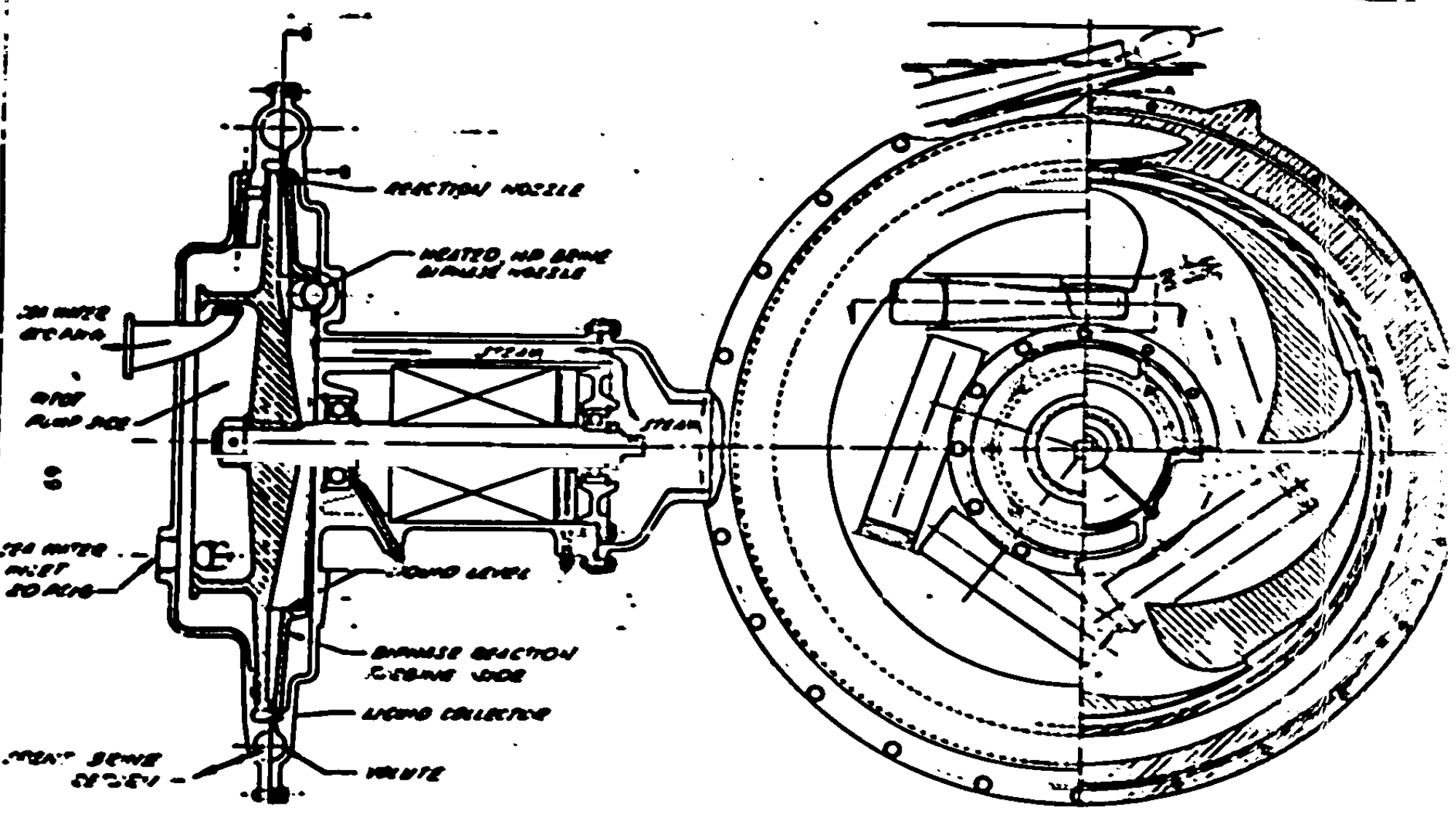
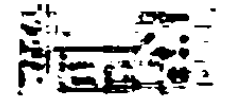


Figure 5-5. Biphase Turbine/Pump/Energy Recovery Unit for Reverse Osmosis Application



the kinetic energy to pressure in the liquid. To get 850 psi required for seawater RO with an 85% pitot diffuser, the liquid must be accelerated to 325 ft/sec. The efficiency of acceleration and efficiency of the pitot diffuser are central to the pump performance.

Figure 5-6 illustrates the four methods of introducing liquid onto the rotor for pumping purposes.

In method 1 in Figure 5-6, liquid contacts the rotor disk near its center and accelerates to the outer radius in the manner of an open unshrouded rotating-cup atomizer. Critical for efficiency is the amount of slip of the fluid in the tangential direction on rotor. Fraser et al (9) give the following condition for nearly slip-free operation.

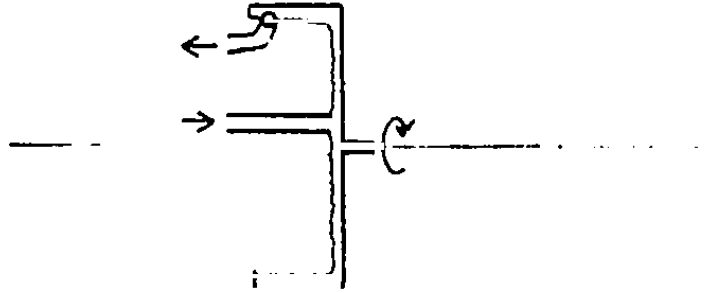
$$\bar{\theta} = \frac{\dot{m}}{n\pi D} < 596.1 \quad (1)$$

where \dot{m} = flow rate (kg/sec)
 n = viscosity (kg/ms)
 D = diameter (m).

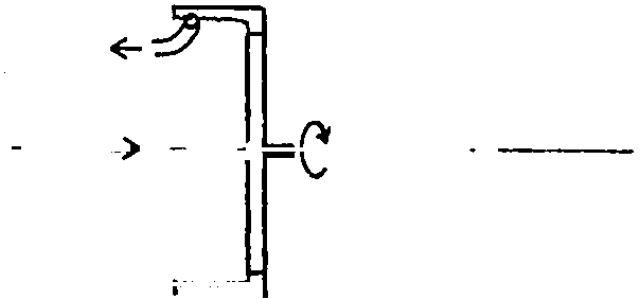
Using a flow of 200 gpm, a water viscosity of 10.3 kg/m·s and a disk diameter of 11 inches yields a value of 14,450 for $\bar{\theta}$, which is 24.2 times larger than the above limit. Hence, slip will be substantial.

The radial velocity of the fluid, as it leaves the face of the rotor and encounters the rim, is also given by Fraser's equations for no-tangential-slip conditions. This gives a lower limit for the radial velocity, which represents kinetic energy which is dissipated at the rim. With a slip-free assumption, the efficiency of fluid acceleration (rate of change of useful kinetic energy in the fluid divided by the power input to the rotor) is only about 27% for typical RO conditions. This is too low for a practical machine.

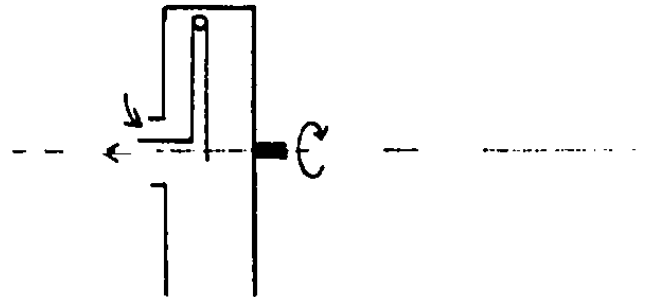
1. OPEN ROTOR



2. OPEN ROTOR WITH SHROUDS
(with and without blades)



3. CLOSED ROTOR



4. 2-SPOOL

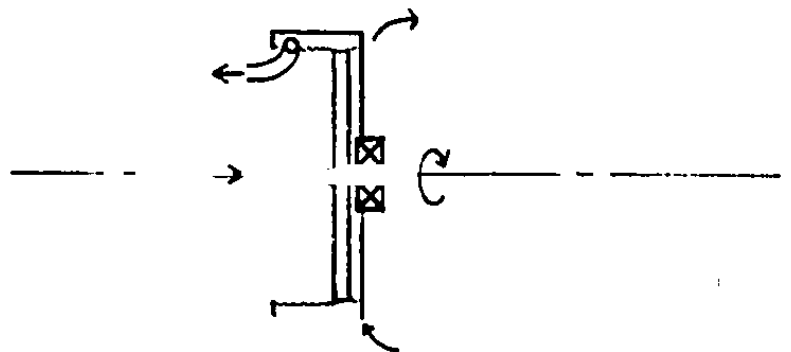


Figure 5-6 Pumping Methods

Method 2 includes shrouded or unshrouded blades attached to the rotor. Even if shrouded, the pressure at both the inlet and outlet of the blades is the housing pressure. A strongly forward-curved blade gives a fluid acceleration efficiency of over 90% for this condition of no-pressure-rise through the blading. However, the efficiency must be multiplied by a low pitot diffuser efficiency (described below) to estimate overall pump efficiency.

Method 3 uses a closed rotor so that a pressure rise can occur between the rotor center and outer rim. The flow then enters a stationary pitot pick-up where the flow diffuses to a higher pressure at the outlet. This is the configuration of commercial rotor-pitot pumps manufactured by Kobe. Overall pump efficiencies of up to 60% are available for typical RO conditions. This is on the threshold of being competitive with other commercially available RO pumps.

Method 4 is a two-spooled geometry, the inner impeller rotates at 1/2 the speed of the center rim. The inner impeller contains strongly forward-curved blades and accelerates the liquid to the same tangential speed as the outer rim. The efficiency of this acceleration can be better than 90% including windage effects.

The controlling factor, then, is the diffuser efficiency. The pitot-scoop diffuser has a potentially higher efficiency because there is zero boundary-layer thickness at the diffuser inlet. However, the diffuser for a seawater RO pressure requirement of over 800 psi has an area ratio of over five and needs a curvature of about 60 degrees. We project a diffuser efficiency of about 53%, on the basis of the diffuser performance data of Eck (10). So overall pump efficiency is also low. This concept may be viable for lower pressure applications, which would employ a lower-area-ratio diffuser.

In the selection of a pumping method, pumps that are integral with the rest of the Biphase turbine give simple equipment. But they must compete on efficiency with pumps that are externally connected to the turbine. So far a competitive pumping method with an integral rotor has not been found.

CONCLUSIONS

1. The Biphase hydraulic reactor turbine can recover the power in the reject brine from a reverse osmosis system with an efficiency of over 70%. The turbine would reduce the pumping power required by the RO plant by 35%.
2. A two phase version of the Biphase turbine can be combined into a reverse osmosis plant to utilize waste-heat energy sources. The system generates 5.6 pounds of fresh water per 1000 Btu of heat input.
3. The combination of the high-pressure reverse-osmosis pump and the power-recovery turbine in the same housing would provide a simple machine. But the combination is not as efficient as using a separate pump and turbine that are coupled together.

6. DESALINATION/POWER CYCLE APPLICATION

The Biphase desalination/power cycle, by itself (not in combination with other water systems) can generate power and fresh water from waste heat sources and salt water. The waste-heat source heats the salt water. The hot salt water expands through the two-phase turbine to generate power. The turbine also separates clean steam which condenses to provide fresh water.

In this section we present a conceptual design for a specific site, San Nicolas Island. Our objective was to determine the system configuration, interfaces with heat sources, and system costs and benefits for a typical installation.

SAN NICOLAS ISLAND

San Nicolas Island, off the coast of California, is a Navy base with about 300 residents. The base supports electronic equipment for the Pacific Missile Test Range. Electricity on the island is generated by diesel-generator sets which are a source of exhaust-gas waste heat. Average power production is about 750 kW.

The San Nicolas power plant is indoors and readily accessible. Figure 6-1 is a rough sketch of the plant layout. Figure 6-2 is a photograph of the plant and the adjacent storage tank for the island's fresh water.

Control of the engines is mostly manual. The operator starts each engine with an air motor controlled by a switch next to the engine. Frequency and generator excitation are controlled manually in the

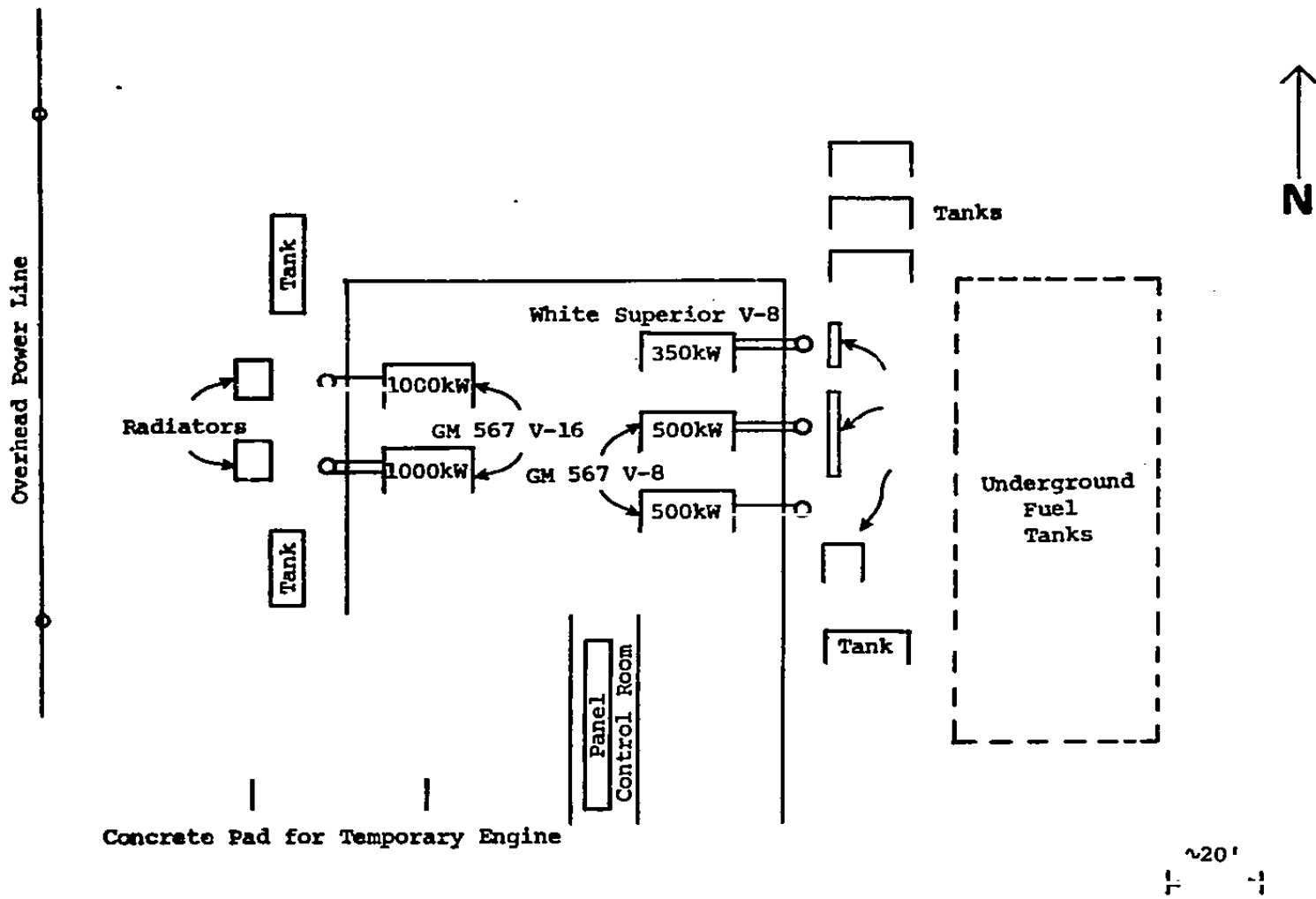


Figure 6-1. Sketch of San Nicolas Island Power Plant



Figure 6-2. San Nicolas Island Power Plant

control room, though an engine governor adjusts for small engine load variations. An operator is on duty 24 hours/day with a maintenance mechanic for one shift. Machine shop facilities are available, though there is no full-time machinist on the island. The bus bar is operated at 4160 volts.

Usually, one of the more efficient 1000 kW engines is used for baseload operation, with the 350-kW or a 500-kW engine for peak loads. Or, as a back-up, both 500-kW engines run together. From January to May in 1979, the frequency of use for each engine was the following:

Engine Number	Power (kW)	% of Total Clock Time
1	500	45
2	500	45
3	350	28
4	1000	12
5	1000	43

} usually run
} together

} 55% total

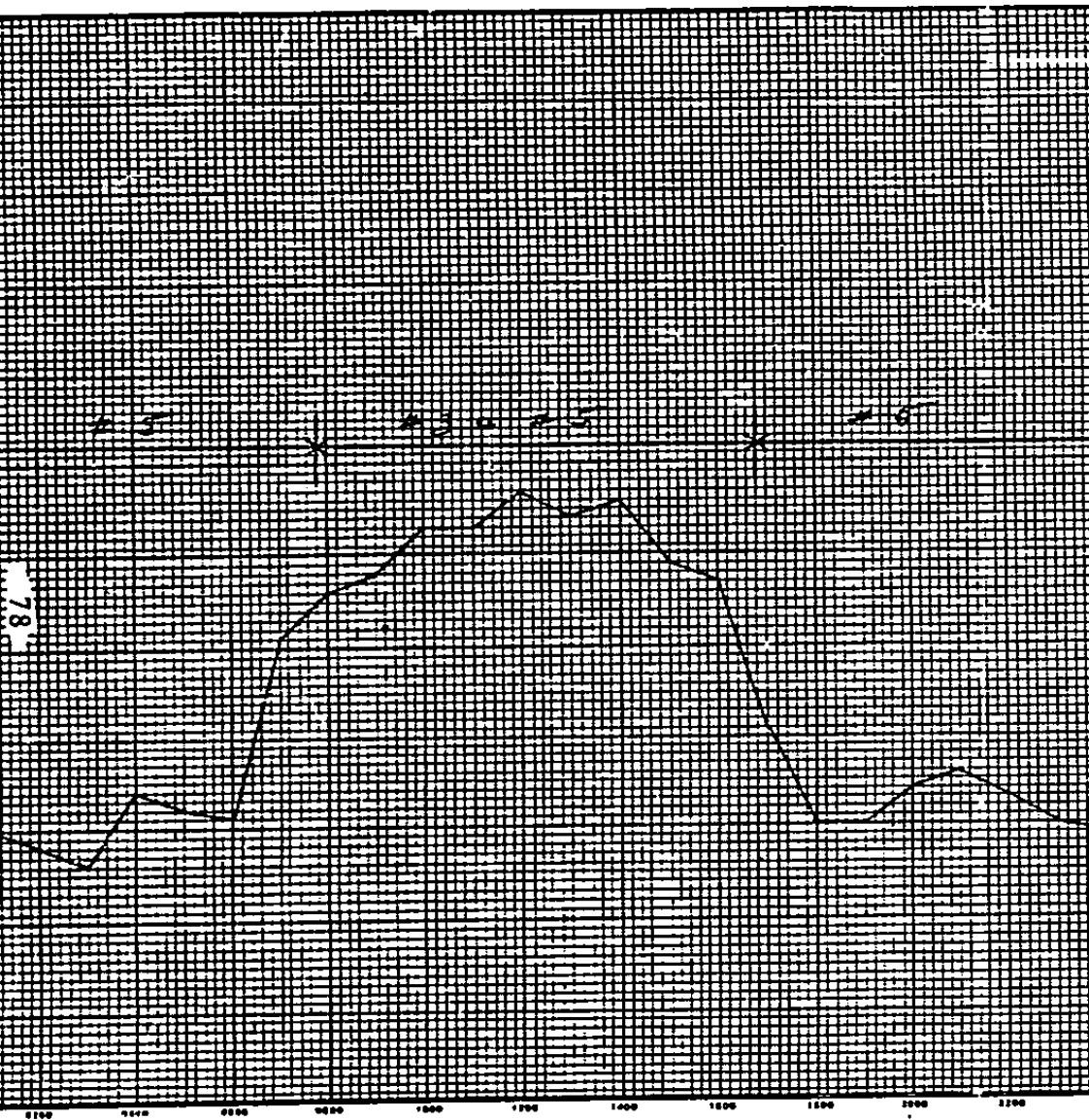
The 55 percent for either 1000-kW engine plus 45% for both 500-kW engines gives 100-percent coverage of the base-load requirement.

Figure 6-3 and 6-4 show power demand for 24 hour periods. Hourly records are made of the exhaust-gas temperatures from each cylinder. Figure 6-5 is a plot of actual exhaust-gas-temperature operating points as a function of engine load. Engine-muffler make and pressure drop are not now known, though pressure drop typically is 10 inches of water in these types of devices.

Island water demand is 25-30 kgpd. Currently, water is supplied by four wells and ground water collection, which has recently been expanded. Some wells were brackish with up to 11,000 ppm TDS. Three 25-kgpd VC distillation units are on location but currently not in use. These are diesel-powered and located near the beach. When in use, these had required more maintenance and operator attention than was originally planned.

DAILY LOG - ELECTRICAL

S. S. I. POWERHOUSE



KWH METER @ 2400 ON LAST DAY OF MONTH		118152
QUARTERLY KWH	TODAY	TOTAL
782400	16000	798400
QUARTERLY ENGINE HOURS	TODAY	TOTAL
2042	33	2075
KWH METER @ 2400	118576	
KWH METER @ 0000	118556	
DIFFERENCE	20	
MULTIPLIER	800	
TOTAL DAILY KWH	16000	
MAXIMUM DEMAND		970
MINIMUM		560
TIME		1200
POWER FACTOR		

ENGINE	ENGINE DATA			
	HOUR METER @ 0000	HOUR METER @ 2400	HOURS RUN DAILY	HOURS SINCE LAST MAINTENANCE
GMC NO. 1	12647	12647	0	12647
NO. 2 - GMC	30675	30675	0	9885
WHITE NO. 3 SUPERIOR	5312	5321	9	5321
NO. 4 - GMC	50376	50376	0	270
NO. 5 - GMC	65326	65350	24	18349
NO. 6 - GMC				

TOTAL FUEL CONSUMPTION 1600 GAL. LUBE OIL 15 GAL.

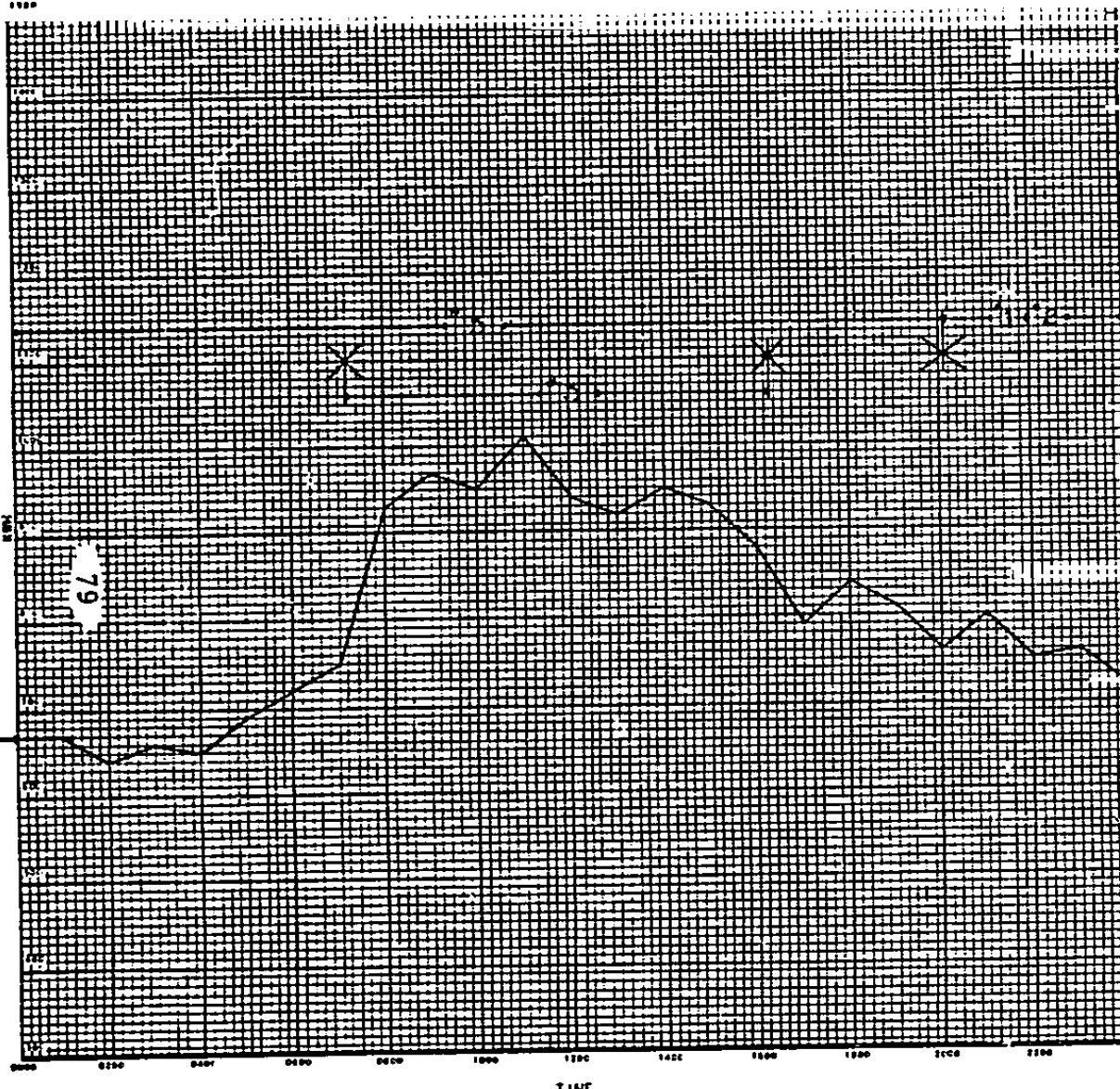
REMARKS
added 15 gal. lube oil in #3 engine

DATE TUES 22 MAY 1979 PREPARED BY R. Ward

Figure 6-3, San Nicolas Island Power Plant Log 5/22/79

DAILY LOG ELECTRICAL

S. N. I. POWERPLANT



KW METER @ 2400 ON LAST DAY OF MONTH		JAN 1979	
QUARTERLY KW	92900	TODAY	17600
TOTAL		TOTAL	340600
QUARTERLY ENGINE HOURS	910	TODAY	37
TOTAL		947	
KW METER @ 2400	11630		
KW METER @ 0000	11670		
DIFFERENCE	-40		
MULTIPLIER	240000		
TOTAL DAILY KW		17600	
ENGINE DATA		POWER FACTOR	
ENGINE	HOW METER @ 0000	HOW METER @ 2400	BURNING HOURS DAILY
NO. 1 - G.P. ENGINE	11268	11270	4
NO. 2 - D/C	20904	20912	4
NO. 3 - D/C	4421	4570	4
NO. 4 - D/C	40106	40104	0
NO. 5 - D/C	68108	68120	20
			HOURS SINCE LAST MAINTENANCE
			11571
			6475
			4550
			30046
			17120
TOTAL FUEL CONSUMPTION		1075 GAL	
		LUBR OIL 20	
REMARKS 5 GALS LUBE OIL ADDED TO UNIT # 1 5 GALS LUBE OIL ADDED TO UNIT # 2 5 GALS LUBE OIL ADDED TO UNIT # 3 5 GALS LUBE OIL ADDED TO UNIT # 5			
DATE		PREPARED BY	
TUES. JAN 23 1979		J. W. Lawson	

Figure 6-4. San Nicolas Island Power Plant Log 1/23/79



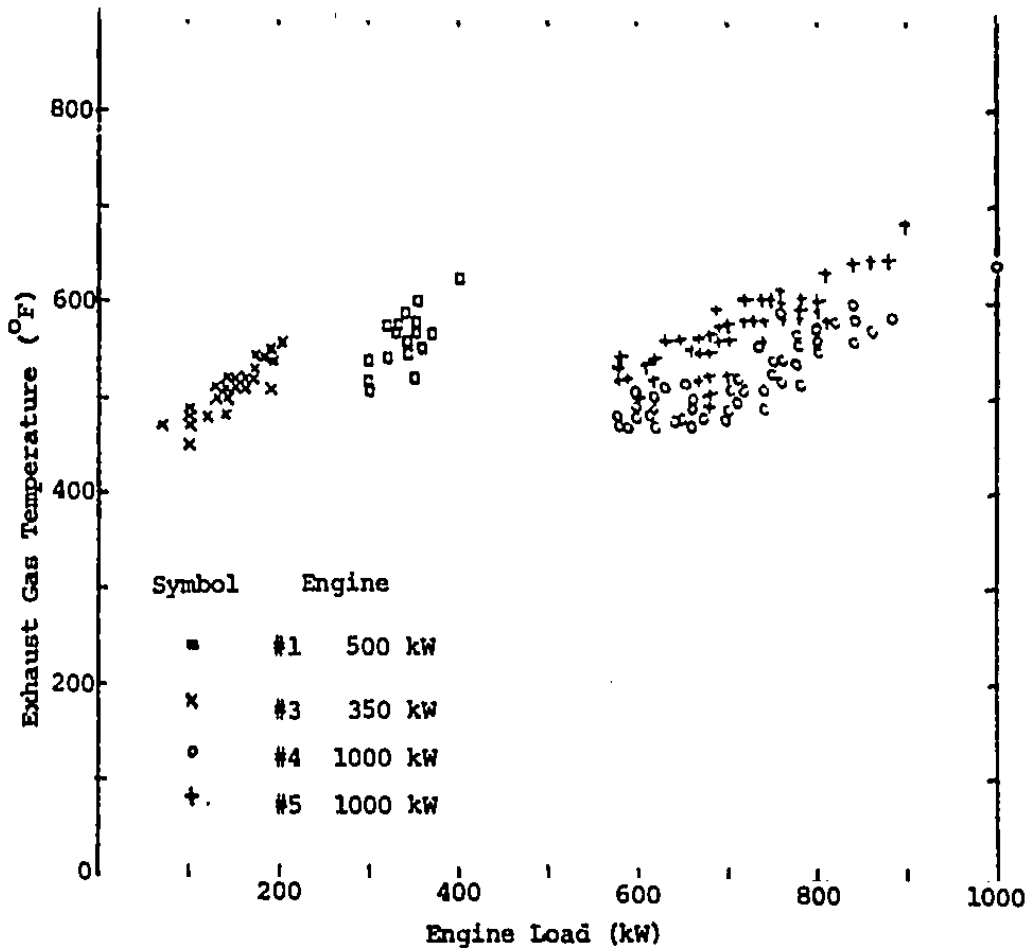


Figure 6-5. Exhaust-Gas Temperature from San Nicolas Engines

BIPHASE DESALINATION/POWER SYSTEM

Different configurations of the Biphase desalination/power cycle are described in a previous report (1). The cycles include single-stage cycles and more complex two-stage cycles. The two-stage cycles offer the advantage of higher power-production efficiency because they include a high-temperature freshwater-working-fluid upper stage. The saltwater-working-fluid second stage has a temperature limited by scale formed by the salt water. The two-stage cycles also offer some flexibility between power and fresh water outputs. However, the design and performance verification of the lower-pressure Biphase turbine is currently more advanced than that of the turbine for the high-pressure stage. For a first demonstration system, the cycle should be the simpler single-stage cycle. A higher pressure stage could then be added later.

Considering engine location and operating practice, the Biphase system should be coupled to the two 1000-kW engines on the west side of the plant. The Biphase system could then be located on an adjacent concrete pad. Figure 6-6 is a photograph of the exhaust ducts and radiators from these engines. The exhaust ducts would connect with a fluidized-bed seawater heater. The exhaust-gas flowrate from either of these engines is estimated to be 5.0 lb/sec at 60% load and 5.5 lb/sec at full load.

Figure 6-7 is a schematic of the system. Seawater is pumped through the condenser where it provides cooling and is heated to 160°F. Then the seawater is heated by the engine exhaust gas in a fluidized-bed heater. The hot seawater flows to the Biphase rotary separator turbine (RST). The seawater expands to a lower pressure and partly flashes to steam. The RST generates power from the expanding seawater and separates clean steam. The steam condenses in the condenser to form the fresh product water. The remaining brine is pumped from the RST back to the ocean.

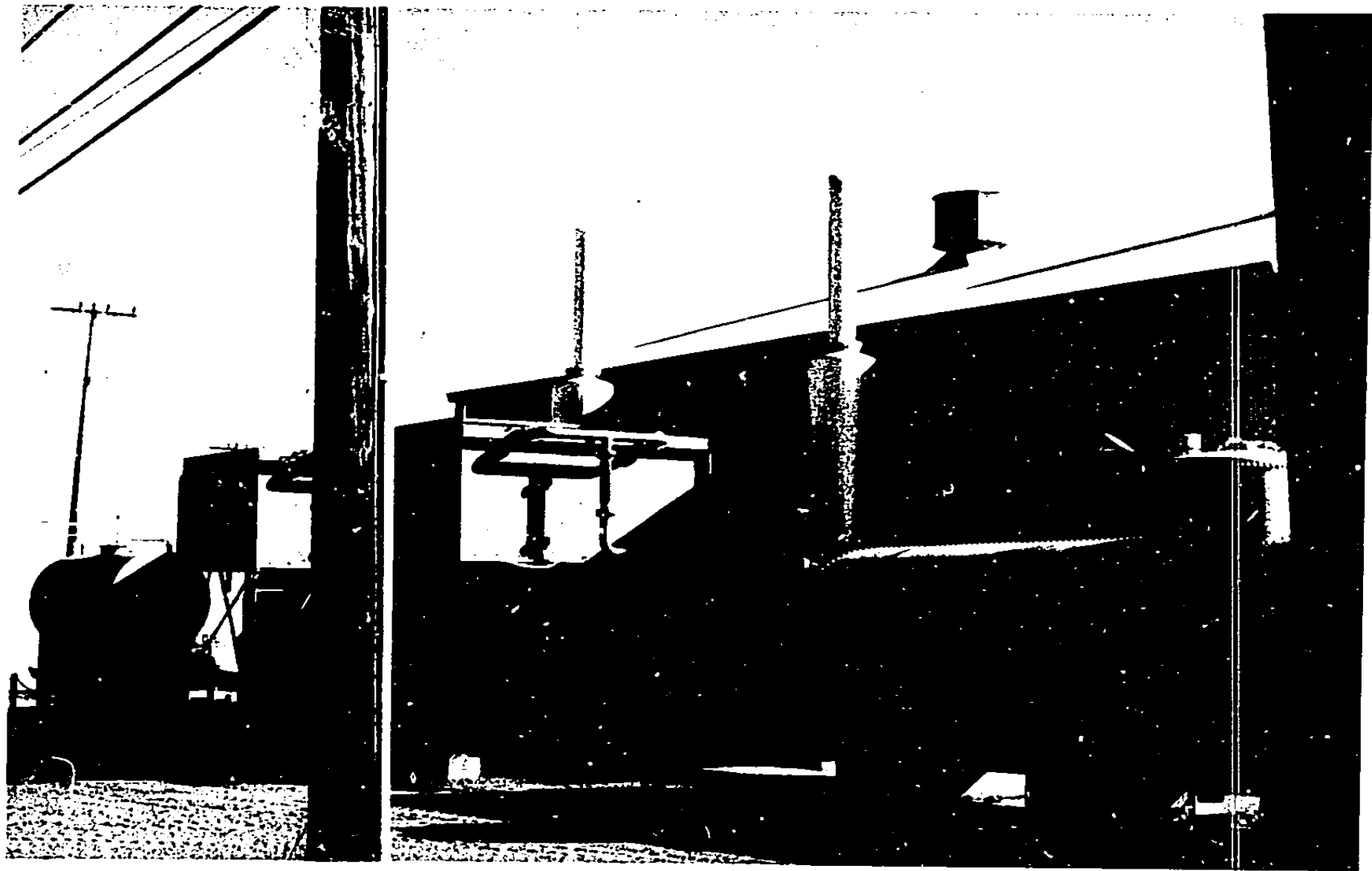


Figure 6-6. Exhaust Ducts from 1000-kw Engines

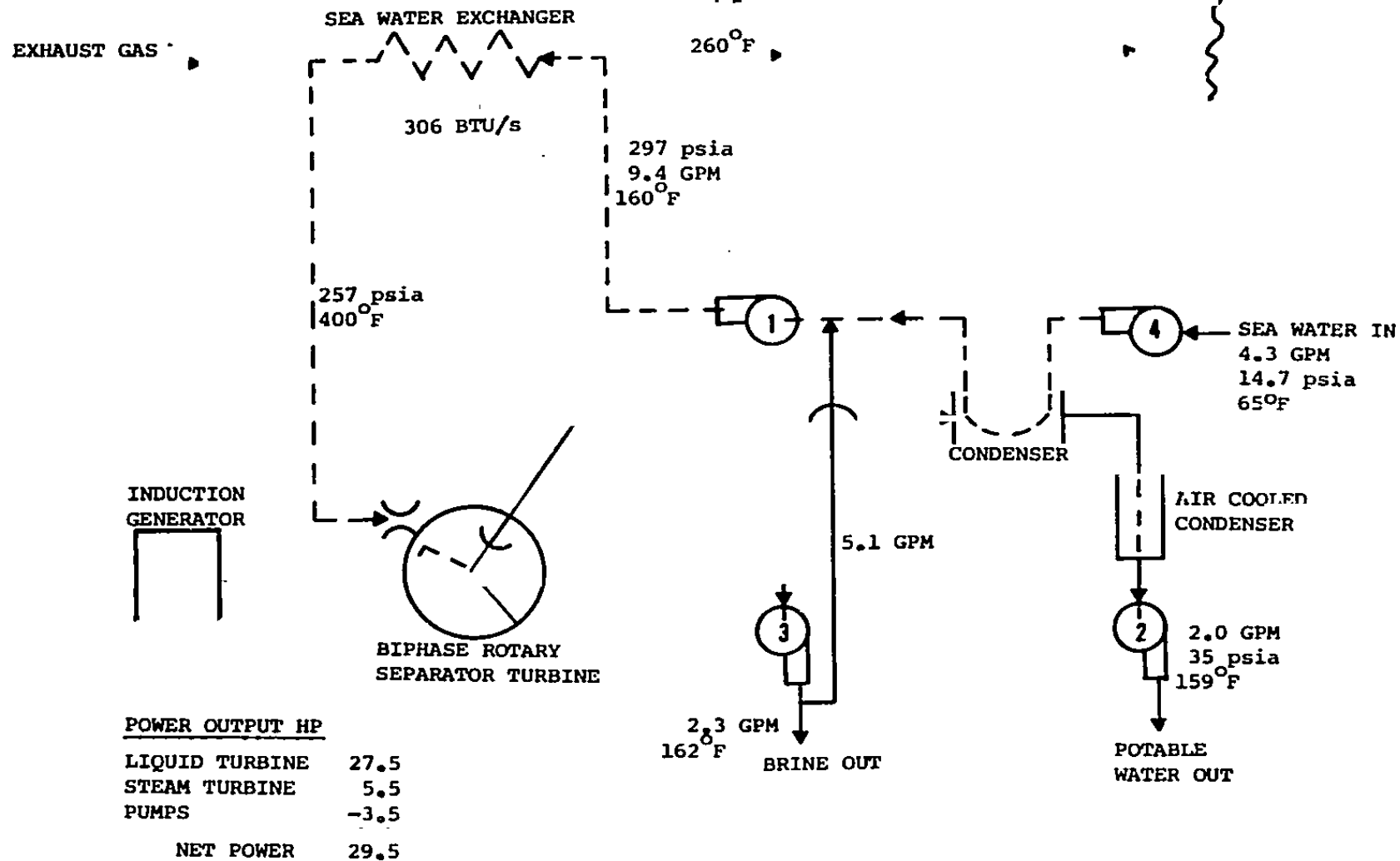


Figure 6-7. Single-Stage Biphase Desalination Cycle 400°F Maximum Seawater Temperature, 5-psia Condensing Pressure

The single-stage Biphase desalination/power cycle system with 400°F seawater maximum temperature can generate up to 57 hp additional shaft power and 5700 gal/day of fresh water. The overall result is summarized in Table 6-1. Figure 6-7 shows the system flowrates during base power generation.

During peak generation, the flowrates increase by a factor of 1.9. The cycle in Figure 6-7 assumes a maximum seawater temperature of 400°F. If this maximum temperature is limited to 330°F, power production drops by 35%, to 19 hp at baseload and 37 hp at the peak. Fresh water production is not affected.

Power from the turbine can be used to drive an induction generator. The power can then be fed into the bus bar. This will reduce the diesel engine load slightly, but not enough to change exhaust gas flow very much.

PROTOTYPE SYSTEM COSTS

Table 6-2 lists breakdown of cost estimate for a prototype system. System cost is \$112,000.

The San Nicolas power plant is at 600 feet elevation, approximately 1.5 miles from the nearest beach. A four-inch pipeline runs from a house next to the unused distillation units (2.5 miles away at the beach) to the main fresh-water storage tanks for the island which are 500 feet from the power plant. This pipeline might be used for seawater supply to the Biphase system at the power plant, but can probably not handle salt-water flow. Pipelines to carry salt water to the power plant and brine back to the beach are estimated to cost \$90,000. This added cost makes the San Nicolas location costly for a prototype test situation.

If capital costs for a developed system are a third of the prototype costs, the specific cost is \$1700 per kW of generated power (at base load). The direct capital costs in terms of fresh water

Table 6-1 San-Nicolas-Island System

Power - Plant Engines:

Either of two GM 567 V-16, each 1000 kW

Load:

Peak: 1000 kW

Base: 600 kW

Low: 590 kW

Energy Recoverable from Exhaust Gas:

Peak - (1000 kW); 5.5 lb/sec @ 680^oF; 589 Btu/sec

Base - (600 kW); 5.0 lb/sec @ 500^oF; 306 Btu/sec

Biphase System with Seawater Working Fluid:

Peak: Generates 57 hp and 5700 gal/day

Base: Generates 29 hp and 2900 gal/day

capacity would be \$14 per gallon per day of fresh water production capability. These costs do not include installation or other direct costs.

CONCLUSIONS

A demonstration desalination system using a Biphase rotary separator turbine can generate 29 hp and 2700 gallons per day using the exhaust gas from the San Nicolas Island power plant. During peak power demand, production increases to 57 hp and 5700 gallons per day.

Table 6-2 Prototype System Cost Estimate

Turbine 13"	\$40,000
Induction motor	2,000
Fluidized Bed Heater	30,000
Air Cooled Condenser	4,000
Condenser/Heat Exchanger	3,000
Pumps - Main	1,000
Recirculating	1,000
Seawater	1,500
Fresh Water	1,000
Vacuum	2,000
Controls	3,000
Instruments and Panel	2,000
Control Valves	2,000
Other Valves	1,000
Piping	2,000
Electrical	2,500
Heat Insulation	1,000
System Structured Skid	6,000
Exhaust Gas Ducts & Insulation	2,000
Gas Duct Valves	2,000
Misc. Parts for Shop Assembly & Test	3,000
	<hr/>
	\$112,000

APPENDIX A
LIQUID FLUIDIZED-BED ANALYSIS

Flow in liquid fluidized beds is correlated by Reynolds Number Re_d and Galileo Number Ga .

$$Re = \frac{\rho_f V d_p}{\mu_f} \quad (1)$$

$$Ga = \frac{\rho_f (\rho_p - \rho_f) g d_p^3}{\mu_f^2} \quad (2)$$

where ρ_f, ρ_p = fluid density, particle density

V = fluid superficial velocity

d_p = particle diameter

μ_f = fluid viscosity

g = gravitational acceleration.

The minimum fluidization velocity, V_{mf} , can be estimated based on equations for pressure drop through fixed beds [11]. Void fraction is about 40 percent for spherical particles at minimum fluidization velocity. Then,

$$Re_{mf} = 25.7 \left\{ \sqrt{1 + 5.53 \times 10^{-5} Ga} - 1 \right\} \quad (3)$$

The maximum velocity at which particles are entrained in the flow, V_t is determined by the balance between particle drag and gravity force.

$$Re_t = \sqrt{\frac{4}{3} \frac{Ga}{D_c}} \quad (4)$$

where $D_c = f(Re_t)$ is the particle drag coefficient. D_c is about 0.4 for our range of interest. Re_t is Reynolds Number based on V_t .

Figure A-1 shows Re_{mf} and Re_t as a function of Ga . Figure A-2 shows V_t as a function of particle size and density. Figures A-3 and A-4 give the relationship between fluid superficial velocity, bed void fraction, and bed expansion.

Veenman [4] has found Ruckerstein and Shorr's correlation to best fit experimental results for wall-to-liquid heat transfer.

$$Nu_{dp} = 0.067 Pr^{0.33} Re_{df}^{-0.273} Ga^{0.522} \quad (5)$$

if $Re_{dp} Ga^{-0.58} > 0.09$ (this condition is satisfied if V is not too close to V_{mf}). Normal sea water at $300^\circ F$ has $Pr = 1.21$. The fluidized beds operate with $V/V_t \sim 0.5$ (see Figures A-3 and A-4). Figure A-1 shows that approximately:

$$Re_{0.5t} = 0.53 Ga^{0.545} \quad (6)$$

Further, approximately:

$$Re = 1.06 \frac{V}{V_f} Ga^{0.545} \quad (7)$$

Then for normal seawater with $Pr = 1.21$ at $300^\circ F$:

$$Nu_{df} = 0.07 \left(\frac{V}{V_f} \right)^{-0.273} Ga^{0.373} \quad (8)$$

This equation can be used to estimate fluidized-bed wall-to-liquid heat-transfer coefficients.

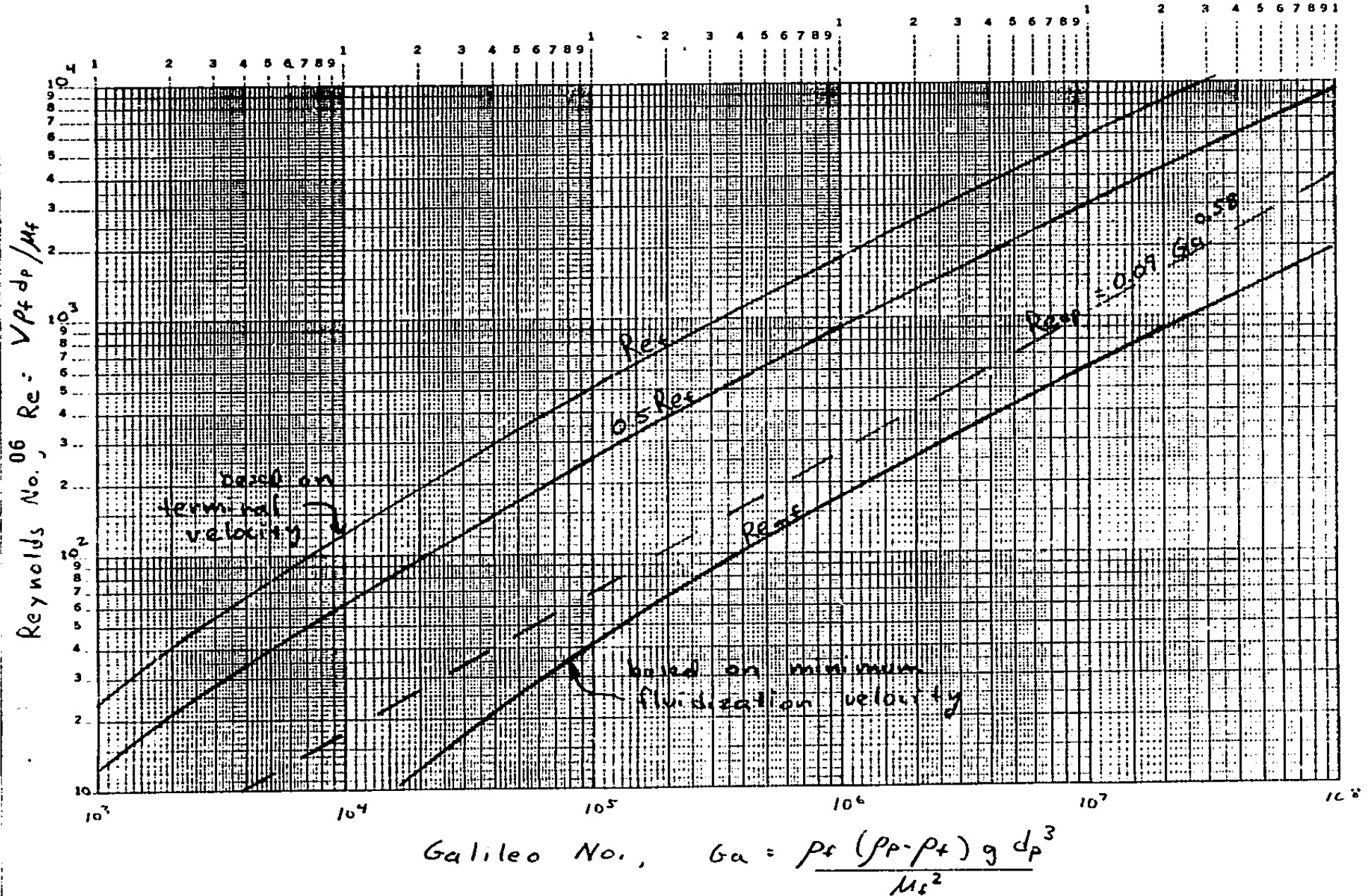


Figure A-1. Reynolds Number vs. Galileo Number for Fluidized Beds

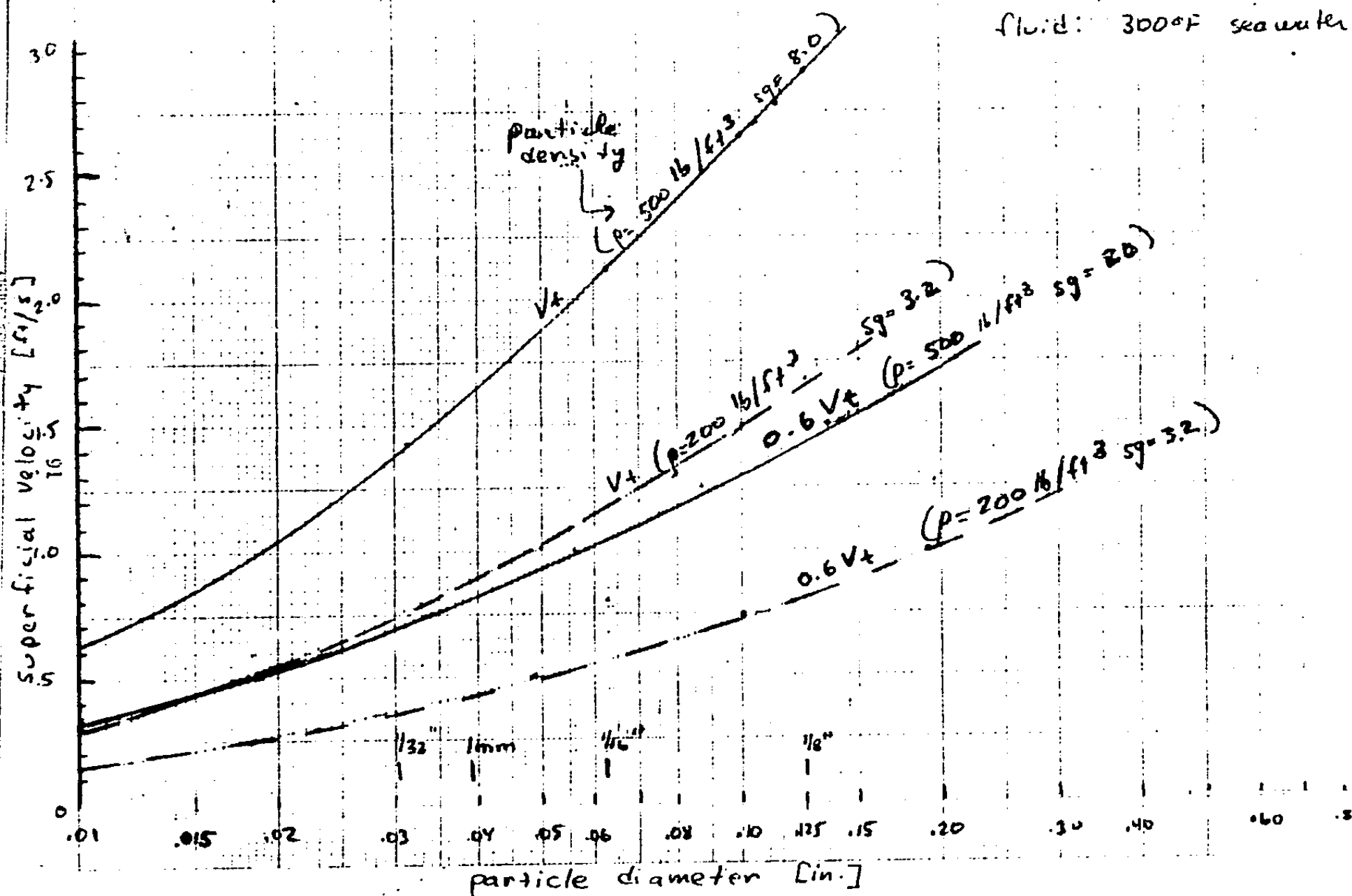


Figure A-2. Fluidized-Bed Superficial Velocity as a Function of Particle Diameter and Density

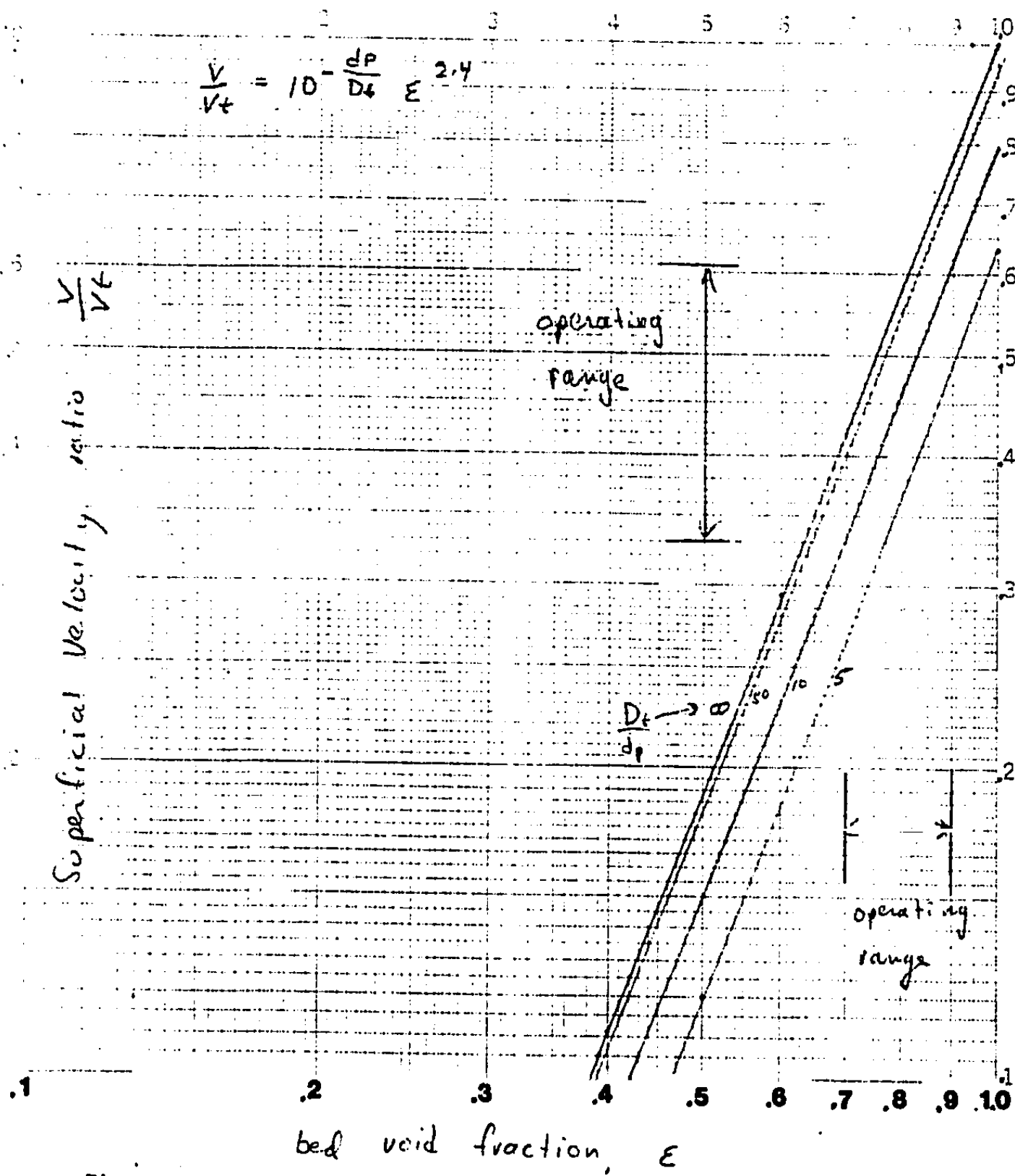


Figure A-3. Bed Void Fraction as a Function of Fluid Velocity

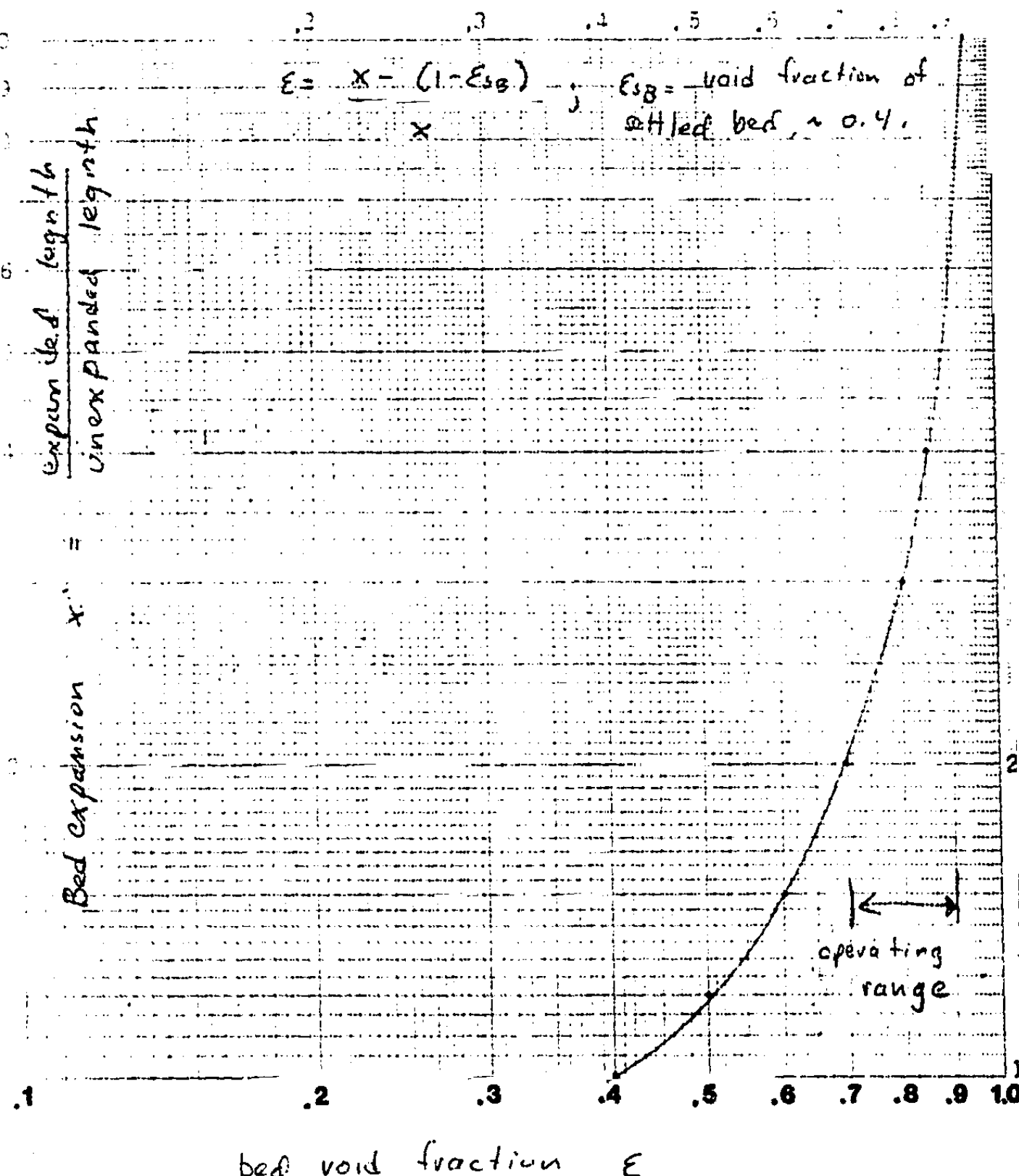


Figure A-4. Bed-Length Expansion as a Function of Bed-Void Fraction

APPENDIX B

TEST SYSTEM INFORMATION

The following figures and tables appear on subsequent pages. They describe the test system used for the fluidized-bed seawater heating tests:

1. Test system detail schematic
2. Valves list
3. Measurements list
4. Data system
5. Seawater heating checklist
6. System shutdown
7. Things to check during testing
8. Calibration/checkout tests
9. Heat exchanger photos

The test system detail schematic shows the details of the test system shown in Figure 3-4 in Section 3. Seawater enters the system from a reservoir (a pool) at the lower right of the detail schematic. The seawater flows through a boost pump, filter and high pressure pump to the tube side of a shell-and-tube preheater. From the preheater, the seawater flows to the test heat exchanger. The detail schematic shows three heat exchanger tubes in series. This was the configuration for bare tube tests. After the test heat exchangers, the hot seawater flowed through the test filter, a back pressure valve and a separation tank which separated any flashed steam. For the corrosion and erosion tests, the corrosion/erosion test fixture replaced the separation tank.

High pressure steam was supplied by a steam generating system (at the top of the detail schematic). An electric Chromalox 25 kW oil heater heated Caloria HT43 heat-transfer oil. The hot oil flowed to the shell side of a shell and tube exchanger. Here the hot oil generated high pressure steam on the tube side. The high pressure steam flowed to the test-heat-exchanger steam jackets. Back pressure valve BPCV8 controlled the steam pressure. From this valve, low pressure steam flowed to the shell side of the preheater. A 100 lb/hr steam boiler supplied additional steam to the preheater. Regulating valve PRV9 controlled the steam pressure in the preheater.

Condensate from the preheater collected in a receiver. From the receiver the water was pumped by a variable speed positive displacement pump back to the high pressure steam generator. The high pressure steam flow was adjusted by adjusting the pump speed.

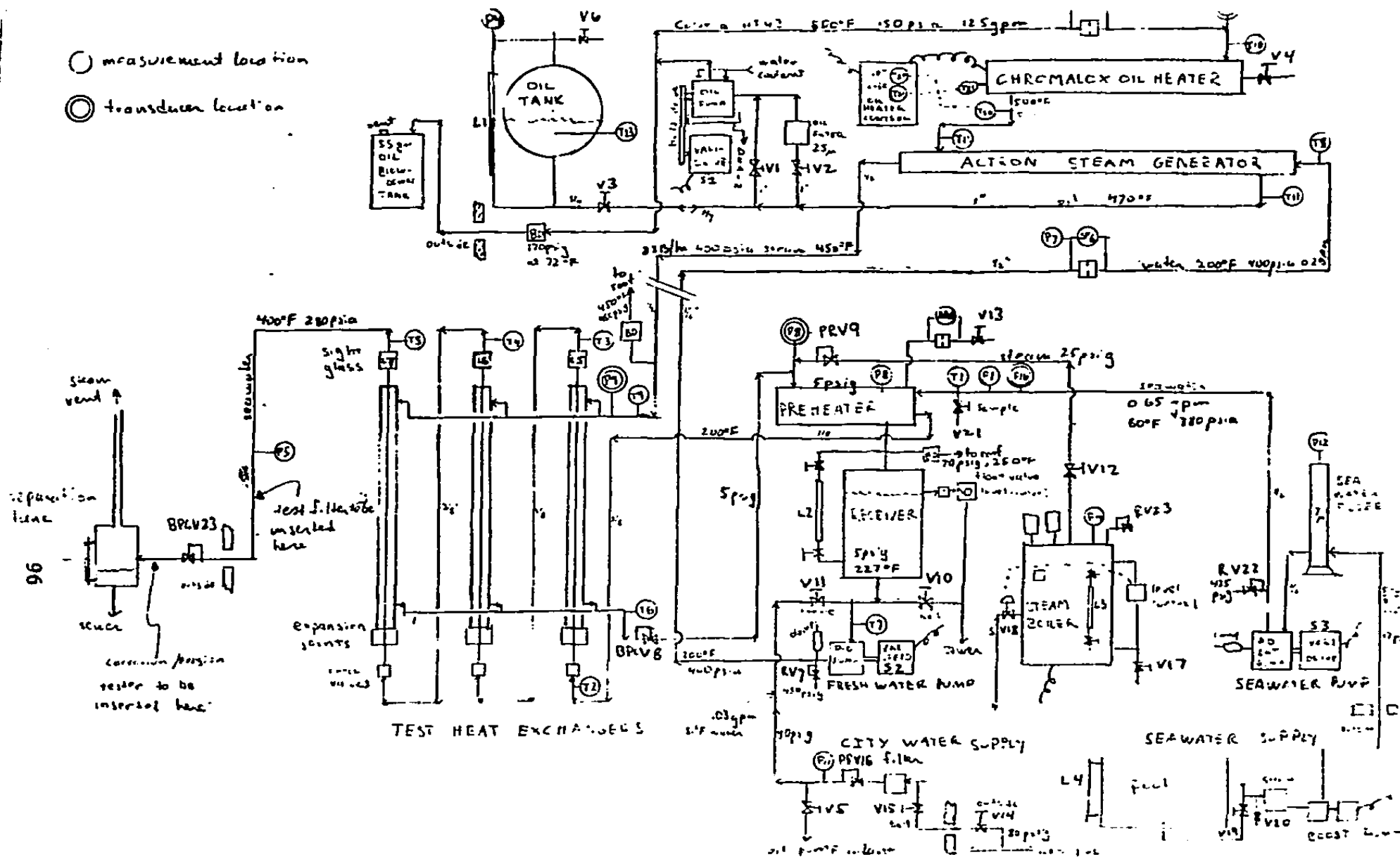


Figure B-1. Test System Detail Schematic



B-2 VALVES LIST

<u>SYMBOL</u>	<u>FUNCTION</u>
V1	Open - oil bypass of filter
V2	Close - oil bypass of filter
V3	Open oil flow to/from accumulator
V4	Open to drain oil heater
V5	Adjust cooling water for oil pump
V6	Open to vent oil accumulator
RV7	Water relief at water pump, 450 psig
BPCV8	Test HX steam pressure control
PRV9	Preheater steam pressure control
V10	Open to drain receiver
V11	Adjust subcooling flow to water pump
V12	Open for l.p. steam flow from boiler
V13	Adjust non-condensibles vent
V14	Open for city water supply
V15	Open for city water supply
PRV16	Control city water supply to system, 40 psig
V17	Open for boiler blowdown
SV18	Automatic control of boiler water level
V19	Open for seawater supply (at pool)
V20	Open to admit fresh water to seawater lines (at pool)
V21	Open for seawater sample
RV22	Seawater relief at seawater pump, 425 psig
BPCV23	Control seawater back pressure in test HX
RV24	Steam relief on boiler
RV25	Oil tank relief, 40 psig
RV26	Regulate Argon gas supply to oil tank
V27	Argon shut off
V28	Open for oil flow to oil tank
V29	Close to bypass oil to oil tank

B-3 MEASUREMENTS LIST

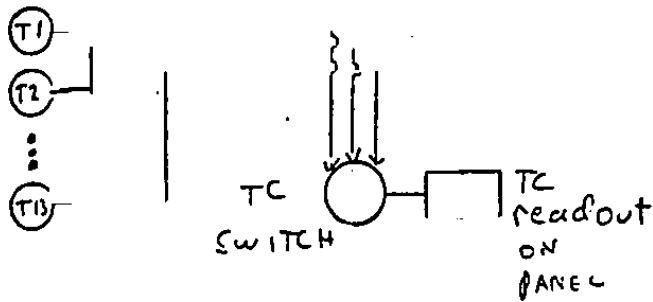
MEASUREMENT	READOUT/RECORDER Kaye # / Panel			SENSOR LOCATION	MEDIA	READOUT LOCATION (If not at panel)
Temperature	T ₁	101	::	preheater inlet	seawater	
	T ₂	102	x	test HX inlet	seawater	
	T ₃	103	x	test HX outlet 1	seawater	
	T ₄	104	x	test HX outlet 2	seawater	
	T ₅	105	x	test HX outlet 3	seawater	
	T ₆	106	x	test HX condensate	water/steam	
	T ₇	107	x	fresh water pump inlet	fresh water	
	T ₈	108	x	steam generator inlet	fresh water	
	T ₉	109	x	test HX steam inlet	steam	Cf P ₉
	T ₁₀	110	x	oil heater inlet	oil	Cf P ₁₀
	T ₁₁	111	x	steam generator inlet	oil	
	T ₁₂	112	x	steam generator outlet	oil	
	T ₁₃	113	x	oil tank	oil	
Pressure	P ₁		x	seawater pump outlet	seawater	
	P ₂		x	oil pump outlet	oil	
	P ₃		x	oil orifice ΔP	oil	

MEASUREMENT	READOUT/RECORDER Kaye # / Panel		SENSOR LOCATION	MEDIA	READOUT LOCATION (If not at panel)	
Pressure	P ₄		oil tank	oil/air	above oil tank	
	P ₅	x	test HX outlet	seawater		
	P ₆	x	fresh water orifice ΔP	fresh water		
	P ₇	x	fresh water pump outlet	fresh water		
	P ₈	208 x	preheater (shell)	steam		
	P ₉	209 x	test HX steam	steam		
	P ₁₀	210	oil heater inlet	oil	Cf P ₂	
	P ₁₁	x	city water regulated pressure	city water		
	P ₁₂		seawater filter	seawater	on seawater filter ne	
	P ₁₃		vent orifice	air/steam	preheater above steam	
	P ₁₄		steam boiler	steam	boiler	
	P ₁₅	x	test filter ΔP	seawater		
	Flow	F ₁₆	216	preheater inlet	seawater	
	Level	L ₁		oil tank level	oil	oil tank
		L ₂		receiver level	water	receiver
L ₃			boiler level	water	boiler	
L ₄			seawater supply	seawater	pool	

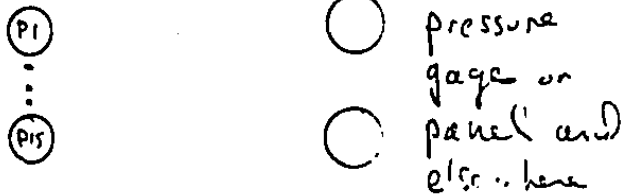
MEASUREMENT	READOUT/RECORDER Kaye # / Panel	SENSOR LOCATION	MEDIA	READOUT LOCATION (If not at panel)
Level	L ₅	test HX 1	seawater/ fluidized-bed	Top of HX's
	L ₆	test HX 2	" " "	Top of HX's
	L ₇	test HX 3	" " "	Top of HX's
Speed	S ₁	oil pump (BLACKMER)		oil pump varidrive
	S ₂	x fresh water pump (JAECO)		panel controller
	S ₃	seawater pump (CAT)		CAT varidrive

TEMPERATURES

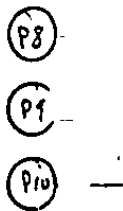
type K thermocouples.



PRESURES



critical pressures have transducers

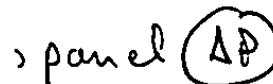


FLOW S

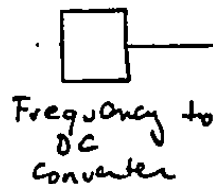
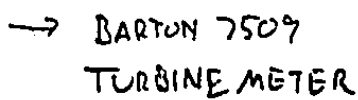
oil
fresh water
non condensibles



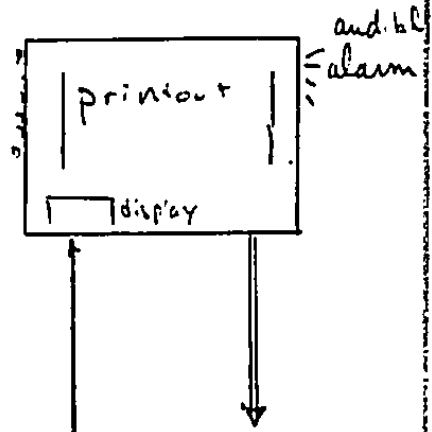
orifice



seawater



KAYE DIGISTRIP



Emergency stop (P8, P9, P10, T)

4. Oil loop Start-up cont'd.

f. Set heater control temperature T_{20} to 175°F.

g. Oil heater ON.

h. Circulate oil through filter for 10 minutes with oil temperature below 200°F.

i. Turn ON/adjust pump coolant water with V_5 .

j. Verify heater control operation.

Verify heater-sheath over-temperature operation, reset to 500°F.

k. Adjust pump speed for $\Delta P_3 = 10$ psi.

l. Open V_7 filter bypass.

m. Close V_2 filter shut-off.

n. Heater set point T_{20} at 175°F.

5. STEAM BOILER and RECEIVER

a. Close V_{10} , open 2 receiver level (L_{12}) gage valves.

b. Fill receiver with V_{11} , verify float valve is OK. SHUT V_{11} .

c. Set boiler pressure control to 25 psig with 6 psi droop.

d. Close V_{12} , turn ON boiler.

e. Verify boiler level control.

Verify boiler pressure control.

f. Open V_{12} . Adjust P_8 to 5 psig with PRV9.

g. Adjust ΔP_{13} to _____ in H_2O with V_{13} .

h. Close V_{12} .

6. FRESHWATER FLOW

a. Open BPCV8 (reduce backpressure).

b. Fresh water pump ON, adjust speed for $\Delta P_6 = 50$ in. H_2O (100 lbm/hr).

c. Open V_{11} to maintain receiver water level if required.

6. Freshwater Flow cont'd.

— — — —
— — — —
d. Adjust P_9 to 210 psig with BPCV8.

e. Allow fresh water temperature T_9 to reach 175°F.

7. HP STEAM FLOW

— — — —
— — — —
a. Turn ON boost pump, seawater pump.

b. Adjust seawater flow for desired flowrate or fluidized-bed expansion.

— — — —
c. Adjust fresh water flow to expected steam rate by adjusting fresh water pump speed S_2 .

— — — —
d. With P_9 at 210 psig, increase heater set temperature T_{20} to 400°F. Flaring should start through BPCV8.

— — — —
e. Gradually increase P_9 with BPCV8 up to expected operating steam pressure. Keep T_9 at 5°F hotter than saturation temperature at P_9 by controlling heater set temperature T_{20} .

— — — —
f. Increase oil flow with oil pump speed S_1 if $T_{20} - T_9 > 40^\circ\text{F}$.

— — — —
g. Adjust T_7 to 200°F with V_{11} .

8. LP STEAM FLOW

— — — —
a. Open V_{12} ; let P_8 settle at 5 psig.

— — — —
b. Adjust ΔP_{13} to _____ in H_2O with V_{13} and adjust seawater temperature T_2 (preheater outlet) to desired level by adjusting P_8 with PRV9.

9. SEAWATER TOP TEMPERATURE

— — — —
a. Readjust P_9 with BPCV8 for desired seawater maximum temperature T_5 .

B-6 SYSTEM SHUTDOWN

DURING TESTS ON SEAWATER, SHUTDOWN PROCESS SHALL AVOID BOILING OF SEAWATER IN THE SEAWATER LINES. KEEP P_5 (TEST HX OUTLET PRESSURE) GREATER THAN SATURATION PRESSURE AT THE MAXIMUM SEAWATER TEMPERATURE IN THE SYSTEM.

PROCEDURE:

1. MAINTAIN OR INCREASE SEAWATER FLOW (MAY NOT BE ABLE TO INCREASE IF BED PARTICLES ARE PRESENT).
2. TURN OFF OIL HEATER AND STEAM BOILER.
3. TURN OFF OIL PUMP.
4. INCREASE FRESH WATER FLOW (S_2).
5. RUN FRESH WATER PUMP UNTIL T_9 COOLS TO 212°F.
6. TURN OFF FRESH WATER PUMP.
7. RUN SEAWATER PUMPS UNTIL T_5 AND T_9 ARE < 200°F.
8. SHUT OFF SEAWATER PUMPS.
9. SHUT OFF CITY WATER, 480 V, AND PULL 120 V PLUG.

B-7 SEAWATER HEATING TEST SYSTEM
THINGS TO CHECK DURING TESTING

- T_2 - in proper range $\sim 220^{\circ}\text{F}$. Indicates steam boiler is ON and providing steam to heat seawater in preheater.
- T_3-T_5 - seawater max temperature at proper point for test.
- T_6 - condensate should not be subcooled. Compare with $T_{\text{sat}} (P_9)$. Increase steam flow (S_2 and P_6) if subcooled.
- T_7 - fresh water temperature should be kept as high as possible but below 180°F to avoid cavitation in freshwater pump.
- T_9 - compare with $T_{\text{sat}} (P_9)$. T_9 should be $3-5^{\circ}\text{F}$ superheated. Increase superheat by keeping freshwater flow (ΔP_6) low and increasing T_{11} .
- T_{11} - check for stable T_{11} , adjust with oil heater control to get proper T_9 steam temperature and steam superheat.
- P_4 - oil tank. Check for rise in temperature indicating build-up of steam in oil tank. Set at 30-40 psig.
- P_3 - check for stable oil flow. No decrease or wild swings (greater ~ 2 psi) indicating pump cavitation or build-up of water in oil loop.
- P_{10} - check for excessive oil pressure (> 100 psig: clog in line). At start-up, keep oil flow low to avoid high pressure until oil heats up and thins out.
- P_9 - check for stable steam pressure, and pressure sufficient to maintain $T_3 - T_5$ at desired levels. Adjust with BPCV 8.
- P_6 - check for stable low pressure steam at value for desired T_2 . Usually set ~ 2 psig.
- P_{12} - seawater filter pressure. Indicates that boost pump is ON.
- F_{16} - check for stable seawater flow at desired level.
- P_5 - test HX outlet pressure. Keep high enough (at least 30 psi above $P_{\text{sat}} (T_{\text{sw}_{\text{max}}})$) to avoid boiling in seawater.
- L_3-L_5 - seawater HX level gages. Check level of fluidized-bed if present and absence of bubbles (bubbles indicate boiling).
- - check for proper oil cooling water flow and drainage. If drain clogs, rap discharge line.

- T₂₀
- check for proper temperature regulation and that needle is not stuck.
 - - oil pump speed. If oil pump quits mysteriously with everything else running, shut power OFF and reset relay in junction box.
 - - check that steam boiler is ON, pipes hot and cut-off reset. Check that automatic refill is maintaining steam boiler water level L₃.
- L₂
- receiver level. Check that level is not too low, or if V₁₁ is open, that float valve is properly maintaining level.
 - - check for leaks in all piping and unusual noises in pumps and varidrives.
 - - check seawater strainer (near pool) for excess air pocket(s).

PLL:jb

B-8 CALIBRATION/CHECKOUT TESTS

1. CALIBRATION

a. CALIBRATE TC's.

Measure output at 3 reference temperatures, ice/water, boiling water, tin melting point (450°F).

b. CALIBRATE PRESSURE TRANSDUCERS.

Hydrostatic test. Compare output over range with reference gage. Reprogram KAYE.

c. FLOW CALIBRATION.

(1) Seawater flow: Plot turbine meter output vs. gpm and pump speed. Reprogram KAYE.

(2) Oil flow: Plot oil pump rpm vs. orifice ΔP . Compare positive-displacement-oil-pump flow rating at various speed with orifice prediction to confirm oil flow as function of ΔP and pump speed.

(3) Fresh water flow: Plot flow vs. orifice ΔP and pump speed. Compare with prediction.

(4) Plot airflow vs. ΔP to confirm orifice characteristic and estimate steam flow vs. ΔP .

2. OIL LOOP HOT TEST

Run oil loop uninsulated to 500°F. Check for leaks, instrument function. No water in tubes of steam generator. Then insulate oil lines.

3. SEAWATER LOOP PRESSURE/FLOW TEST

Hydrostat seawater loop to 600 psi (test pressure of preheater tubes). Flow test seawater loop with freshwater. Check for leaks, valve and instrument operation. Check preheater for leakage to shell.

4. LOW PRESSURE STEAM LOOP

Generate steam up to 30 psig in preheater. Check boiler operation, for leaks and instrument operation. With fresh water flowing in preheater tubes, measure heat rate to water at different water flow rates and steam pressures.

5. HP STEAM LOOP

(1) Hydrostat to 900 psig; (2) Performance test of steam generator. Following procedure in heating test checklist, measure oil temperature T_{12} required to generate saturated liquid and 5°F superheated steam (T_g) at 300 psia and 400 psia (P_g) as function of water flow rate (at inlet to steam generator).

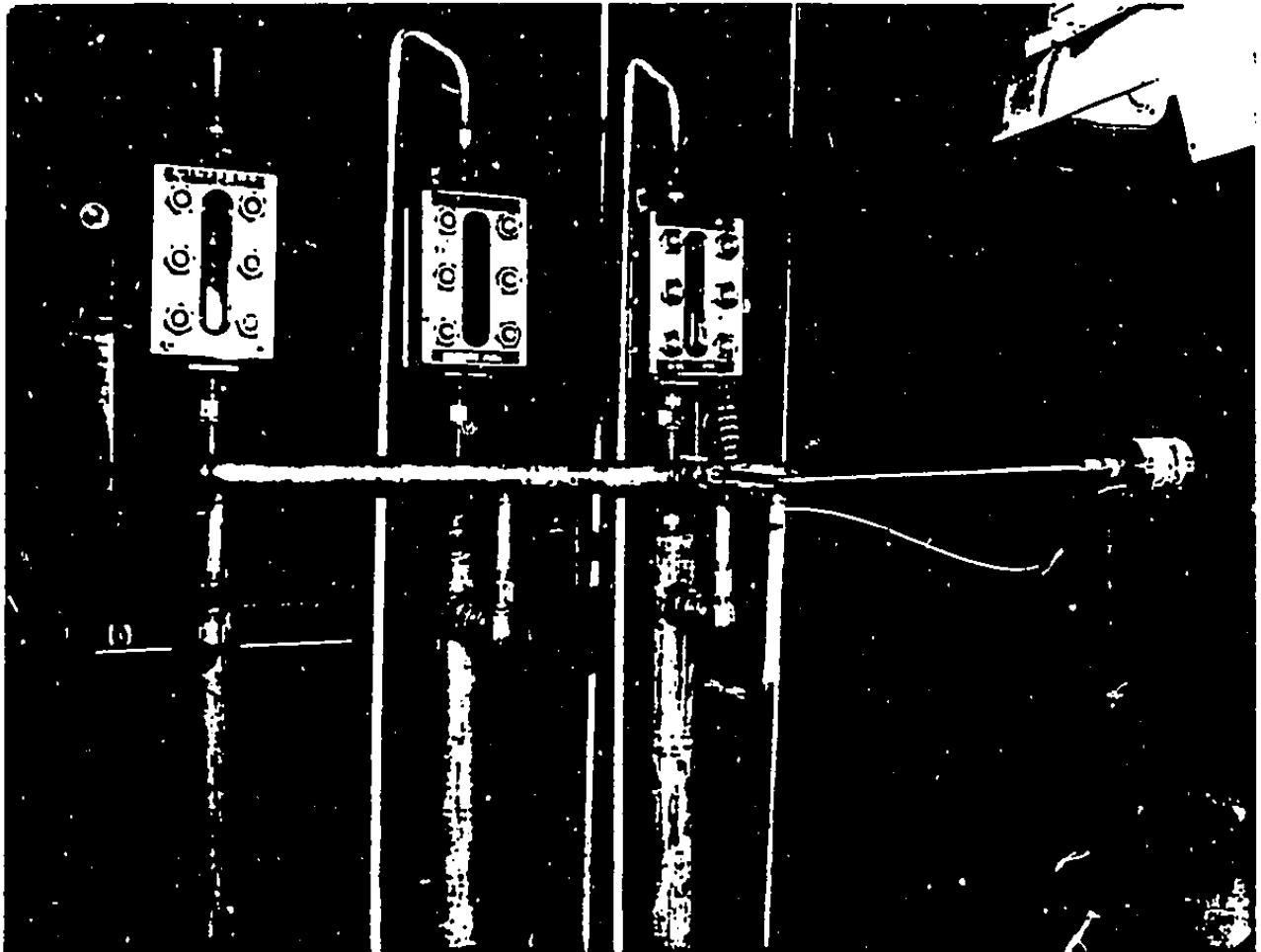


Figure B-9a. Three Uninsulated Test Heat Exchangers, Top Section
Showing Sight Glasses

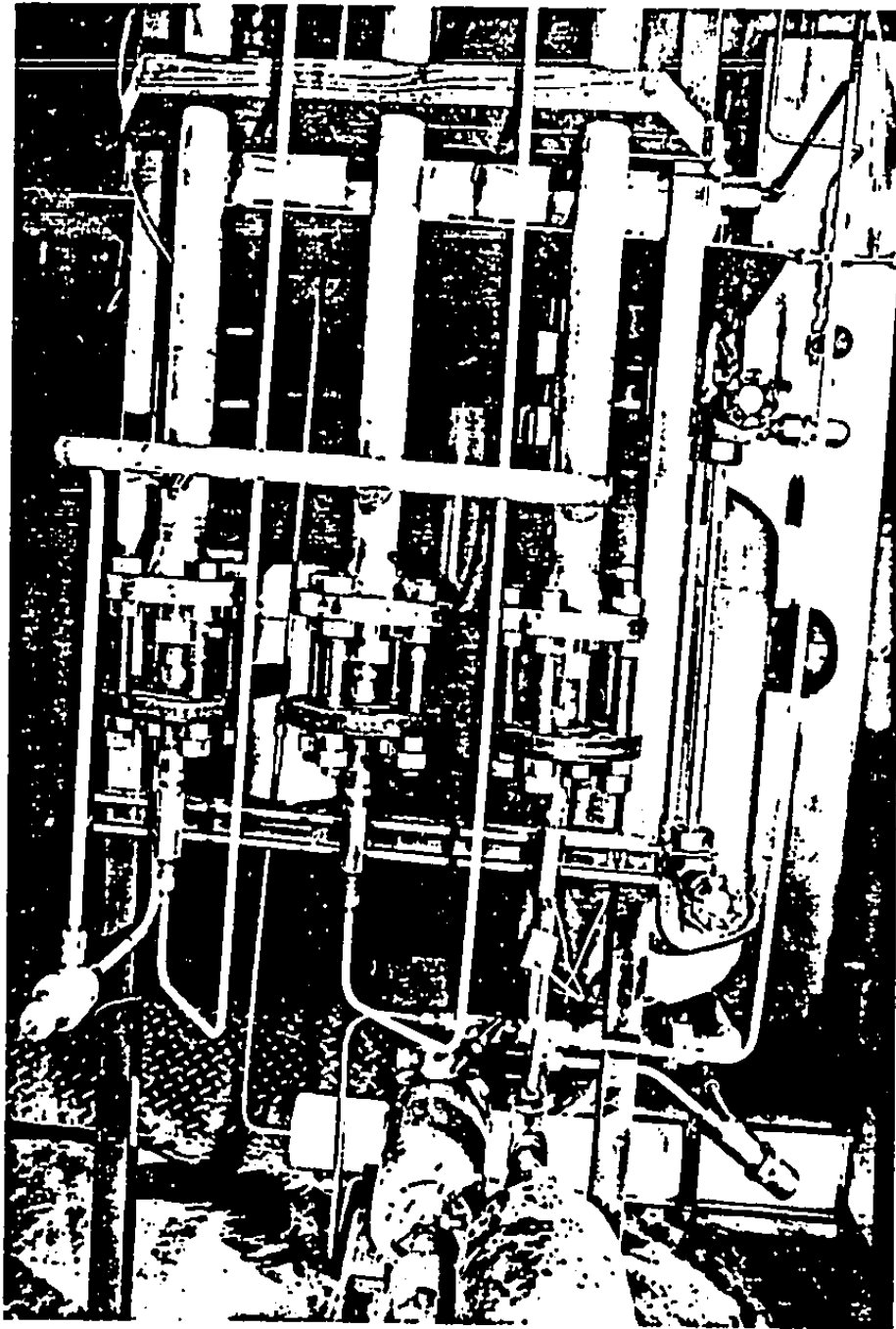


Figure B-9b. Three Uninsulated Test Heat Exchanger, Lower Section Showing Expansion Joints

APPENDIX C

REACTION TURBINE FLUID MECHANICS AND THERMODYNAMICS

In the reaction turbine the flow first accelerates through inlet nozzles with efficiency η_N . The velocity of the fluid jet c_1 is

$$\frac{c_1^2}{2} = \eta_N(h_0 - h_{1s}) + \frac{c_0^2}{2} \quad (1)$$

The fluid kinetic energy of the flow entering the nozzle, $c_0^2/2$, is small and usually can be neglected. Figure C-1 shows the nozzle expansion from the nozzle inlet pressure P_0 to nozzle exit pressure P_1 on an enthalpy-entropy plot (Mollier diagram).

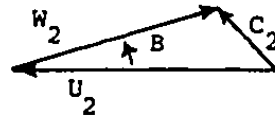
The nozzle jet (state 1) next enters the reaction rotor at an inner radius. The flow leaves the rotor at an outer radius at the same static pressure (state 2). Figure C-2 is a schematic of the reaction rotor and flow velocity triangles at the inlet and outlet. At the inlet, the nozzle jet is in the plane of rotation of the rotor. The jet velocity makes an angle α relative to the rotor speed u_1 (along a tangent) at the point of contact of the jet with the rotor. So,

$$c_{\theta 1} = u_1 + w_{\theta 1} \quad (2)$$

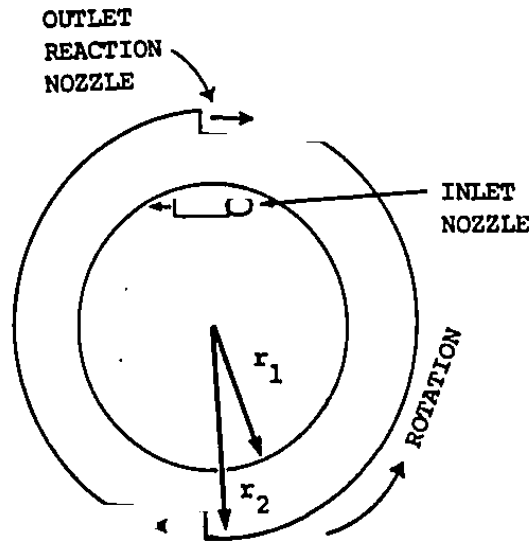
$$c_1^2 = c_{\theta 1}^2 + w_{m1}^2 \quad (3)$$

$$c_{\theta 1} = c_1 \cos \alpha \quad (4)$$

OUTLET VELOCITY TRIANGLE



U = ROTOR VELOCITY
 W = FLOW VELOCITY
 RELATIVE TO ROTOR
 C = ABSOLUTE FLOW
 VELOCITY



INLET VELOCITY TRIANGLE

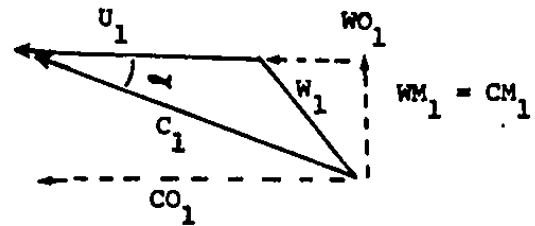


Figure C-2. Reaction Rotor and Velocity Triangles

At the outlet, the reaction jets expel the fluid from the rotor with a velocity making an angle β with the rotor tip speed u_2 . Then

$$c_{\theta 2} = u_2 - w_2 \cos \beta \quad (5)$$

The conservation of angular momentum in the rotor requires that the torque T is

$$T = \dot{m}(c_{\theta 1} r_1 - c_{\theta 2} r_2) .$$

Multiplying by the rotor angular speed and dividing by the mass flow \dot{m} gives the specific power P/\dot{m} .

$$\frac{P}{\dot{m}} = c_{\theta 1} u_1 - c_{\theta 2} u_2 \quad (6)$$

This is Euler's turbine equation.

The conservation of energy also specifies the specific power.

$$\frac{P}{\dot{m}} = \left(h_1 + \frac{c_1^2}{2} \right) - \left(h_2 + \frac{c_2^2}{2} \right) \quad (7)$$

Equating (6) and (7) and rearranging, gives

$$h_1 + \frac{c_1^2}{2} - c_{\theta 1} u_1 = h_2 + \frac{c_2^2}{2} - c_{\theta 2} u_2 = I \quad (8)$$

The function $I = h + 1/2 c^2 - u c_{\theta}$ remains constant anywhere throughout the flow in the rotor. We will use this relationship to determine the velocity of the flow leaving the rotor.

Figure C-1 depicts the rotor energy relationships specified by Equations (6), (7), and (8). To determine the power output and efficiency of the rotor, we start with the angular momentum Equation (6) and substitute in (5) for c_θ^2 .

$$\frac{P}{\dot{m}} = c_{\theta 1} u_1 - u_2^2 + w_2 u_2 \cos \beta$$

Now, defining a rotor efficiency η_r we get

$$\eta_r \equiv \frac{P/\dot{m}}{c_1^2/2} \quad (9)$$

$$\eta_r = 2 \cos^2 \alpha \left[\frac{u_1}{c_{\theta 1}} - \left(\frac{r_2}{r_1} \right)^2 \left(\frac{u_1}{c_{\theta 1}} \right)^2 + \cos \beta \left(\frac{r_2}{r_1} \right)^2 \left(\frac{u_1}{c_{\theta 1}} \right)^2 \frac{w_2}{u_2} \right] \quad (10)$$

The speed of the turbine is specified by $u_1/c_{\theta 1}$ and the geometry (so far) is specified by α , β and the radius ratio r_1/r_2 . Note also that η_r specified by (10) does not yet include windage and bearing losses. The first of the three terms in the bracket in (10) is the normalized power of the inlet flow. The second term is a loss due to radially outward pumping of the flow. And the third term is the reaction power contribution of the reaction nozzles.

We must determine w_2 , the relative velocity of the reaction-nozzle jet. Using (8), we will substitute the relative velocity w and rotor velocity u for the absolute velocity c using the absolute velocity triangle relationships. At the rotor inlet, using (2), (3), and (4) we have

$$I = h_1 + \frac{c_1^2}{2} - c_{\theta 1} u_1$$

$$I = h_1 + \frac{w_{m1}^2}{2} + \frac{(u_1 + w_{\theta 1})^2}{2} - (u_1 + w_{\theta 1})u_1$$

$$I = h_1 + \frac{w_{m1}^2}{2} + \frac{w_{\theta 1}^2}{2} - \frac{u_1^2}{2}$$

$$I = h_1 + \frac{w_1^2}{2} - \frac{u_1^2}{2} \quad (11)$$

Similarly, using the velocity triangle relationships at the rotor outlet, we have

$$I = h_2 + \frac{w_2^2}{2} - \frac{u_2^2}{2} \quad (12)$$

With (11) equal to (12), and solving for w_2 ,

$$\frac{w_2^2}{2} = h_1 - h_2 + \frac{w_1^2}{2} + \frac{u_2^2}{2} - \frac{u_1^2}{2} \quad (13)$$

Now we must consider irreversibilities as the flow moves on to and through the rotor. We assume the fluid is incompressible. By design, the pressure at states 1 and 2 is the same. So the change in enthalpy is due only to a change in internal energy from irreversibilities. Consider a two-step process from state 1 to state 2. During the first step, the jet from the entry nozzle contacts the rotor. The flow slows to the speed of the rotor so that there is no relative velocity between the flow and the rotor. During this step the flow remains at the inner radius r_1 . In (13) this step is the irreversible change

of the kinetic energy into an increase in enthalpy of the flow h_2 . So far then

$$h_2 - h_1 = \frac{w_1^2}{2} \quad (14)$$

Now consider a second ideal step as the flow moves through the rotor and reaction nozzles. With no irreversibilities and the pressure remaining constant, h_2 will not increase anymore. Then, combined with (14), Equation (13) for the complete two-step process gives an ideal w_2 .

$$\left(\frac{w_2^2}{2}\right)_{\text{ideal}} = \frac{u_2^2}{2} - \frac{u_1^2}{2} \quad (15)$$

Now, we characterize the friction and losses in the rotor passages using a rotor velocity ratio ϕ_r .

$$\phi_r \equiv \frac{w_2 \text{ actual}}{w_2 \text{ ideal}} \quad (16)$$

Then, dividing (15) by u_2^2 , w_2 is given by

$$\frac{w_2}{u_2} = \phi_r \left[1 - \left(\frac{r_1}{r_2}\right)^2 \right]^{1/2} \quad (17)$$

With (17) replacing w_2/u_2 , (10) gives the rotor efficiency, though now in terms of the velocity ratio ϕ_r . We assume ϕ_r is a constant in the rest of this analysis. Based on pipe friction factor formulas, ϕ_r is at least 0.975 and could be as high as 0.995. Experimental tests are required to measure ϕ_r . We will use $\phi_r = 0.975$ hereafter.

Note that our assumption that all of $w_1^2/2$ in (13) irreversibly converts to enthalpy is conservative. The rotor might be designed to take advantage of some of that energy to increase w_2 . However, our analysis does consider that as the flow slows down, the angular momentum of the relative flow contributes to the torque on the rotor.

Using (17) to substitute for w_2 in (10) gives the rotor efficiency.

$$\eta_r = 2 \cos^2 \alpha \left\{ \frac{u_1}{c_{\theta 1}} + \left(\frac{r_2}{r_1} \right)^2 \left(\frac{u_1}{c_{\theta 1}} \right)^2 \left[\phi_r \cos \beta \sqrt{1 - \left(\frac{r_1}{r_2} \right)^2} - 1 \right] \right\} \quad (18)$$

Summarizing, the overall turbine efficiency η_T is the product of the nozzle efficiency (1) and the rotor efficiency (18)

$$\eta_T = \eta_N \eta_r \left(\alpha, \beta, \frac{u_1}{c_{\theta 1}}, \frac{r_1}{r_2}, \phi_r \right) \quad (19)$$

By differentiation of (18) the optimum values of the radius ratio and speed ratio $u_1/c_{\theta 1}$ are the following ($\beta=0$).

$$\left(\frac{r_1}{r_2} \right)_{\text{opt}} = \left\{ \frac{2}{\phi_r^2} \left[(1 - \phi_r^2)^{1/2} - (1 - \phi_r) \right] \right\}^{1/2} \quad (20)$$

$$\left(\frac{u_1}{c_{\theta 1}} \right)_{\text{opt}} = \frac{\left(\frac{r_1}{r_2} \right)^2}{2(1 - \phi_r) \sqrt{1 - \frac{r_1^2}{r_2^2}}} \quad (21)$$

Interestingly, when these optimum values (which depend on ϕ_r) are used in (18) to determine η_r , the result is that

$$\eta_r = \cos^2 \alpha \left(\frac{u_1}{c_{\theta 1}} \right)_{\text{opt}} . \quad (22)$$

Figure C-3 shows r_1/r_2 , $u_1/c_{\theta 1}$ and $\eta_r/\cos^2 \alpha$ as a function of ϕ_r . With $\phi_r = 0.975$, $(r_1/r_2)_{\text{opt}}$ is 0.605 and $(u_1/c_{\theta 1})_{\text{opt}} = 0.817$. With an inlet angle α of 15° and a hydraulic-entry-nozzle efficiency η_N of 0.95, the overall turbine efficiency is 72%. This efficiency does not include bearing and windage losses.

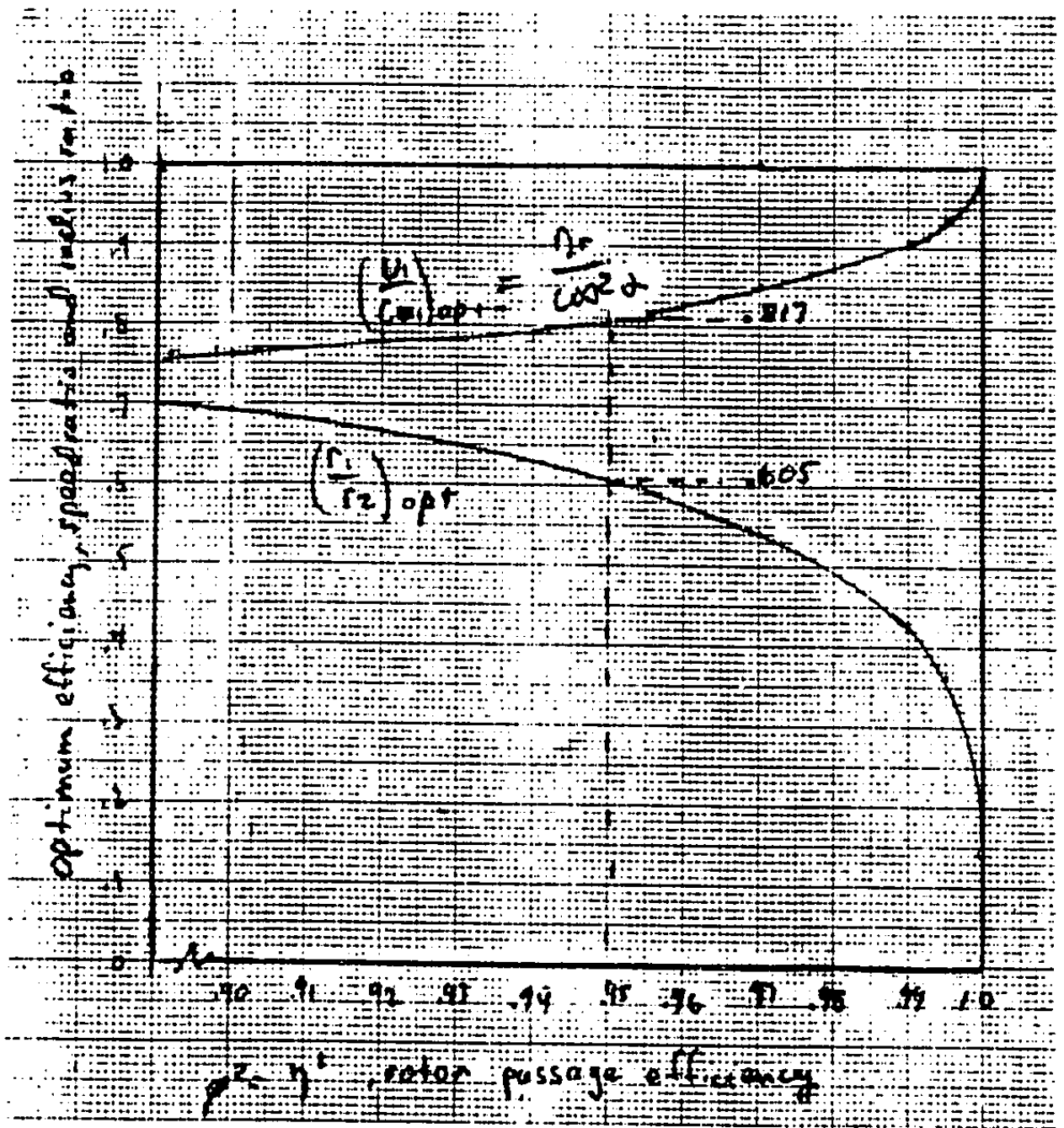


Figure C-3. Optimum Efficiency, Speed Ratio and Radius Ratio

REFERENCES

1. Biphase Energy Systems. "Desalination/Power Cycles with the Biphase Rotary Separator and Turbine." Final Report to OWRT, DOI, Contract No. 14-34-0001-9407, September 1980.
2. Hatch, L.P. and G.G. Weth. "Scale Control in High-Temperature Distillation Utilizing Fluidized-Bed Heat Exchangers." U.S. Department of the Interior, R&D Progress Report No. 571, July 1970.
3. Swaidan, B.E. and E.E. Cooper. "Analysis of Scale Control in Fluidized-Bed Heat Exchangers." U.S. Navy Laboratories Technical Note N-1340, Port Hueneme, California, April 1974.
4. Veeman, A.W., J.D. Broekens, C.M. Dissel. "The Fluidized-Bed Heat Exchanger in an MSF/FBE, Its Self-Cleaning and De-Scaling Capabilities" in Proceedings of the 6th International Symposium on Fresh Water from Sea. Las Palmas, Grand Canaria, Spain. Vol. 2, pp. 61-73, 1978.
5. Veenman, A.W. "The Fluidized-Bed Heat Exchanger in a Vertical Multi-Stage Flash Evaporator." NWSIA Journal, July 1977, Vol 4, No. 2, pg. 31.
6. Cole, L.T. and C.A. Allen. "Liquid Fluidized-Bed Heat Exchanger Flow Distribution Models." Allied Chemical Corporation, Idaho Chemical Program, No. ICP-1153, April 1978.
7. Allen, C.A. and E.S. Grimmett. "Liquid Fluidized-Bed Heat-Exchanger Design Parameters." Allied Chemical Corporation, Idaho Chemical Program, No. ICP-1153, April 1978.
8. Allen, C.A., R.E. McAtee, and E.S. Grimmett. "Liquid Fluidized-Bed-Heat-Exchanger Scale Control and Corrosion Tests." Allied Chemical Corporation, SAE/P-78/75.
9. Fraser, R.P., E.P. Eisenklam, and N. Dombrowski. "Liquid Atomization in Chemical Engineering: Part 2. Rotary Atomizers." British Chemical Engineering, September 1957.
10. Eck, Bruno. Technische Stroemungslehre. Springer-Verlag, Berlin, 1961.
11. Davidson, J.F. and D. Harrison, eds. Fluidization. Academic Press, London 1971.